SURFACE FORCES IN THIN WATER FILMS ON SMOOTH QUARTZ

BY

RICHARD MARK PASHLEY

Thesis Submitted For The Degree of
Doctor Of Philosophy

Department of Mineral Resources Engineering,
Imperial College of Science and Technology,
London, SW7 2BP.

August, 1978.

Surface forces in thin water films on smooth quartz

by

Richard Mark Pashley

ABSTRACT

The wetting characteristics of pure water on clean, fully hydroxylated, crystalline quartz and on quartz which had been rendered hydrophobic have been investigated. The water adsorption isotherm on clean quartz, determined by ellipsometry, corresponded to that of a perfectly hydrophilic solid. Isotherms for hydrophobic quartz surfaces showed limited adsorption at saturation, and were similar to results previously reported for vitreous silica; the latter were probably obtained with surfaces which were not sufficiently rigorously cleaned. A short-range "structural" interaction appears to be the major factor controlling the difference in wetting properties between hydrophobic and hydrophilic quartz.

As the wetting properties of high energy surfaces are very sensitive to contamination, it was necessary to investigate methods of cleaning and storing of polished quartz samples. Rigorous conditions were required to obtain and maintain clean quartz surfaces. Methods of producing and monitoring surfactant-free water were also studied.

The crystalline quartz plates used were specially polished, etched and then characterised. They were found to be very smooth and free from amorphous material and foreign elements.

The affect of surface roughness on the ellipsometric measurement of thin water films on quartz was investigated theoretically; large errors in measurement may be incurred if the water film is comparable in thickness with the surface roughness.

Lifshitz theory for the calculation of the macroscopic van der Waals interaction was applied to water/quartz systems, using recent spectral data. For water films thicker than about 60 nm on quartz the van der Waals component of the disjoining pressure becomes weakly negative, but this will normally be obscured by electrical double-layer repulsion.

Current approximate theory for electrical double-layer forces in liquid films was investigated. For thick water films on quartz the theory agrees roughly with experimental measurements, however, in thin films these forces appear to be underestimated.

ACKNOWLEDGEMENTS

I would like to express my most sincere thanks to my supervisor, Dr. J. A. Kitchener, for his invaluable help over the past three years.

I am also indebted to Kodak Ltd. for assistance received under a CASE studentship and for encouragement and valuable discussion with members of the surface chemistry group at Kodak Ltd., Harrow, with special thanks to Dr. J. F. Padday.

This work was funded by the Science Research Council to whom I am most grateful.

I would also like to thank members of the Department of Mineral Resources Engineering for their assistance and useful discussions.

The ellipsometer used in this work was constructed with the kind advice of Dr. B. T. Ingram and co-workers at Procter and Gamble Ltd., Newcastle for which I am very grateful.

CONTENTS

LIST OF TABLES

LIST OF FIGURES

CHAPTER 1

INTRODUCTION

The study of thin liquid films - such as "free" lamellae of surfactant solutions or "supported" films of liquids on solid substrates - has provided important information about the nature and magnitude of surface forces. The results are relevant not only to the lamella systems themselves (e.g. foams, spreading and wetting phenomena) but also to disperse systems such as sols and emulsions, where the forces which control stability are not accessible to direct measurement.

The aim of this work was to study experimentally the adsorption isotherm of water on smooth crystalline quartz surfaces (using the method of ellipsometry) and to compare the results obtained with current theoretical understanding of surface forces in thin films. A flat solid substrate was chosen so that multilayer adsorption could be studied very close to the saturated vapour pressure; inter-particulate capillary condensation would occur in this region if adsorption on a powder were studied.

When a thin liquid film exists in equilibrium with its vapour at a partial pressure, P, less than the normal saturation vapour pressure, P_o, it can be considered to be subject to a surface force, normal to its plane, which is known as the "disjoining pressure", Π. This pressure depends on the thickness of the film, h, and can be calculated from the relative vapour pressure (P/P_o) in equilibrium with the film by the equation derived by Derjaguin and Shcherbakov (1.1):

$$\Pi = -\frac{RT}{V_m} \ln. \frac{P}{P_o} = -\left(\frac{\partial G}{\partial h}\right)_T \qquad 1.1$$

where G is the specific excess free energy of the film (due to the action of surface forces) and V_m is the molar volume of the liquid in the film. The disjoining pressure concept, introduced by Derjaguin, may be thought of as an excess pressure within a thin film which prevents the film draining (i.e. the pressure difference between liquid in the film and liquid in bulk (1.2)). If the disjoining pressure is positive, the film is mechanically stable and tends to thicken (or can come to equilibrium under the action of gravitational forces). A negative disjoining pressure produces instability and collapse of the film.

The pressure, Π, is generally assumed to be a function (dependent on film thickness) which can be split up into several separate components. For example, Derjaguin and Churaev (1.3) proposed three terms:

$$\Pi = \Pi_{el} + \Pi_{vdw} + \Pi_s \qquad 1.2$$

Here Π_{el} is the disjoining pressure in the film due to electric double-layer repulsion (or attraction); Π_{vdw} is the component due to van der Waals interaction and Π_s is a postulated "structural" component of disjoining pressure. Theoretical calculations of Π_{vdw} and Π_{el} are discussed in Chapters 2 and 3. Π_s is the component due to interaction between the substrate surface and adjacent liquid molecules. It may be either positive or negative in sign, but it is believed to be of relatively short range. For the case of a strongly hydrogen -bonded or polar liquid (e.g. water) this structural interaction may be the predominant force controlling the wetting properties of a particular material - determining, for example, whether a finite contact angle will be formed. That this is apparently the case is well illustrated by the different wetting

properties of water on fully hydroxylated silica (contact angle $\sim 0^{\circ}$) and heat dehydroxylated silica (contact angle $\sim 40^{\circ}$). It has been argued (1.4) that many strongly hydrophobic solids (e.g. graphite, paraffin wax, molybdenite etc.) would behave as hydrophilic solids if Π_{vdw} and Π_{el} were the only significant surface forces.

Experimental evidence for Π_s and theoretical understanding of its origin are still inadequate at present (1.3). It was planned in this work to experimentally measure the adsorption isotherms on clean (hydroxylated), heat dehydroxylated and surface methylated quartz surfaces in order to evaluate the importance of this short-range structural component.

It has long been known (e.g. by Freundlich in 1926 (1.5)) that the intercept and form of the water adsorption isotherm, near $P/P_o = 1.0$, are related to the contact angle (i.e. wetting properties) of water on the substrate (1.6, 1.7). For surfaces on which a finite contact angle is formed the adsorption isotherm intersects the axis ($P/P_o = 1.0$, $\Pi = 0$) at a definite, small, film thickness (Figure 1.1, curve (b)). A zero or very small contact angle corresponds to a very thick film at saturated vapour pressure (Figure 1.1, curve (a)).

Thus, at saturated vapour pressure for a non-wetting system, bulk water can be in equilibrium with a thin film via a finite contact angle (Figure 1.2). When a contact angle of a liquid on a solid is measured, at equilibrium, the solid surface necessarily carries an adsorbed vapour layer, as noted by Frumkin in 1938 (1.8).

Fig 1.1 Adsorption isotherms expected for water vapour on flat silica substrate where (a) bulk water wets the solid and (b) a contact angle is formed.

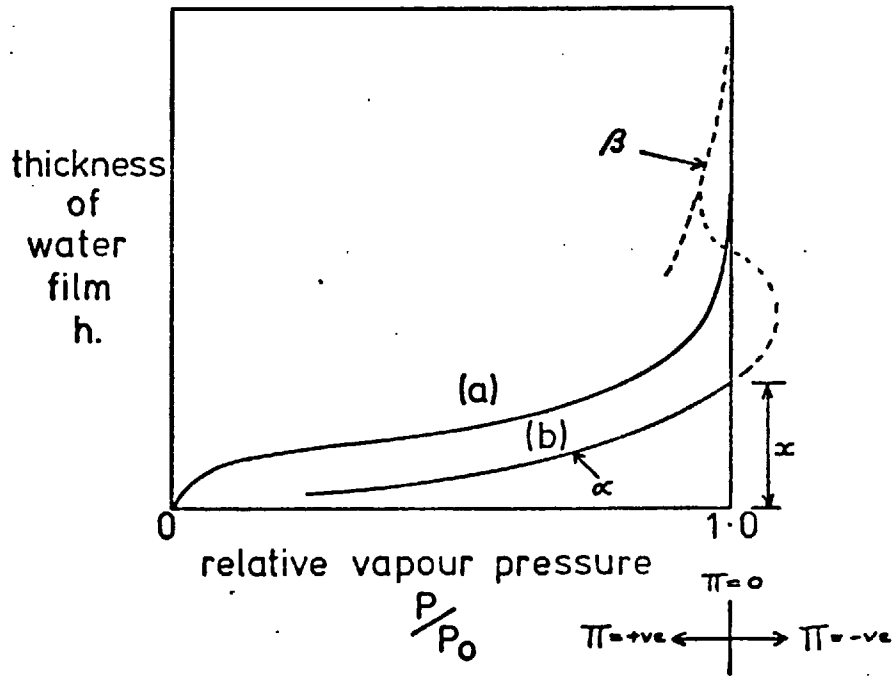

Fig 1.2 Bulk contact angle, θ, on solid substrate in equilibrium with thin film.

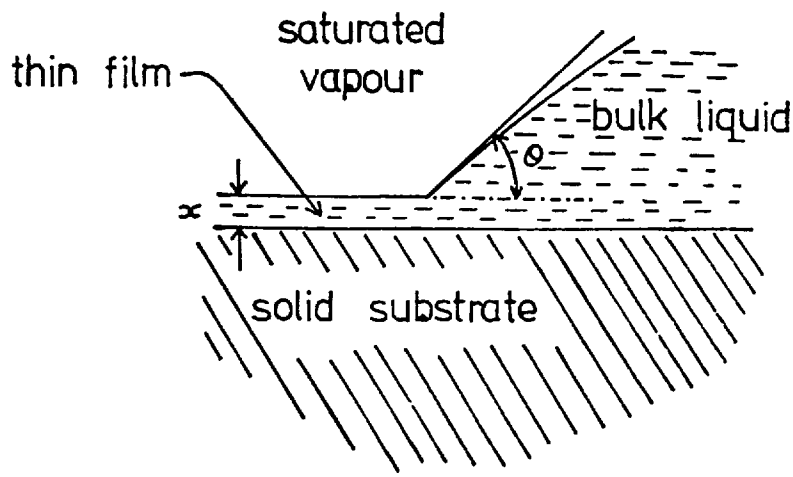

It has been postulated that where a finite contact angle exists between bulk and thin film the film must have a different "structure" to that of the bulk (1.6). In a recent review Drost-Hansen (1.9) discusses evidence in favour of the existence of structured water layers adjacent to solid surfaces, but firm evidence on this question is scarce.

Derjaguin and Zorin (1.6) termed this thin "structured" layer the α-film (see Figure 1.1) and the thick film formed by thinning of bulk liquid (e.g. by pressing a bubble against a plate) the β-film. For very thin films ($\lesssim$ 11 nm) Derjaguin and Churaev (1.10) conclude that only these structural forces are important (for the case of polar liquid films). Derjaguin and Zorin (1.6) further postulated that the α and β portions of the adsorption isotherm may therefore belong to different forms of the polar liquid and hence to two separate isotherms, where no continuous transition between the two is possible.

Derjaguin and Zorin (1.6), Ershova, Zorin and Churaev (1.11) Derjaguin, Zorin (1.12) and Hall (1.13) reported adsorption isotherm measurements on apparently clean, fully hydroxylated, vitreous silica surfaces which give finite water film thicknesses of about 4-7 nm at saturated vapour pressure (i.e. Figure 1.1, (b) type isotherm). Derjaguin, Zorin, Churaev and Shishin (1.12) state that the clean silica plates used had a water contact angle of about 20°. This would mean that vitreous silica, when clean and fully hydroxylated, is hydrophobic and that a structured layer of water 4-7 nm thick (at $25^{\circ}C$) can exist in equilibrium with bulk water on its surface, at saturated vapour pressure. Such a contact angle on silica (and quartz) is contrary to what is commonly accepted by research workers in mineral flotation, namely, that

silica and quartz when clean and fully hydroxylated are perfectly hydrophilic (i.e. Figure 1.1, (a) type isotherm).

However, isotherms corresponding to perfect wetting by water on glass surfaces have been reported by Garbatski and Folman (1.14, 1.15). Water films of 62 nm thickness were reported at a relative vapour pressure of 0.9976. The results indicated that there was a continuous transition between thin and thick water films and that the adsorption isotherm was of type (a) in Figure 1.1 Characterisation of the surfaces used in these measurements was insufficient and further investigation of the nature of the forces was recommended.

Experience has shown that the wetting properties and adsorption isotherms for water on quartz are extremely sensitive to the surface cleanliness of both the solid substrate and of the water used. Attention was therefore given to the charact erisation of both the quartz surfaces and the water used in the present work. The effect of alteration of the quartz surface on its wetting properties was also investigated in order to obtain a better understanding of the surface forces involved. A theoretical analysis of the van der Waals and electric double-layer forces in water films on quartz was also carried out for comparison with experimental results, because, as pointed out by Derjaguin and Churaev (1.3), it should be possible to deduce the influence of structural forces by this approach.

A better understanding of the surface forces which determine whether water wets a particular solid or not is of importance in many industrial processes (e.g. flotation, lithography), and knowledge of the effect of structural water (or short-range forces) adjacent to a surface may also be necessary to achieve a comprehensive description of colloid stability.

A. THEORETICAL SECTION

CHAPTER 2

THEORETICAL CALCULATION OF THE MACROSCOPIC VAN DER WAALS INTERACTION

Historical Introduction

That forces of attraction exist between gaseous molecules was first recognised in 1881 by van der Waals in relation to deviations from ideality of real gases, though without knowledge of the molecular origin of the forces. These attractive forces exist between both polar and non-polar molecules, the latter being due to the formation of instantaneous dipoles. The pair-wise interaction between vapour molecules was calculated by Keesom (2.1), Debye (2.2) and London (2.3) who derived interaction forces related to molecular polarizabilities. The application of such interactions for macroscopic bodies is more complicated and was first attempted using a pair-wise summation process which calculated the sum of interactions between their incremental parts (2.4), the polarisabilities of each part being the fundamental property which determines the interactive force. Casimir and Polder (2.5) first pointed out the retardation effect in the dispersion force (non-polar) interaction. Only the dispersion force is an additive property for macroscopic bodies.

After the advent and understanding of quantum theory a new approach followed which was based on continuum properties of macroscopic bodies. Thus Lifshitz (2.6) and later Dzyaloshinskii, Lifshitz and Pitaevskii (2.7) derived, using the theory of quantum electrodynamics, the van der Waals force between planar macroscopic

bodies related to the spectral absorption characteristics of the media considered. The Lifshitz equation embraces all types of van der Waals forces (e.g. London and dipole-dipole interactions), as well as the effect of retardation. In order to use the full Lifshitz equation, spectral data for the media involved are required, extending from far infra-red (i.r.) to far ultra-violet (u.v.) frequencies. Such data, and suitable methods for handling the data, were not available in 1960 when the Liftshitz equation was derived, and only approximate calculations were then possible.

Techniques for creating spectral models to represent the spectral data required, using incomplete data available were more recently (1969) developed by Parsegian and Ninham (2.8). Such advances made accurate calculations of the macroscopic van der Waals interaction possible.

Introduction

The simple non-retarded Hamaker-type equation is given in equation 2.1 for the planar interaction system illustrated in Figure 2.1 :

$$\Pi = - A/6 \pi l^3 \qquad 2.1$$

where Π is the disjoining pressure (force of repulsion) between media 1 and 2 and A is the Hamaker coefficient which is a function of the media considered. This simple equation does not take into account the affect of retardation. The retardation effect is the reduction of the coefficient A with distance, and arises due to the fluctuations in dipole becoming out of phase with the second polarisable system owing to the distance the electromagnetic fluctuation has to travel.

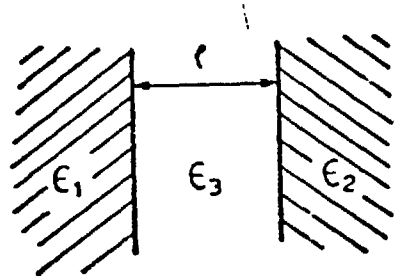

Figure 2.1. Two semi-infinite half-spaces separated by distance l.

If the interacting bodies are far apart the interaction force is said to be "fully retarded" and the law of interaction for planar bodies becomes:

$$\Pi = - B/l^4 \qquad 2.1a$$

At intermediate distances there is a gradual transition from the l^{-3} to the l^{-4} law (2.9). The full Lifshitz equation, which includes retardation effects, for the system shown in Figure 2.1 is given below:

$$G(l) = \frac{kT}{8\pi l^2} \sum_{\xi_n}{}' \left(\frac{\xi_n}{\xi_s}\right)^2 \int_1^\infty dp.p.ln\left[\left\{1 - \Delta(p;s_1).\right.\right.$$

$$\left.\Delta(p;s_2).exp\left(-\frac{\xi_n p}{\xi_s}\right)\right\}.\left\{1 - \bar{\Delta}(p;s_1).\right.$$

$$\left.\left.\bar{\Delta}(p;s_2).exp\left(-\frac{\xi_n p}{\xi_s}\right)\right\}\right]$$

where $$\Delta(p;s_j) = \frac{\epsilon_j p - \epsilon_3 s_j}{\epsilon_j p + \epsilon_3 s_j}$$

$$\bar{\Delta}(p;s_j) = \frac{p - s_j}{p + s_j}$$

$$s_j^2 = p^2 - 1 + \epsilon_j/\epsilon_3 \;, \qquad j = 1,2$$

$$\xi_s = c/2l(\epsilon_3)^{1/2} \;, \quad \xi_n = (2\pi kT/\hbar).n$$

where:

c = velocity of light in a vacuum, T = temperature and

G(1) is the free energy of interaction.

ϵ_j is the dielectric constant as a function of the imaginary frequency for medium "j", i.e. $\epsilon_j = \epsilon_j (i\xi)$. Thus, basically if ϵ is known throughout the electromagnetic spectrum (in practice from far i.r. to far u.v. is sufficient), the interaction energy may be calculated using equation 2.2. Equation 2.2 is the form of the Lifshitz equation given by Richmond (2.10). The dielectric constant $\epsilon(i\xi)$ can be obtained for a particular frequency by using the Kramers-Kronig equation (2.9) derived from complex variable theory:

$$\epsilon(i\xi) - 1 = \frac{2}{\pi} \int_0^\infty \frac{x\epsilon''(x)\,dx}{x^2 + \xi^2} \qquad 2.3$$

where:

$$\epsilon''(x) = 2n(x).k(x) \qquad 2.4$$

and n and k are the real and imaginary parts of the refractive index at frequency x. Equation 2.3 in effect means that $\epsilon(i\xi)$ can be calculated for any given frequency (ξ), assuming complete knowledge of the absorption properties; since k is directly related to the absorption coefficient of the material via the equation:

$$k(x) = \frac{c.\ \mu(x)}{2.\ x} \qquad 2.5$$

where $\mu(x)$ is the optical absorption coefficient at frequency x.

The extent of spectral data required, into the ultra-violet, for the Lifshitz calculation is determined by the "cut-off frequency" (2.10) given by:

$$\xi = \xi_s > c/2l\sqrt{\epsilon_3} \qquad 2.6$$

Thus, from retardation considerations, for $l \gtrsim 10$ nm the higher frequencies are strongly retarded and hence lack of data in the far u.v. will not greatly affect the calculation (for $\epsilon_3 = 1.0$). However, for $l < 5$ nm the cut-off frequency is $\xi_s \gtrsim 3 \times 10^{16}$, which lies well into the u.v. region. Since these frequencies are now no longer so damped, data in the far u.v. are necessary for accurate calculations.

From comparison of the non-retarded equation 2.1 with the full equation 2.2 it may be seen that the Hamaker coefficient $A = f(l)$. It is predicted that A is a constant only for short distances of separation (i.e. $\lesssim 5$ nm).

Experimental measurements of van der Waals forces have been shown to be in reasonable agreement with theory. Blake's (1.2) measurements of octane and decane films on sapphire surfaces are in close agreement with Lifshitz theory for films > 20 nm. Wittman et al (2.11) measured the force between quartz plates for separations of about 10 to 100 nm and reported fair agreement with the van der Waals force calculated by the Lifshitz theory, using experimentally determined adsorption data for quartz. More recently, Splittgerber and Wittmann (2.12) re-measured the force between quartz plates but with 3 - 4 molecular layers of water present on the two interacting surfaces. Excellent agreement was reported with Lifshitz theory where bulk dielectric properties were assumed for the adsorbed water layers.

Smooth vertical fluoride substrates have recently been used to study forces in helium films; excellent agreement was obtained for films of 1 to 25 nm thickness (2.13). Chan and Richmond (2.14) recently compared theory and experiment for forces between quartz

and mica plates. They found rough agreement but concluded that more accurate experimental measurements over a wider range are required for a precise comparison for the case of quartz plates.

As mentioned previously, the van der Waals force calculation depends on the bulk spectral characteristics of a material. It is, however, possible that the structure of a liquid adjacent to a solid substrate may be different from that of the bulk. In this case the calculated force would be incorrect. Israelachvili (2.15) has recently measured the force between two mica cylinders in aqueous solutions and has reported that down to 2 nm separation the water interlayer has a refractive index within 1% of the bulk value. This suggests that the calculated van der Waals force should be correct at least down to separations of about 2 nm for water/silicate systems.

As a very thorough review of van der Waals force calculations has recently been published by Mahanty and Ninham (2.16), further discussion will not be given here.

Method

A computer program was written to solve the Lifshitz equation (eqn. 2.2); a flow-chart for this program is given in Appendix 2.1. The inner integral was solved using a Gauss-Laguerre quadrature technique (2.17) following a method devised by Dr. L.R. White (private communication). The outer summation was calculated for n = 0,500.

Equation 2.2 gives the free energy of interaction, G. In order to calculate the force between the planar media the simple relation:

$$\text{force of attraction, } F = + \frac{\partial G}{\partial l} \qquad 2.7$$

was used. The calculation requires knowledge of G over a small change in l, where the gradient is essentially linear. For regions where a Hamaker constant is valid the simple relations:

$$F = A_F/6\pi l^3 \qquad 2.8$$

$$G = A_G/12\pi l^2 \qquad 2.9$$

hence $$F = 2G/l \qquad 2.10$$

may be used in order to calculate the force from the free energy. But where A is not constant the values calculated from force and energy equations are not identical, $A_G \neq A_F$ (2.18). The correct force is that obtained by computation by using equation 2.7.

The basic input data for the program were the spectral data of the materials involved. At present, "spectral models" are commonly used to represent the actual spectral characteristics of the materials. Two types of such models are given below:

$$(I)\ \frac{\epsilon(i\xi) - 1}{\epsilon(i\xi) + 2} = \sum_i \frac{F_i}{\omega_i^2 + \xi^2 - \gamma_i \xi} \qquad 2.11$$

where F_i is a constant related to the oscillator strength of an absorption peak and ω_i is the frequency of that peak, γ_i is the bandwidth or damping constant, which can usually be neglected.

$$(II)\ \epsilon(i\xi) = 1 + \sum_m \frac{C_m}{1 + \xi\tau_m} + \sum \frac{C_l}{1 + (\xi/\omega_l)^2 + \gamma_l(\xi/\omega_l^2)} \qquad 2.12$$

where $1/\tau_m$ and ω_l are resonance frequencies of absorption peaks of oscillator strengths related to C_m and C_l. The first sum refers

to Debye type microwave relaxation (2.19).

The first, simpler model (2.20) can be used for systems where the spectral data can be approximated to two main peaks (2.21). For the case of water and silica, for example, these peaks would be in the infra-red and the ultra-violet regions of the spectrum (2.21). Thus for equation 2.11, i = 1,2. In the visible region for materials such as water and quartz, the spectral properties may be assumed to be dominated by a single absorption peak in the u.v.; thus equation 2.11 becomes:

$$\frac{n(\omega)^2 - 1}{n(\omega)^2 + 2} = \frac{F_{uv}}{\omega_{uv}^2 - \omega^2} \qquad 2.13$$

Thus if the refractive indices at different wavelengths in the visible region are accurately known, the constants F_{uv} and ω_{uv} can be calculated.

An alternative approach is to assume that ω_{uv} corresponds to the first ionizationpotential of the material (e.g. $\omega_{uv}^{H_2O} = 1.906 \times 10^{16}$ rads/sec). Typical constants used by Ingram (2.21) for the i.r. region for silica and water were used in this work with the u.v. constants calculated as explained above. This simple equation was used to calculate the force for the water/vac./water interaction in order to compare the results obtained with those using a different, more fundamental, approach (see Appendix 2.2).

If spectral data (and hence ϵ'' values) are available for the materials over a sufficiently wide range then the Kramers-Kronig equation (eqn. 2.3) can be used to calculate $\epsilon(i\xi)$. Such data are now available for materials such as crystalline quartz, liquid water and polystyrene. Table 2.1 gives the data sources used in

Table 2.1. Spectral data sources for water, quartz and polystyrene

material	region	frequency range (rad/sec)	source
water	i.r.	$6.1 \times 10^{7} - 7.6 \times 10^{12}$	2.29
	i.r.	$9.1 \times 10^{12} - 3.8 \times 10^{13}$	2.30
	i.r.	$4.6 \times 10^{13} - 1.8 \times 10^{15}$	2.31
	u.v.	$1.2 \times 10^{17} - 3.8 \times 10^{16}$	2.32
	u.v.	$3.8 \times 10^{16} - 1.5 \times 10^{17}$	2.33
quartz	i.r.	$5.7 \times 10^{12} - 5.7 \times 10^{13}$	2.34
	i.r.	$6.3 \times 10^{13} - 2.7 \times 10^{14}$	2.35
	u.v.	$3.8 \times 10^{14} - 3.3 \times 10^{16}$	2.36
	u.v.	$3.3 \times 10^{16} - 6.1 \times 10^{16}$	2.37
polystyrene	u.v.	$6.8 \times 10^{15} - 9.1 \times 10^{16}$	2.38

this work for these materials. The computer program written was used for both the spectral model and Kramers-Kronig integration calculations for the water/vac./water interaction. A simple numerical integration technique was used to integrate the spectral data, via the Kramers-Kronig equation, in order to calculate $\epsilon(i\,\xi)$ for each sampling point required for the Gauss-Laguerre quadrature.

The amount of spectral data required into the u.v. for short distances of separation can be estimated by the use of plasma frequency limiting equations for very high frequency. At these high frequencies the dielectric characteristics are essentially those of a plasma (2.22) and are given by the equation:

$$\epsilon(i\,\xi) = 1 + (4\pi\, Ne^2/m\,\xi^2) \qquad 2.14$$

where the plasma frequency, $\omega_p = (4\pi\, Ne^2/m.)^{\frac{1}{2}}$ and N is the number of electrons (of mass and charge, m and e) per unit volume.

This equation is valid only for $\omega_p \ll \xi \ll 2\pi c/a$ where "a" is a length of atomic dimensions. For liquid water $\omega_p^2 \simeq 10^{33}$ $(\text{rad/sec})^2$ and $2\pi\, c/a \simeq 6 \times 10^{18}$ rad/sec. Thus, for water, the limiting equation is valid over the range 0.2×10^{18} to 1.0×10^{18} rad/sec.

Over this range the value of ϵ calculated from the spectral data can be compared with the limiting values in order to determine whether the data used are adequate. The limiting equation itself can be used to calculate the value of ϵ over this range.

Results and Discussion

1. Water/vacuum/water interaction

The dielectric constant as a function of imaginary frequency ($\epsilon(i\xi)$) was calculated for water using the Kramers-Kronig integration and also using a spectral model of the type given in equation 2.12 for comparison (see Figure 2.2). Table 2.2 also compares the result with the values calculated using an oscillator model (of type equation 2.11) with $\omega_{uv} = 3.0 \times 10^{16}$ rad/sec. This latter frequency appears to give results in better agreement with those from the full spectral data calculation. It is of interest to note that this frequency is, in fact, the "effective frequency" used by London (2.23) as long ago as 1937.

For very high frequencies, the limiting equation was used to calculate $\epsilon(i\xi)$ and these values are compared with those obtained using the full spectral data in Table 2.3. It can be seen that the Kramers-Kronig treatment agrees very well with that of the limiting equation for high frequencies.

Table 2.4 shows a comparison of the value A_G ($= -12\pi l^2 G$) for the water-water interaction calculated using both oscillator models and the Kramers-Kronig integration method. From these results it is apparent that the full spectral data approach is well approximated by an oscillator model of assumed u.v. frequency, $\omega_{uv} = 3.0 \times 10^{16}$ rad/sec.

Visser (2.24) recommended a value of 4.4×10^{-20} J for the Hamaker constant (in the non-retarded region); this corresponds to the value calculated here at 5 nm separation. Nir (2.25) reported values of Hamaker constants calculated for this system using a macroscopic approach which included a retardation effect, using a spectral model. For separations of 10 to 50 nm the two different

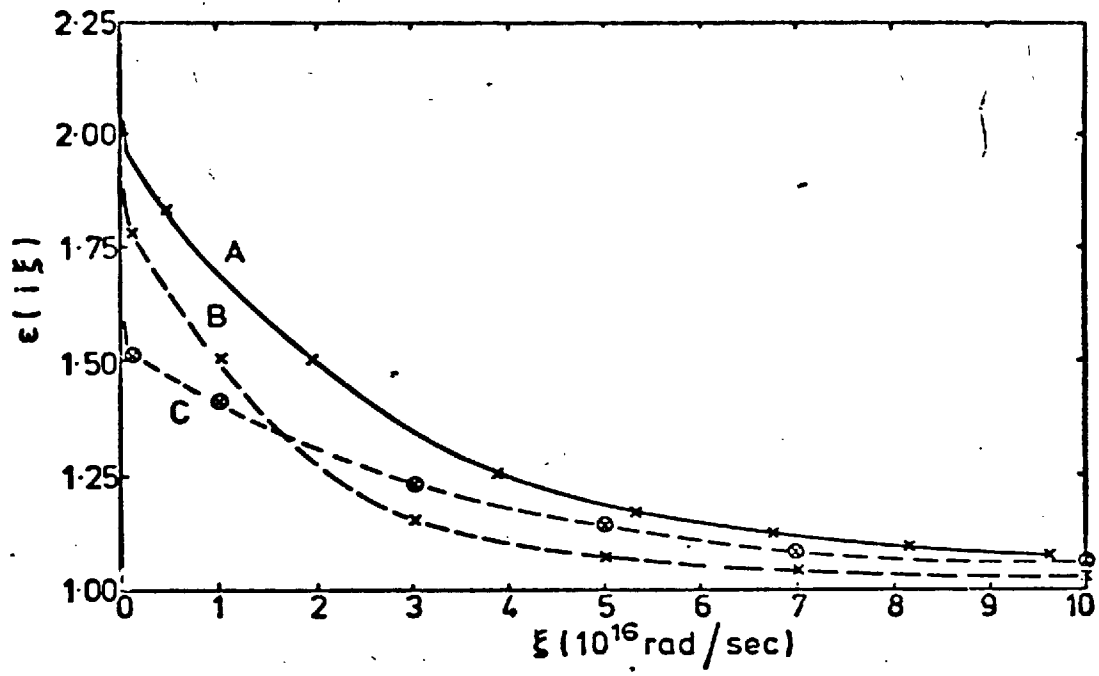

Fig. 2.2

Calculated dielectric "constant" as a function of imaginary frequency

A This study - full spectral data and Kramers-Kronig equation

B Nir et al (2.39) - oscillator model equation

(ω_{uv} = 1.906 x 10^{16} rad/sec)

C Nir et al (2.39) - full spectral data and Kramers-Kronig equation

At ξ = 0.001 rad/sec Nir et al (2.39) reported

$\epsilon(i\xi)$ = 93.6 ± 21.4 (from full spectral data)

This study: $\epsilon(i\xi)$ = 85.2

Table 2.2 Comparison of $\epsilon(i\xi)$ calculated using full spectral data and oscillator equation (for water)

	frequency (ξ) (rad/sec) x 10^{16}				
	0.4816	0.853	6.742	9.632	12.04
full spectral data (K-K equation)	1.832	1.255	1.120	1.068	1.047
oscillator model ($\omega_{uv}=3\times10^{16}$ rad/sec)	1.882	1.282	1.117	1.062	1.041

Table 2.3 Comparison of $\epsilon(i\xi)$ calculated using full spectral data and limiting equation (eqn. 2.14) for water

	frequency (ξ) (rad/sec) x 10^{18}			
	0.2504	0.3468	0.4045	0.4816
full spectral data (K-K equation)	1.013	1.007	1.005	1.003
limiting equation	1.016	1.008	1.006	1.004

Table 2.4. Hamaker function, A_G, calculated using full spectral data and two different oscillator models (of type shown in equation 2.11) for the interaction between two water half-spaces.

	separation distance (nm)					
	0.2	5	10	20	50	100
A_G (i) ($\times 10^{-20}$ J)	3.7	3.3	2.8	2.2	1.4	1.0
A_G (ii) ($\times 10^{-20}$ J)	5.5	4.3	3.4	2.5	1.5	1.0
A_G (iii) ($\times 10^{-20}$ J	5.7[a]	(5.3) 4.3 (3.4)	3.4	2.4	1.4	0.9

(i) oscillator model where: $\omega_{uv} = 1.906 \times 10^{16}$ rad/sec; $F_{uv}/\omega^2_{uv} = 0.202$

$\omega_{IR} = 5.66 \times 10^{14}$ rad/sec; $F_{IR}/\omega^2_{IR} = 0.377$

(ii) oscillator model where: $\omega_{uv} = 3.0 \times 10^{16}$ rad/sec; $F_{UV}/\omega^2_{UV} = 0.203$

$\omega_{IR} = 5.66 \times 10^{14}$ rad/sec; $F_{IR}/\omega^2_{IR} = 0.377$

(iii) spectral data.

[a]This calculation was also carried out using n = 4,000, A_G calculated = 5.7×10^{-20} J.

approaches give similar results.

Figure 2.3 shows the disjoining pressure between two water half spaces calculated using full spectral data and using the simple non-retarded Hamaker equation. The inverse case of a free water film is expected, from simple theory, to have the same interaction energy (2.26). The disjoining pressures calculated for a free water film by Vassilieff and Ivanov (2.27) agree very well with the results given here in Figure 2.3. In Appendix 2.3 the full equation was used to calculate the interaction energy for the two inverse cases. At very short distances the energy is very similar; as the separation becomes larger the difference becomes greater.

In these calculations n = 0,500 was used. This determines the range of frequencies summed (see eqn. 2.2). For very short distances of separation, where high frequencies are important, n = 500 was found to be sufficient (see Table 2.4a).

In order to obtain a rough estimate of the possible error involved in the calculation due to the spectral data, all the u.v. data for water were first increased by 15 - 25% and then decreased. The corresponding calculated values of A_G are given in parenthesis in Table 2.4 for 5 nm separation. These values will however be a gross overestimate of the errors expected from the u.v. data.

2. Crystalline quartz/vacuum/crystalline quartz

The force of attraction between quartz plates as a function of distance calculated using the full spectral data for crystalline quartz is given in Table 2.5. Chan and Richmond's recently calculated values (2.14) are shown in parenthesis for comparison.

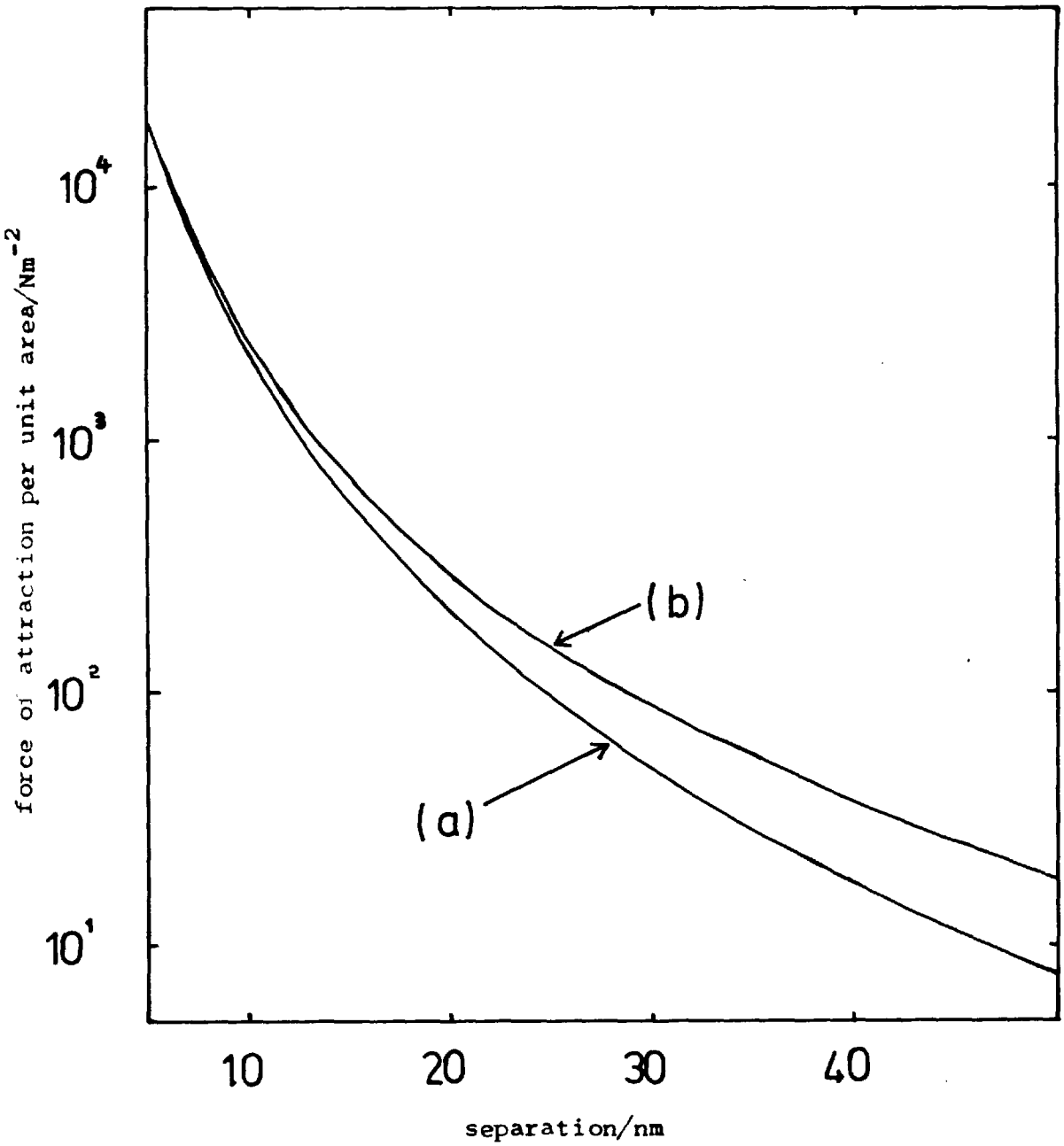

Figure 2.3. Calculated macroscopic van der Waals force of attraction between two water half-spaces as a function of separation.

(a) force calculated using Lifshitz equation and full spectral data.

(b) force calculated using Hamaker-type equation, where $A = 4.34 \times 10^{-20}$ J.

Table 2.5. Force of attraction between quartz half-spaces calculated using full spectral data

separation (nm)	1.0	3.16	10	31.6	100
force Nm^{-2}	4.7 x 10 (4.91×10^{6})	1.4×10^{5} (1.45×10^{5})	3.5×10^{3} (3.66×10^{3})	6.3×10^{1} (6.61×10^{1})	7.9×10^{-1} (9.15×10^{-1})

Chan and Richmonds (1977) calculated values are given in parenthesis for comparison.

Table 2.6. Calculated energy and disjoining pressure for water films on quartz, using full spectral data

film thickness (nm)	5	11	25	35	55
interaction energy, G mJm^{-2}	$+9.4 \times 10^{-3}$	$+1.2 \times 10^{-3}$	$+7.0 \times 10^{-5}$	$+8.9 \times 10^{-6}$	-7.6×10^{-6}
disjoining pressure Π, Nm^{-2}	$+4.5 \times 10^{3}$	$+3.1 \times 10^{2}$	$+1.5 \times 10^{1}$	+2.8	$+1.1 \times 10^{-1}$

Again there is good agreement with the latter authors, who used a spectral model approximation.

3. Crystalline quartz/water/vacuum

The disjoining pressure and free energy of water films on quartz due to van der Waals interaction was calculated using full spectral data for both materials. Figure 2.4 compares the calculated disjoining pressure with that obtained using the simple non-retarded Hamaker-type equation $\Pi = A/6\pi l^3$ with $A = -1.12 \times 10^{-20}$ J (1.3). For films of thickness $l \lesssim 5$ nm, the non-retarded equation is valid; but already at 10 nm this approximation is about 40% too high, because of the effect of retardation. Table 2.6 gives the calculated values of Π and G for films of 5 to 55 nm thick.

The interaction energy calculated for various quartz/water systems is plotted in Figure 2.5. From the results of curve A for a water film on quartz calculated with full spectral data it may be seen that the free energy becomes negative for films $l \gtrsim 40$ nm and that the disjoining pressure becomes negative for $l \gtrsim 60$ nm (Figure 2.6). That this result is due to the strong i.r. absorption of water (i.e. large static dielectric constant) can be seen from curves B and C. Removal of the i.r. data of water causes the disjoining pressure (and G) to be everywhere positive.

The sign of Π (i.e. whether the force of repulsion is positive or not between the half-spaces) is determined for large distances of separation by the static dielectric constants of the three media. This follows from a simplication of the full interaction equation which has been discussed by Dzyaloshinskii et al (2.28). From this simplified equation if $\epsilon_{o_1} = \epsilon_{o_2}$ (where ϵ_{o_n} is the static dielectric

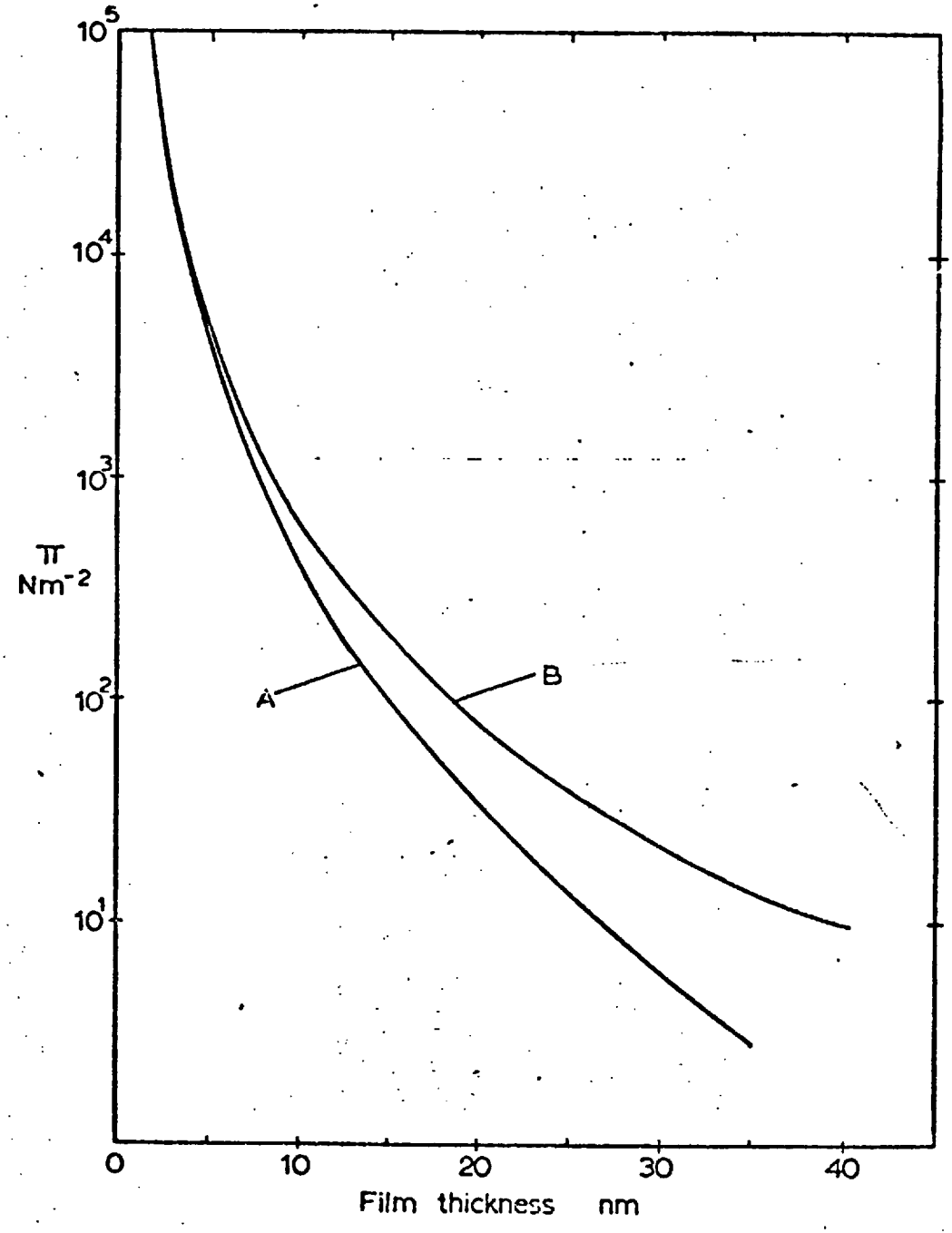

Figure 2.4. Disjoining pressure, Π_{vdw}, in thin water films on quartz

A - results calculated using the Lifshitz equation and full spectral data

B - calculated using simple non-retarted Hamaker-type equation, with $A = -1.12 \times 10^{-20}$ J.

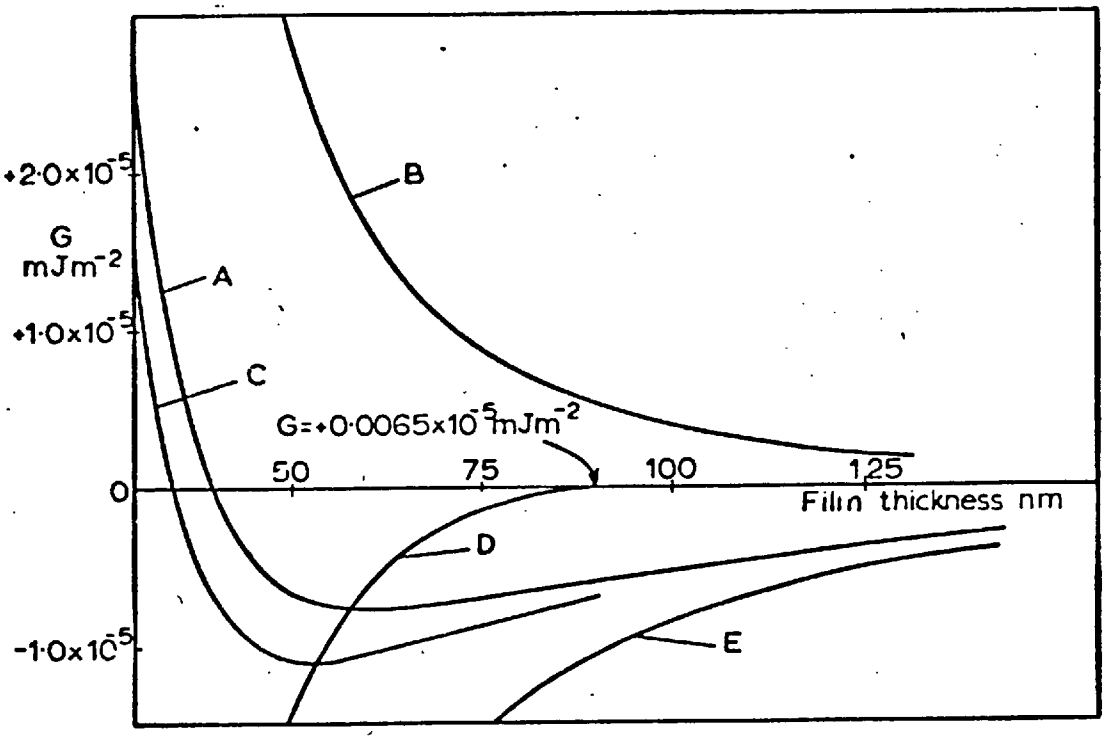

Figure 2.5. Free energy as a function of separation for the macroscopic van der Waals interaction

(A) quartz/H_2O/vac. using full spectral data for both

(B) quartz/H_2O/vac. omitting i.r. data for both

(C) quartz/H_2O/vac. omitting i.r. data for quartz only

(D) H_2O/quartz/vac. using full spectral data for both.

(E) quartz/H_2O/quartz using full spectral data for both.

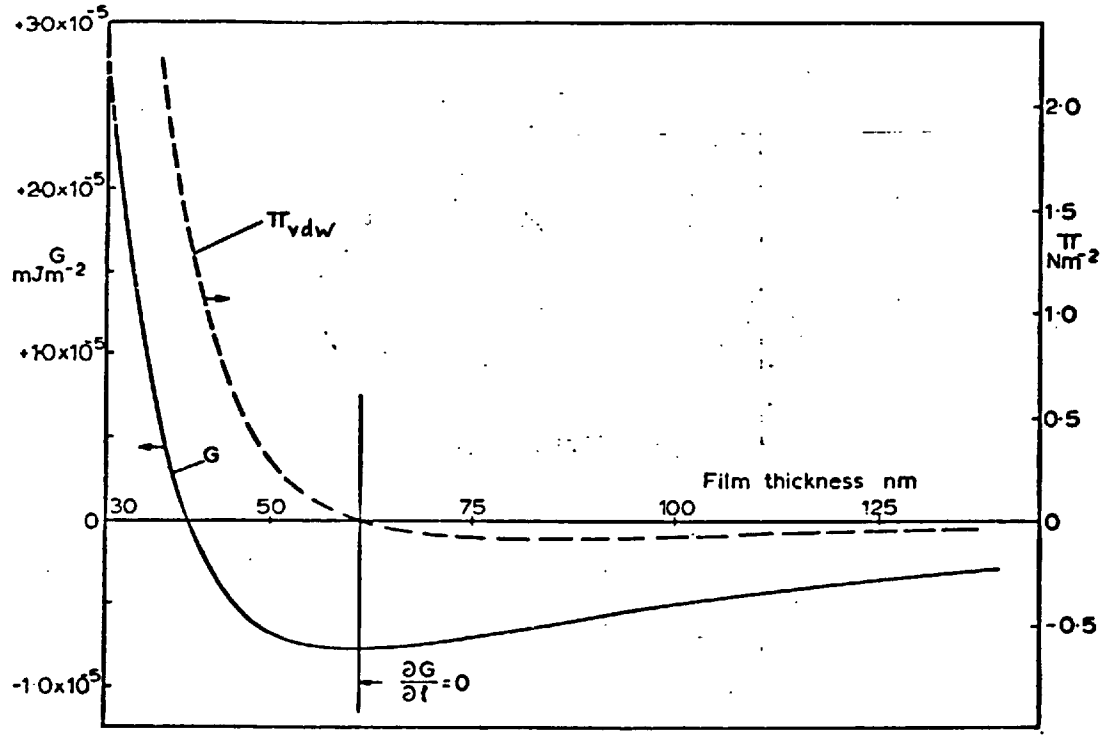

Figure 2.6. Disjoining pressure and free energy calculated as a function of film thickness using the Liftshitz equation with full spectral data for water films on quartz

constant of medium n) the force between media 1 and 2 is always attractive (Figure 2.5., curve E), independent of the intervening medium. For the case $\epsilon_{o_3} > \epsilon_{o_1} > \epsilon_{o_2}$ (e.g. a water film on quartz), at large distances of separation the force between media 1 and 2 must be attractive (Π negative as in Figure 2.5 and 2.6). The inverse case of a hypothetical film of quartz on water (Figure 2.5, curve D) is subject to attraction at short distances and very slight repulsion at large distances.

Corresponding calculations for hypothetical water films on polystyrene gave a very similar result, i.e. a transition to negative disjoining pressure for thick films, Figure 2.7. Polystyrene has rather similar u.v. absorption properties to quartz and has negligible i.r. absorption.

It should be emphasised that the negative disjoining pressures in thick water films on quartz are only of the order 0.1 N m^{-2}. This is negligibly small compared with the likely positive disjoining pressure due to electrical double layer repulsion. For example, for quartz substrates and a low concentration symmetrical electrolyte aqueous film, Derjaguin (1.3) estimated a positive disjoining pressure of about 400 N m^{-2} for an 80 nm thick film. If the double layer component could be reduced to zero by reduction of the surface potential or by increase in electrolyte concentration, the tendency towards thinning in the thick film may theoretically be observed. However, the interaction energy calculated for water may be invalid for strong electrolyte solutions (2.10). Also, the energy difference between thick film and bulk at equilibrium (at $\Pi = 0$) even in this ideal case is only of the order 10^{-4} m Jm^{-2}, which if manifested as a surface energy difference between bulk and thick film would have no practical significance.

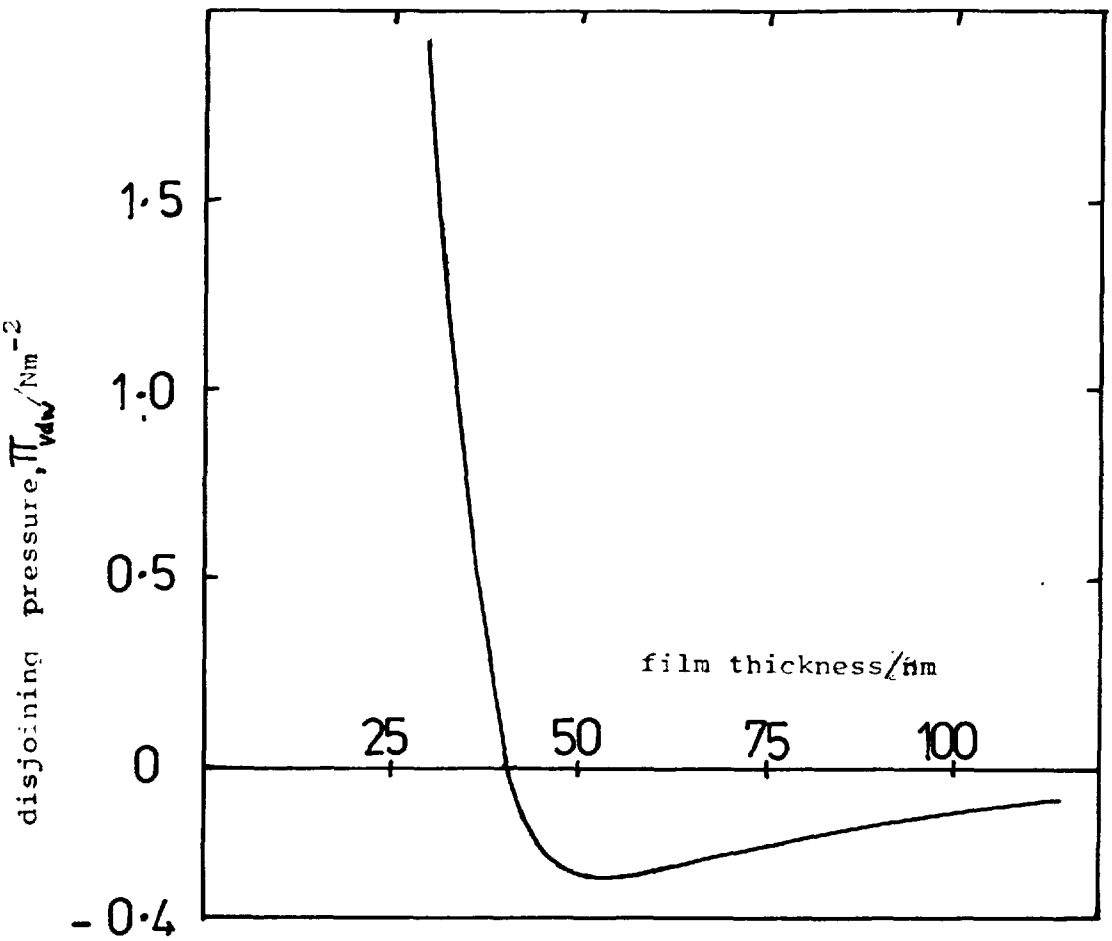

Figure 2.7. Disjoining pressure calculated using the Lifshitz equation and full spectral data for hypothetical water films on polystyrene.

Main Conclusions

1. The simple non-retarded calculation for the disjoining pressure due to van der Waals interaction is valid for water films on quartz up to 5 nm thickness, with a Hamaker constant $A = -1.12 \times 10^{-20}$ J.

2. The full spectral data - Kramers-Kronig method is a more fundamental method of calculating the van der Waals interaction. However, in the cases considered here good agreement was obtained with results calculated using spectral models.

3. Water films on crystalline quartz are subject to a strong positive disjoining pressure (with respect to van der Waals interaction) up to about 60 nm thickness. For thicker films Π_{vdw} becomes negative but very small.

This negative value of Π will normally be masked by a large positive contribution due to electric double layer forces and is unlikely to have any measurable effect.

CHAPTER 3

ELECTRIC DOUBLE-LAYER FORCES IN WATER FILMS ON QUARTZ SURFACES

Introduction

The existence of relatively thick, stable, water films on glass as a result of double-layer forces was first proposed by Langmuir in 1938 (3.1) as an explanation of the Jones-Ray effect (3.2). The anomalous minimum in the surface tension/concentration curve, for dilute aqueous electrolyte solutions measured by capillary rise, was explained by a decrease in thickness of wetting films with increase in electrolyte concentration. The effect of a thick wetting film is to reduce the capillary radius so that the solution rises to a greater height. The theory used by Langmuir to calculate the repulsive force in the wetting film (and hence its thickness) is discussed in the following section.

Derjaguin first calculated the repulsive forces between plates separated by electrolyte solution at constant surface potential (3.3) and together with Kusakov started experimental studies of those forces in relatively thick water films on glass (3.4). Significant experimental measurements on thick water films (> 30 nm) on vitreous silica have since been reported by Read and Kitchener (3.5), Blake and Kitchener (3.6), Callaghan and Baldry (3.7) and Schulze and Cichos (3.8). All these researchers measured positive disjoining pressures for thick films and reported that electric double-layer force theory at least approximately explained experimental results. The usual procedure has been to press a small bubble against an optical silica plate and to measure

the equilibrium thickness corresponding to a known disjoining pressure. Read and Kitchener (3.5) concluded, theoretically, that for films >30 nm the electrical double-layer force should be the predominant component of the total disjoining pressure.

Various methods for the calculation of the electrical double-layer force have been used for comparison with experimental measurements. These methods are discussed in the following section.

Methods of calculation of the electrical double-layer force in films

The potential distribution assumed for the case of a water film on silica is illustrated in Figure 3.1. From electrophoretic or streaming potential measurements the silica surface potential (at pH 7) may be estimated as approximately -150 mV (assuming that the zeta-potential may be equated to the surface potential (of the whole of the diffuse double-layer). This surface potential will be the approximate value for the case of very thick films ($d \gg \kappa^{-1}$, where κ^{-1} is the Debye-Huckel length). However, for thin films, ψ_o may be a function of d. If, however, it is assumed that ψ_o remains constant with changing thickness then as the film is compressed the charge density on the plate must diminish.

Measurement of the potential at the air/water interface is difficult and no definitive value has been established. Read and Kitchener suggested a value of -10 mV (3.5) and some very recent measurements of the zeta-potential of gas bubbles in distilled water suggest a potential of -15 mV (3.9) (although values ranging from -9 mV to -24 mV were measured). The negative potential is commonly assumed to be due to the preferential adsorption of hydroxyl ions (or desorption of hydrogen ions) and is therefore dependent on pH. Once again, however, the air/water potential may alter as a function

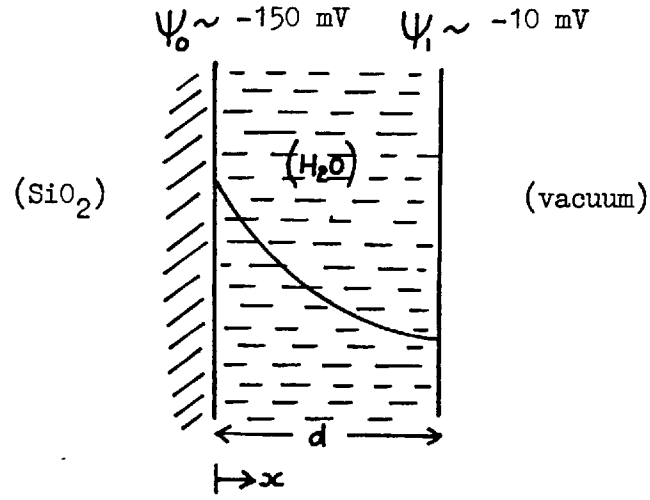

Figure 3.1. Potential distribution assumed for a water film on quartz

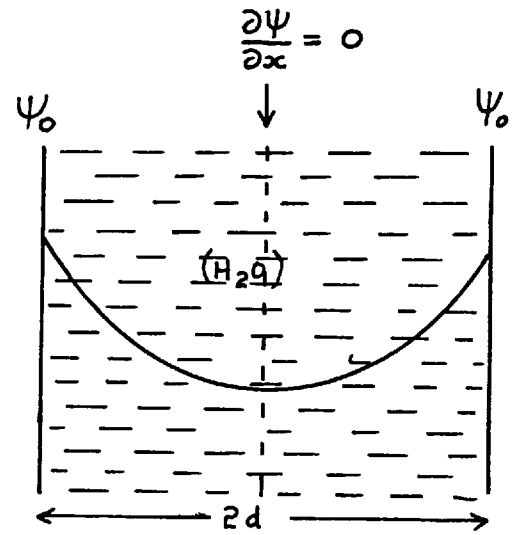

Figure 3.2. Potential distribution in thin film assumed to be identical to one side of that for symmetrical plates (Langmuir - Frumkin model)

of film thickness.

Methods used to calculate the double-layer force vary in the conditions selected for Ψ_o and Ψ_1. A reasonable method may be to assume constant charge (same sign but different magnitude) for the two interfaces and use heterocoagulation theory, as given, for example, by Bell and Peterson (3.10). However, no reasonable estimate of the charge densities can be made at present. Neither constant charge nor constant potential models are physically ideal; it really depends on the charging mechanism and the kinetics of approach of the surfaces and of redistribution of the potential determining ions. The truth probably lies somewhere between the two models.

Two different methods of calculation are examined initially here:

(a) Langmuir-type model and (b) Heterocoagulation - constant potential model.

(a) Langmuir-type model

This model was first considered by Langmuir (3.1) and Frumkin (1.8) and later developed by Jones and Frizzell (3.11). The principle of this method is illustrated in Figure 3.2. It is assumed that at the air/water interface $(\partial\Psi/\partial x)_{x=d} = 0$, which implies that the charge at this interface is zero (i.e. no electric field passes through the interface). Thus the force in the thin film (arising from the potential distribution) is identical to that between two parallel plates (both with potential Ψ_o) separated by twice the thickness of the film.

Assuming that Ψ_o is known (or can be estimated) the double-layer force can be easily obtained by using the extensive tables of Devereux and de Bruyn (3.12). Figure 3.3 gives the double-layer force as a function of film thickness, calculated with these tables.

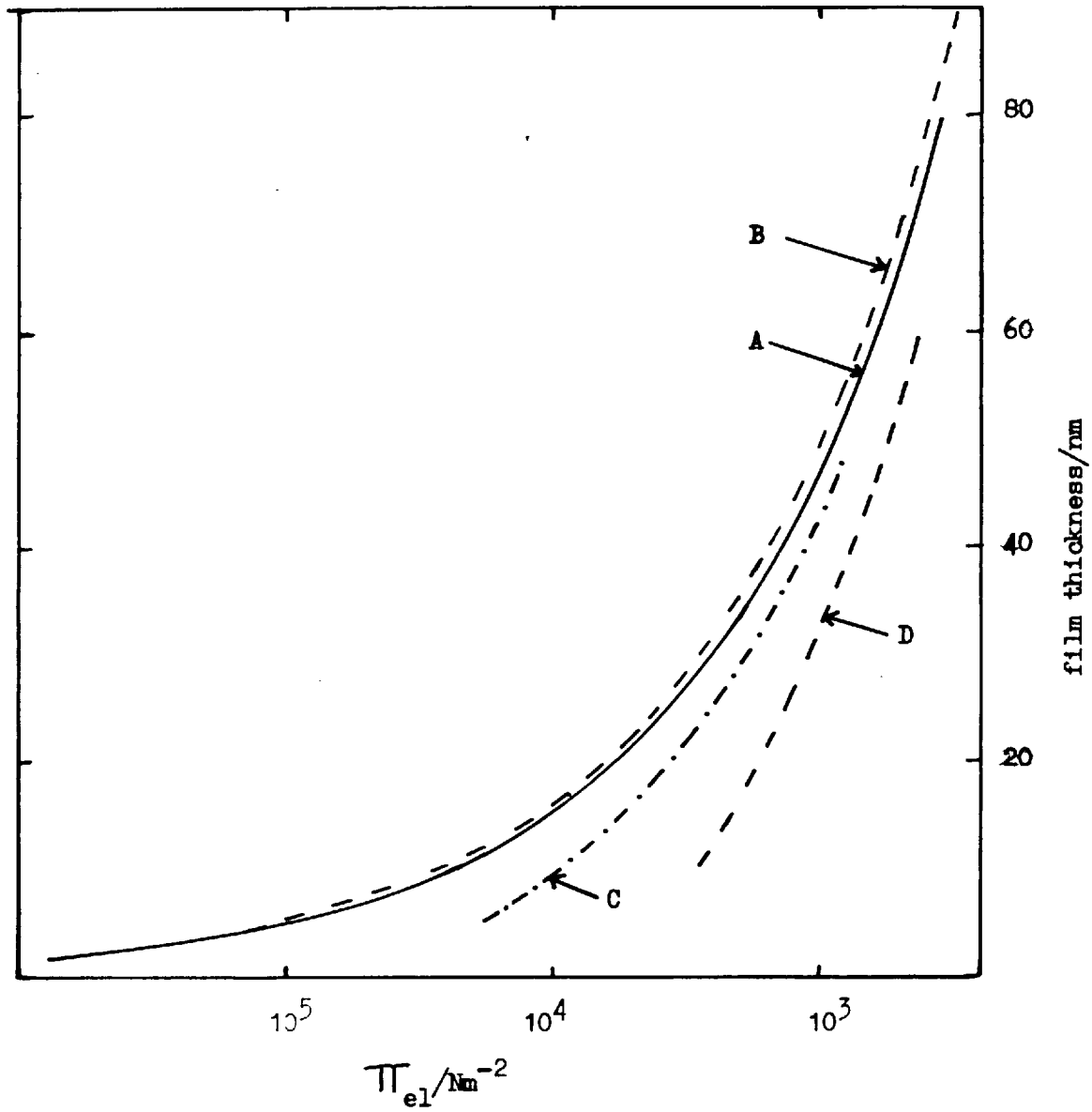

Fig. 3.3. Calculated disjoining pressure from electric double-layer interaction for water films on quartz

A - values calculated using the Langmuir equation

B - values calculated using Devereux and de Bruyn tables for a surface potential of 520 mV and film of conductivity water

C - as for previous case but with 260 mV potential

D - as for previous case but with 207 mV potential

Using the Poisson and Boltzmann equations, Langmuir (3.1) derived a limiting equation for the case of a film of very dilute solution of symmetrical electrolyte on a plate with a high surface potential, such that everywhere between the plates the potential, $\psi \gg {}^{kT}/_{e}$:

$$\Pi_{el} = \frac{\pi \epsilon}{8} \left(\frac{RT}{eZ}\right)^2 \frac{1}{d^2} \qquad 3.1$$

where Π_{el} = disjoining pressure due to the double-layer

ϵ = dielectric constant of water

R = Boltzmann constant

e = electron charge

Z = valency of electrolyte ions

This equation is independent of both surface potential and electrolyte concentration. According to Derjaguin (1.3) equation 3.1 is in good agreement with experimental measurements (3.5, 3.6, 3.8) of relatively thick water films on quartz (i.e. 50 to 240 nm) and may be used for thin films also. The disjoining pressure (Π_{el}) as a function of film thickness calculated from equation 3.1 is plotted for comparison in Figure 3.3.

The double-layer force calculated for a water film on quartz using this Langmuir-Frumkin method is always repulsive (i.e. Π_{el} is always +ve.) From Figure 3.3. it is also apparent that equation 3.1 agrees with the interaction calculated (using the Devereux and de Bruyn tables) for symmetrical plates with equal potentials of about 400 mV, for a film of conductivity water (i.e. corresponding to 5×10^{-7} N-KCl (3.13)).

The important assumptions in the Langmuir-Frumkin model are that the potential at the air/water interface approaches that at the solid/water interface as the film thickness decreases and that this interface carries zero charge. However, experimental evidence suggests that the air/water interface is weakly negatively charged (3.9). Read and Kitchener (3.5) estimated, by superimposition of the air/water double layer on the Langmuir-Frumkin model, that film thicknesses would be increased by about 25% for an assumed -10 mV potential at the air/water interface.

(b) Heterocoagulation-constant potential model

If it is assumed that ψ_o =-150 mV and ψ_1 = -10 mV and that the potentials remain constant with respect to variation of film thickness, then the tables of Devereux and de Bruyn can be used to calculate the double-layer force. Derjaguin was first to calculate the interaction between surfaces of dissimilar potentials (3.14) i.e. heterocoagulation theory.

For the potentials given, the calculated force in a film of conductivity water becomes attractive for films thinner than about twice the Debye-Huckel length (about 450 nm for conductivity water (3.13)). Such films would therefore spontaneously collapse below a critical (relatively large) film thickness.

Schulze and Cichos (3.8) have also calculated the affect of dissimilarity of potentials and ionic strengths using heterocoagulation theory. They found that as the difference between the interacting potentials (of same sign) becomes greater the interaction becomes less repulsive and eventually becomes attractive. The effect of increasing the ionic strength of the film is to reduce the value of the critical thickness for the onset of collapse.

This theoretical attraction arises because the potential at the air/water interface would be expected to approach the value of ψ_o as the film thickness decreases, if there were no charge at the interface. However, since a small constant negative potential is assumed in the calculation, this must be maintained by the build-up of an excess positive charge at the interface (3.15) and of course, a build-up of positive charge causes an attractive force between the surfaces (because their diffuse double layers are of opposite sign and partially cancel one another).

A constant potential model might be plausible for the interface of an amphoteric oxide with water; but there is no firm evidence for the air/water interface adopting a positive sign.

Discussion

From previously reported experimental observations it is apparent that for relatively thick water films on vitreous silica (namely 50 to 240 nm) the disjoining pressure is positive (i.e. the force between the two interfaces is repulsive). It appears that the Langmuir-Frumkin approach gives a better explanation of the interaction than does heterocoagulation theory with assumed constant potentials. The assumption of a constant potential (with respect to film thickness) at the air/water interface thus appears to be invalid for this case.

Several workers have reported that the film thicknesses measured (in the range 20 to 100 nm) are substantially thicker than those predicted using the Langmuir-Frumkin method (3.5, 3.7). However, as a convenient and reasonable estimation this method was used here for comparison with experimentally measured values.

A more physically realistic model would be one in which the

interfaces are assumed to be charged with ions which are in equilibrium with the film and hence the degree of ionisation changes with film thickness. This calculation, however, would be mathematically more complex (3.16). A suggested procedure for deriving the electrical double-layer force in such a thin film is given in Appendix 3.1.

Another problem associated with double-layer forces in thin films is the lack, at present, of an appreciation of the possible difference between the interaction for the case of a bubble pressed against a plate in a dilute solution and of a pure water film condensed onto a plate (as in the present experiments). In the former case there is a bulk reservoir of electrolyte, whereas in the latter there is equilibrium only through the vapour phase.

CHAPTER 4

THE THEORY OF ELLIPSOMETRY : A SUMMARY WITH SPECIAL REFERENCE TO THE MEASUREMENT OF WATER FILMS ON QUARTZ

Introduction

The term ellipsometry refers to the measurement of the change in polarisation of monochromatic light reflected from a surface with or without a film. Plane polarised light is a particular case of the more general elliptically polarised light. Plane polarised light may be considered to consist of two orthogonal components each at 45° to the plane of polarisation (see Figure 4.1). Thus the plane polarised wave (P) is equivalent to two orthogonal equal amplitude components (S_1 and S_2). When these two components are out of phase the resultant electric vector traces out an ellipse as viewed from the direction of propogation. The degree of phase difference (Δ) between the two components determines the type of ellipse. The parameter Ψ (the azimuth) defines the relative magnitude of the electric vectors of the two components. The types of elliptical polarisation corresponding to values of Δ and Ψ are given in Figure 4.2. Thus two parameters are required to define the state of polarisation. The change in these two parameters during reflection from a surface is measured by means of an ellipsometer (see Chapter 7 for ellipsometer details).

Azzam and Bashara have recently published a very thorough review of ellipsometry and polarised light (4.1).

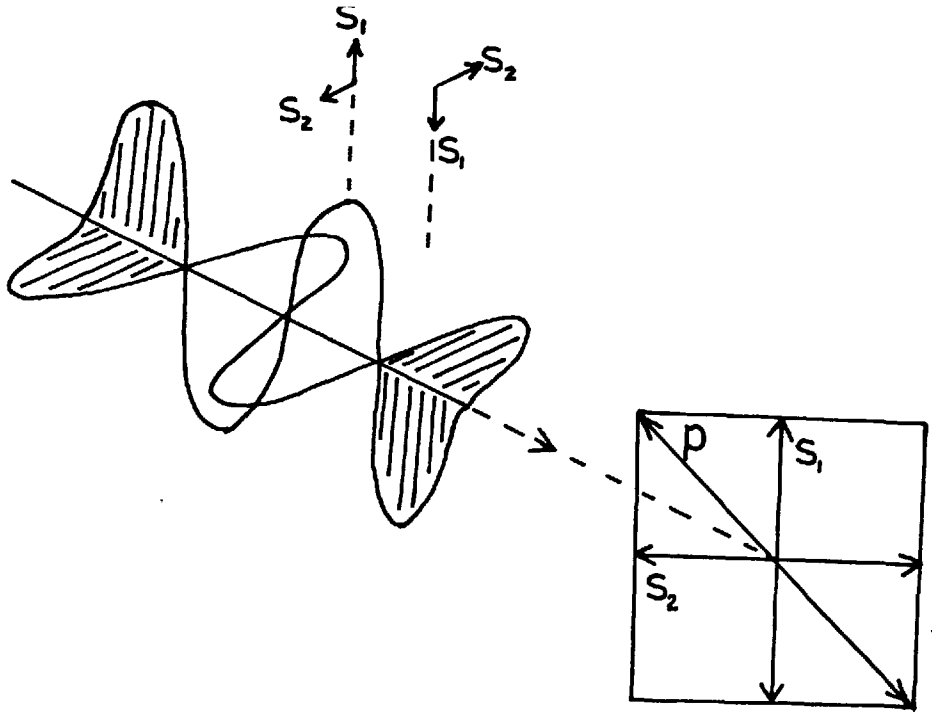

Figure 4.1. Illustration of plane polarised light (electric vector)

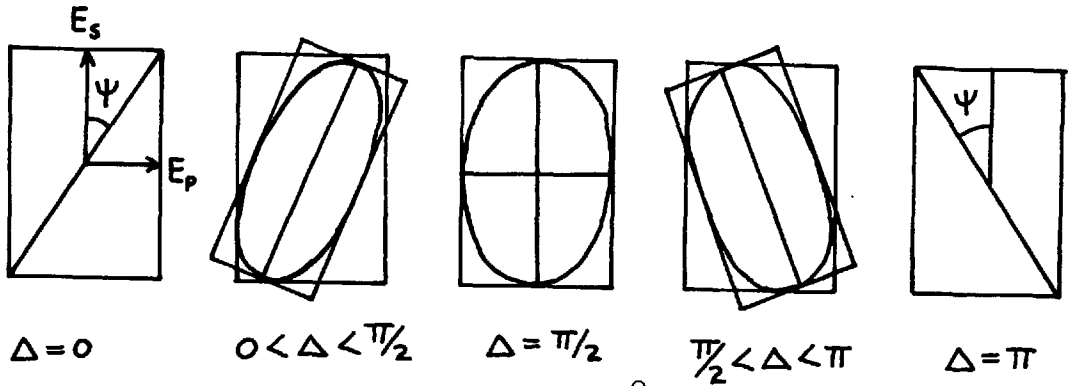

(if $\psi = 45^{\circ}$ is circular)

Figure 4.2. Depencence of elliptically polarised light on Δ and ψ.

General theory of ellipsometry

For convenience the incident and reflected light (from the substrate) is decomposed into two components. The "s" component has its electric vector normal to the plane of incidence (i.e. parallel to the plane of the reflecting surface), the "p" component corresponds to that parallel to the plane of incidence. In the theoretical calculations it is usual to assume that the s and p components are equal for the incident beam ($\tan \Psi = 1$) and that they are in phase ($\Delta = 0$).

The general case considered here is shown in Figure 4.3.

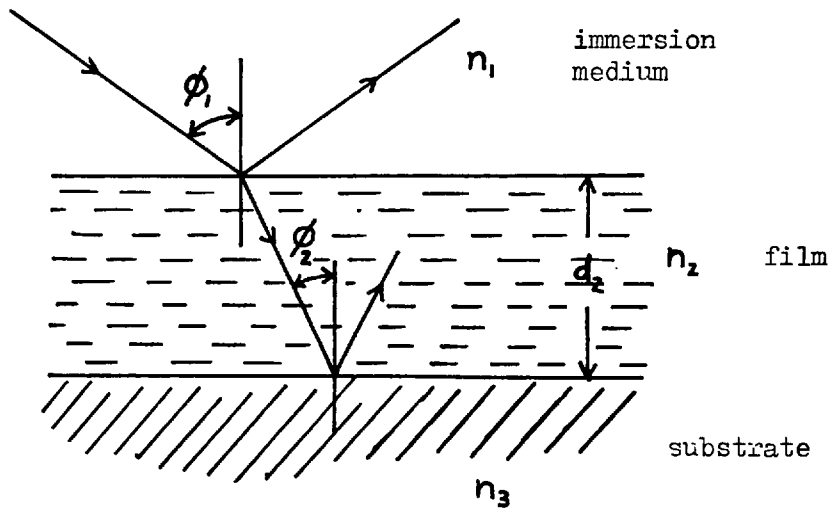

Figure 4.3. Parallel film on smooth substrate.

The parallel and normal reflection coefficients for the light incident at the n_1/n_2 boundary are:

$$r_{12}^{p} = \frac{n_2 \cos\phi_1 - n_1 \cos\phi_2}{n_2 \cos\phi_1 + n_1 \cos\phi_2} \qquad 4.1$$

$$r_{12}^{s} = \frac{n_1 \cos\phi_1 - n_2 \cos\phi_2}{n_1 \cos\phi_1 + n_2 \cos\phi_2} \qquad 4.2$$

These are the Fresnel equations (4.2) for the boundary.

For absorbing film or substrate the refractive indices are given by complex numbers. Snells law is still valid in such cases (4.3):

$$n_c = n - ik$$

$$n_o \sin\phi = n_c \sin\phi_c' \qquad 4.3$$

Thus the angle of refraction becomes a complex number, as do the reflection coefficients.

Similar reflection coefficients are obtained for the n_2/n_3 boundary. The total coefficients are given by the Drude equations (4.2):

$$R^{p} = \frac{r_{12}^{p} + r_{23}^{p} \exp. D}{1 + r_{12}^{s} r_{23}^{s} \exp. D} \qquad 4.4$$

$$R^{s} = \frac{r_{12}^{s} + r_{23}^{s} \exp. D}{1 + r_{12}^{s} r_{23}^{s} \exp. D} \qquad 4.5$$

where $D = -4\pi i n_2 \cos\phi_2 d_2/\lambda$ 4.6

and λ = wavelength.

The ratio of these total reflection coefficients is defined as ρ :

$$\rho = R^p/R^s \qquad 4.7$$

ρ may be expressed in terms of the azimuth angle (Ψ) and the relative phase shift (Δ):

$$\rho = (\tan \Psi). \exp (i \Delta) \qquad 4.8$$

The value of ρ (i.e. Δ and Ψ) is determined from ellipsometric measurements. Since n_1, n_3, ϕ_1 and λ are known, it should be possible, using the equations given, to calculate both the refractive index and thickness of the film.

Methods of solution and results

The use of computers has made ellipsometric calculations easier and hence the technique of ellipsometry has recently become more popular.

A computer program was written to calculate Δ and Ψ as a function of d_2 for assumed values of n_1, n_2, n_3, ϕ_1, and λ , using the equations already given. For the quartz/water film system and helium-neon laser light source, the variation of Δ and Ψ with film thickness was calculated for a selected angle of incidence near the Brewster angle ($\phi_B = \tan^{-1} n_3$) for crystalline quartz (see later for discussion on choice of ϕ_1).

The results calculated are shown in Figure 4.4. The effect of variation of the refractive index of the film is also shown. From these results it is apparent that for measurements of accuracy

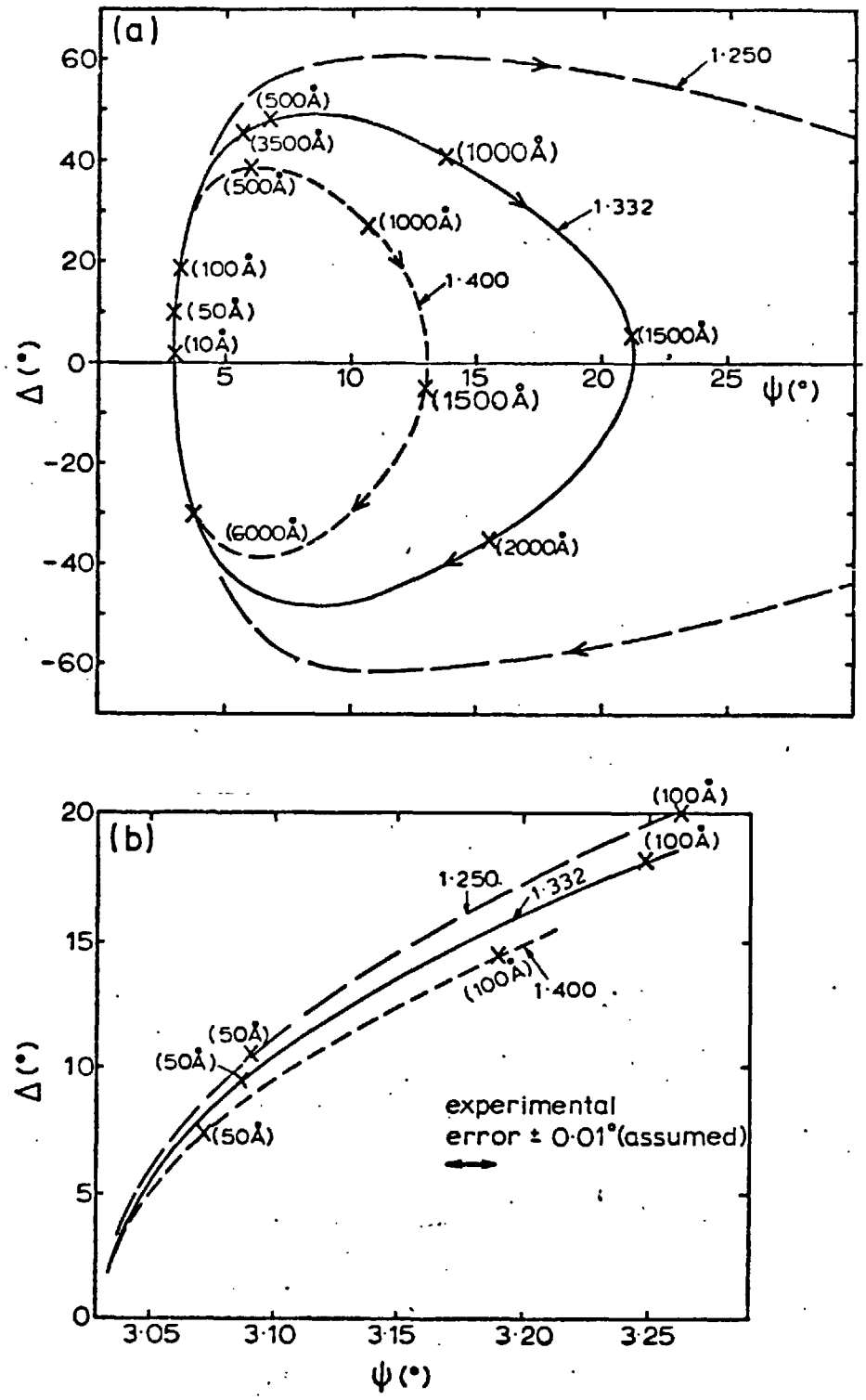

Figure 4.4. Theoretically calculated variation of phase change (Δ) and azimuth (Ψ) with film thickness

$n_1 = 1.0$; $n_2 = 1.250$, 1.332, 1.400; $n_3 = 1.543$ (quartz); $\phi_1 = 59.3^{\circ}$ and $\lambda = 632.8$ nm

$0.1 - 0.2^{o}$ (for Δ and Ψ, typical error obtained here, see Chapter 7) the thickness of a 5 nm water film of assumed refractive index can be determined to about $\pm$ 0.2 nm. However, for films of less than about 20 nm the error in Ψ prevents determination of the refractive index of the water film. This observation has been reported also by Hall (1.11). Therefore the refractive index of very thin water films was assumed to be that of bulk water.

The effect of the value of ϕ_1 (angle of incidence) on Δ and Ψ variation with film thickness is shown in Figure 4.5. The sensitivity of Δ to film thickness increases as $\phi_1 \rightarrow \phi_B$. However, although theoretically ϕ_B ought to be the best choice for angle of incidence it has been previously found that at this point experimental uncertainty increases. A value of ϕ_1 $2 - 3^{o}$ above ϕ_B has therefore been recommended by Vedam and Malin (4.4). From Figure 4.5. it is apparent that variation in ϕ_1 alters the value of Ψ for a bare substrate ($d_2 = 0$). Thus, the measured value of Ψ accurately defines the angle of incidence.

For thin water films on quartz (i.e. up to about 10 nm) the phase change is very nearly a linear function of the film thickness (see Table 4.1). As the thickness of the film becomes large (i.e. $>$ 300 nm) the parameters Δ and Ψ are repeated (Figure 4.4a). The behaviour shown in Figure 4.4a is typical for transparent dielectric films and substrates. From Figure 4.4 it is apparent that the larger the difference between the refractive indices of the film and the substrate the greater is the change in Δ for a given film thickness. Thus water films on crystalline quartz ($n_3 = 1.543$) produce a larger phase change than on vitreous silica ($n_3 = 1.46$).

The curves calculated for Δ and Ψ (Figure 4.4) give the thickness of a water film (of assumed index) on quartz directly.

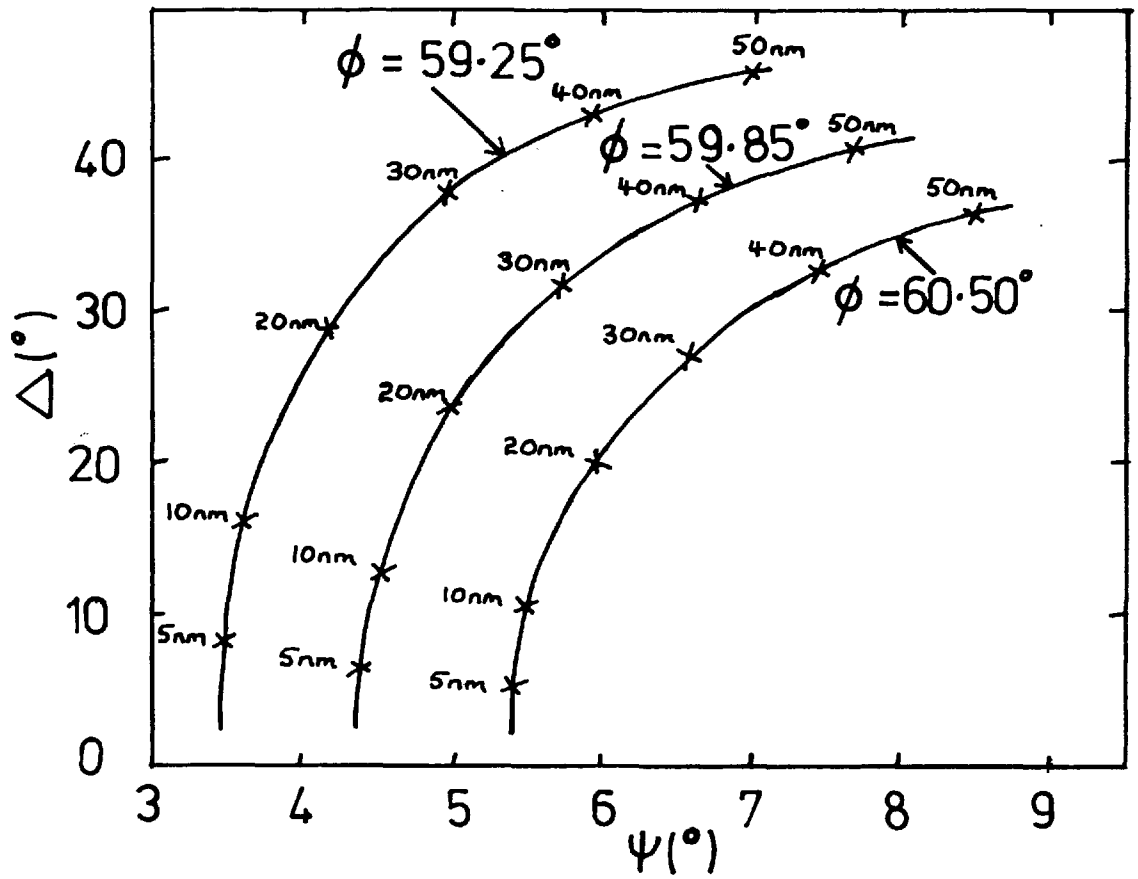

Figure 4.5. Variation of Δ and Ψ with water film thickness for different angles of incidence (ϕ_1) on quartz

(n_2 1.332, n_3 1.543, λ = 632.8 nm)

Table 4.1. Calculated values of Δ and Ψ for water films (1.33) on crystalline quartz (1.543)

water film thickness (nm)	phase change (Δ°)	azimuth (Ψ°)
1	1.33	4.36
5	6.58	4.40
10	12.87	4.53
20	23.74	5.00
30	31.81	5.73
40	37.27	6.64
50	40.63	7.69

($\phi_1 = 59.85^{\circ}$ and $\lambda = 632.8$ nm)

Only these curves are therefore necessary to convert measured Δ and Ψ values into film thicknesses. Experimentally measured values of Δ and Ψ for films of varying thickness must fall on this curve if the assumptions made about the system are correct. This method was found easier to use than calculating thicknesses from each measured set of values of Δ and Ψ .

Theoretical analysis of the effect of surface roughness on the measurement of thin films by ellipsometry

Introduction

The ellipsometric theory outlined in the previous section applies to the ideal case of an isotropic film on a smooth substrate surface. However, real surfaces are not perfectly smooth and surface roughness of the substrate may cause errors in thin film measurement. Since surface roughness is often on the micro-scale (i.e. projections $< \lambda$), optical effects appear as averaged characteristics. Fenstermaker and McCracken (4.5) used a volume average method (see later) to show the effect of surface roughness (up to 30 nm) on the apparent refractive index of glass. The refractive index theoretically calculated in this way was complex i.e. the rough surface substrate should appear to be (by ellipsometry) not completely transparent.

Archer (4.6) used a simple surface roughness model and estimated the effect of this roughness on thin film measurement, again using a volume average method for carbon tetrachloride films on silicon. Archer reported that because of surface roughness the film thickness as measured could be less than the true value by more than 50%. More recently Loschke and Kuhn (4.7) used the Fenstermaker-McCrackin roughness model to explain discrepancies found in film thickness measurements on GaAs surfaces.

Errors in thin film measurement due to substrate roughness must obviously depend on the degree of roughness and on the refractive indices of the media, and may also depend on the type of surface roughness. In this work the effect of roughness of quartz surfaces with respect to the ellipsometric measurement of thin water films was analysed by a theoretical model.

Theoretical model and calculations

Fenstermaker and McCrackin (4.5) used the Garnett theory (4.8, 4.9, 4.10) to calculate refractive indices for horizontal sections of a rough surface. This method assumes the validity of the Clausius-Mossotti relation in order to calculate polarisabilities of the components in the horizontal section, which are then volume-averaged to obtain the mean refractive index of the section. A series of layers of different refractive indices (n_e) are obtained (see Figure 4.6). The refractive index and film thickness that is ellipsometrically equivalent to these combined layers was calculated by using the equations of McCrackin and Colson (4.11):

$$N_{cal.} = \left[\int_0^t n_e (n_e - n_1)\, dt \right] \left[\int_0^t (n_e - n_1)\, dt \right]^{-1} \qquad 4.9$$

$$T_{cal.} = \left[\int_0^t (n_e - n_1)\, dt \right] (N_{cal.} - n_1)^{-1} \qquad 4.10$$

N_{cal} is the average refractive index and T_{cal} is the effective thickness.

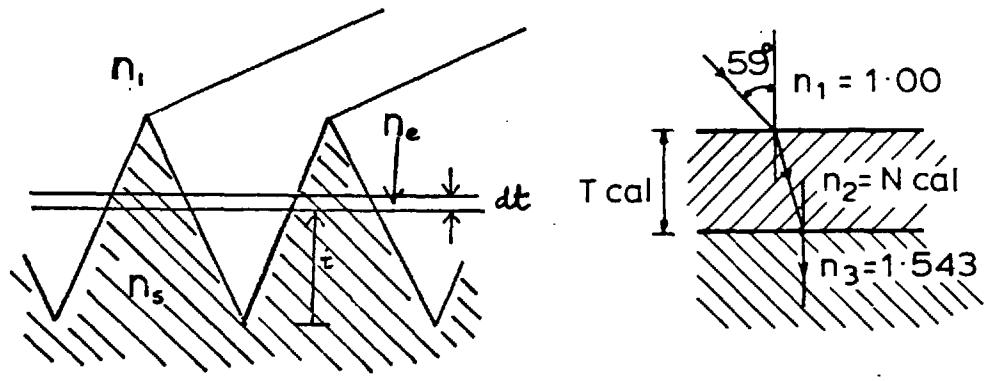

Figure 4.6. Triangular ridge model rough surface and ellipsometrically equivalent film on quartz.

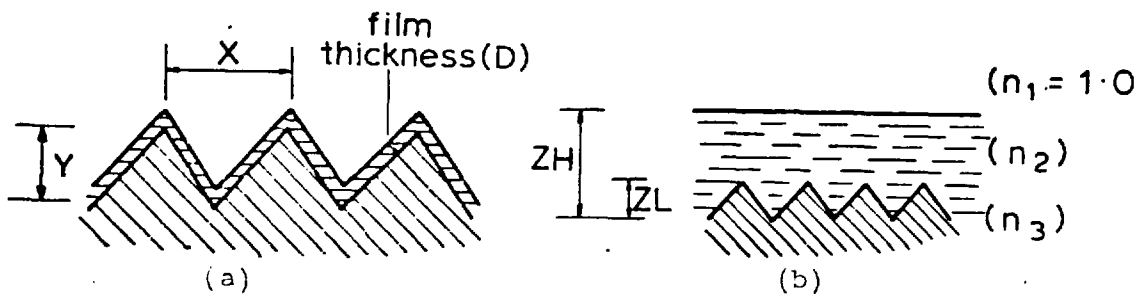

Figure 4.7. Triangular ridge model rough surface with (a) contoured film and (b) flat surface film (i.e. low substrate surface roughness)

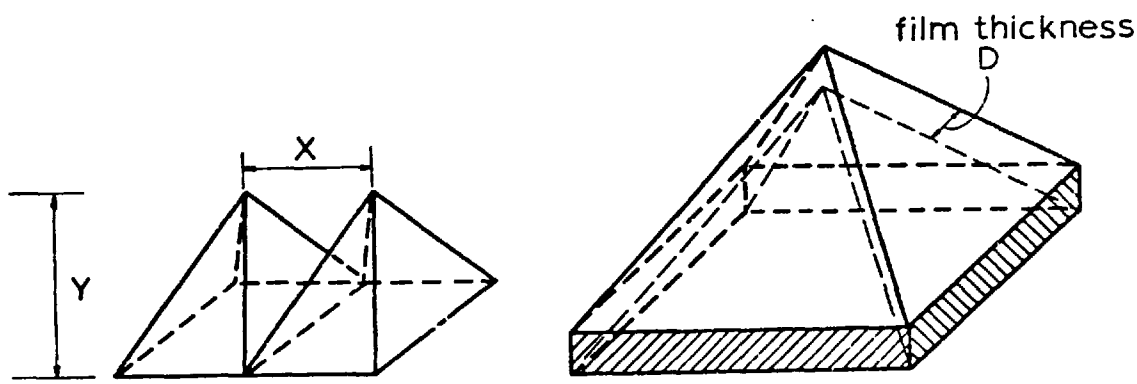

Figure 4.8. Square-based pyramid model rough surface, with and without film.

Thus Fenstermaker and McCrackin were able to calculate the thickness and refractive index of a film which was ellipsometrically equivalent (with respect to observed phase change (Δ) and azimuth (Ψ)) to various rough model surfaces on several substrates. The Δ and Ψ values calculated could then be used to calculate an apparent refractive index of the substrate, assuming its surface were perfectly smooth. This procedure was followed for the quartz ($n_3 = 1.543$) substrates considered here.

All the ellipsometric calculations were carried out by computer.

If a water film ($n_2 = 1.332$) is placed on a rough surface and the form of the surface and film is assumed (i.e. contoured or flat surface, Figure 4.7) it is again possible to calculate the thickness and refractive index of an ideal smooth film which is ellipsometrically equivalent to that model. From this equivalent film system the values Δ and Ψ which would be observed may be calculated. This method assumes that the Fenstermaker-McCrackin treatment may be applied to a three-phase system.

Using this method the values of Δ and Ψ which would be measured both on a bare quartz surface and on a surface with a water film could be calculated

Two different methods were used for analysing (in terms of the thickness of the film) these Δ and Ψ values which would be experimentally measured but which were calculated here:

(a) For thin water films (< 20 nm) on quartz, it has been shown (Figure 4.4b) that for measured Δ and Ψ accuracy of $\pm 0.01^{\circ}$ (optimistic error limit) ellipsometric measurements, at a single angle of incidence, do not accurately define the refractive index of a film as well as its thickness. Thus we must assume a refractive

index in order to calculate the corresponding nominal film thickness. From Table 4.2 it is apparent that rough surfaces on quartz are ellipsometrically equivalent to films of refractive index (N_{cal} = 1.35) near to that of water. Hence, for convenience in this method, the rough surface and rough surface with water film were assumed to be equivalent to different thicknesses of films of refractive index of water, 1.332. The actual measured water film thickness on a rough substrate is then, simply, the difference betwee these two thicknesses.

(b) The values of Δ and Ψ measured for a rough surface (which are theoretically calculated here) are different from those expected for a smooth surface. If the substrate refractive index is calculated from these values (supposing the substrate to be smooth) the refractive index is found to be apparently complex. In this second method the substrate surface was assumed to be smooth and the substrate to possess this complex refractive index. The thickness of the transparent film of refractive index 1.332 present on this absorbing substrate corresponding to the measured Δ and Ψ values (theoretically calculated here) was then calculated. The results from these two methods are compared.

An iterative computer solution was written to calculate the thicknesses of the films in both methods. Two solutions were obtained in each case - one each from equating real and imaginary parts of the equations. The valid solution was proved to be that obtained from the imaginary equation since only this value gave the original starting values on re-calculation.

Table 4.2 Calculation of apparent thickness of film of 1.332 equivalent to triangular ridge rough surface of quartz.

Y(Å)	N_{cal}	T_{cal} (Å)	tan Ψ. exp (iΔ)	$\Delta°$	$\Psi°$	D_i (Å)
5	1.3512	3.655	0.05298+i0.0006105	0.66	3.03	3.45
10	"	7.3102	0.05299+i0.001221	1.32	3.03	6.93
15	"	10.965	0.05299+i0.001832	1.98	3.035	10.40
20	"	14.620	0.05300+i0.002442	2.64	3.04	13.87
25	"	18.276	0.05301+i0.003052	3.295	3.04	17.33
50	"	36.55	0.05312+i0.006104	6.556	3.06	34.5
100	"	73.10	0.05355+i0.01238	13.02	3.15	69.4
200	"	146.2	0.05520+i0.02439	23.84	3.45	138.5
300	"	219.3	0.05802+i0.03653	32.20	3.92	207.4
500	"	365.5	0.06727+i0.06056	41.99	5.17	343.9

λ = 6328.0 Å; ϕ_1 = 59.0°; n_3 = 1.543.

The models used here for the rough surfaces are shown in Figures 4.6, 4.7 and 4.8. In order to calculate the film equivalent (i.e. N_{cal} and T_{cal} from equations 4.9 and 4.10) to a rough surface, using the Fenstermaker-McCrackin method, the averaged horizontal layer indices, n_e are required as a function of vertical height, t. For triangular ridge surfaces n_e is a direct function of t, which is easily integrated; hence equations 4.9 and 4.10 were solved directly. However, for square-based pyramid models this was not the case and n_e was therefore calculated for 0.1 nm intervals and the summation, for N_{cal} and T_{cal}, was carried out numerically.

The average horizontal layer indices (n_e) were calculated for a 3-phase system using the following equation, which is directly analogous to that used by Fenstermaker-McCrackin:

$$\frac{n_e^2 - 1}{n_e^2 + 2} = q_1 \frac{N_1^2 - 1}{N_1^2 + 2} + q_2 \frac{N_2^2 - 1}{N_2^2 + 2} + q_3 \frac{N_3^2 - 1}{N_3^2 + 2} \qquad 4.11$$

where n_e is calculated from the volume fractions (q_n) and refractive indices (N_n) of the three components in a horizontal layer of thickness dt in the model surface/film system. Equation 4.11 is essentially a volume average of polarisabilities.

Calculated values (from eqn. 4.11) for n_e as a function of height (t) are plotted in Figure 4.9 for the case of a contoured water film on a square-based pyramid rough surface.

Results and discussion

Table 4.2 gives the results of the Fenstermaker-McCrackin method used to calculate Δ and Ψ from the dimensions of triangular-

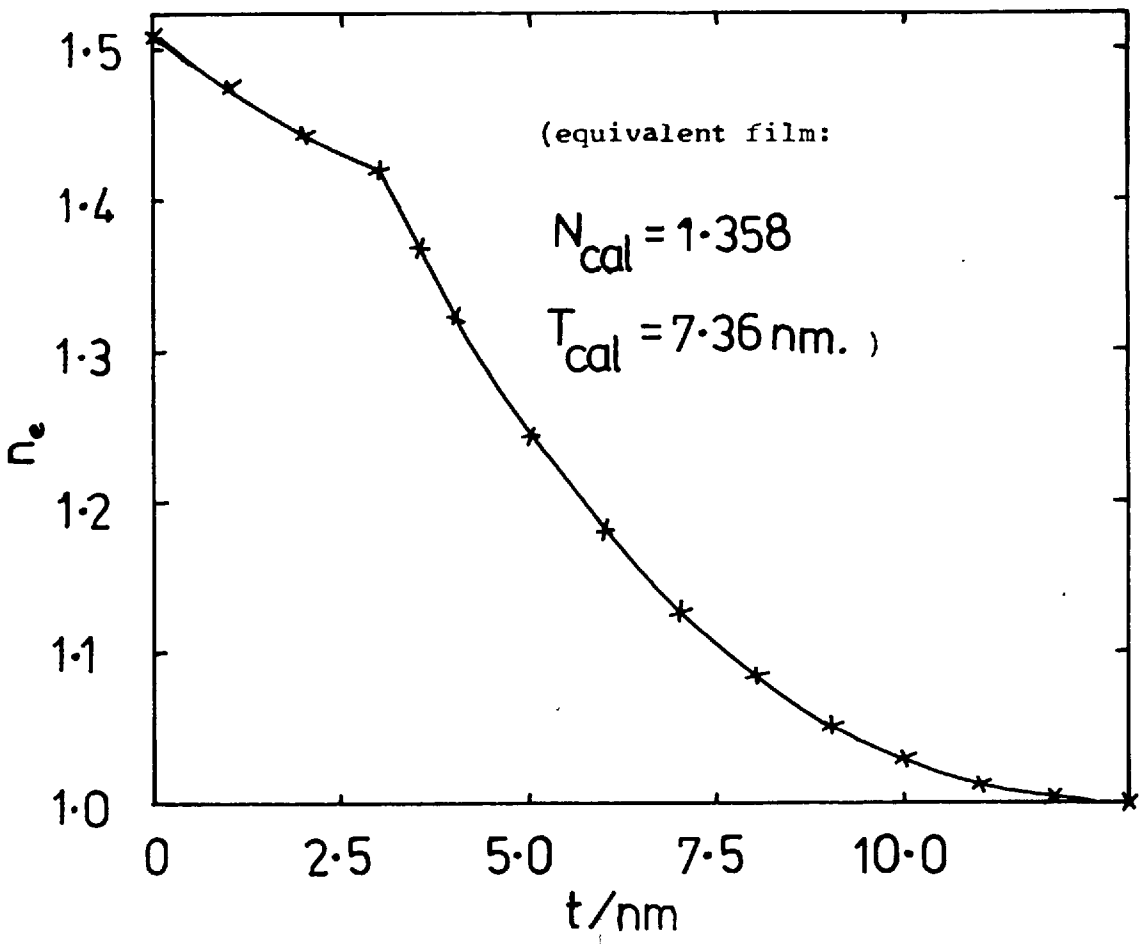

Figure 4.9. Layer average refractive index (n_e) as a function of height for water film contoured on square-based pyramid rough surface (where Y = 10 nm, X = 30 nm, D = 2.5 nm) (in Fig. 4.8), n_3 = 1.51, n_2 = 1.332 and n_1 = 1.00)

ridge model rough surfaces. D_i is the thickness of a film of refractive index 1.332 (on a 1.543 smooth substrate) which would give the same Δ and ψ values. It may be seen, as expected from Figure 4.4b, that for Δ and ψ to $\pm 0.01^{\circ}$ a film of a particular index and thickness is ellipsometrically equivalent to a thinner film of lower index. It is of interest to note that N_{cal} and Tcal values in Table 4.2 are independent of the X dimension (see Figure 4.7), assuming that the latter is small compared with the wavelength of the incident light.

Tables 4.3, 4 and 5 similarly give calculated $\tan\Delta . \exp(i\psi)$ values (from which Δ and ψ can be easily calculated) and the corresponding 1.332 index film thickness to which they are equivalent. By subtracting the latter value from that given in Table 4.2, the values for water film thicknesses which would be ellipsometrically measured on these rough surfaces (using this method) are obtained; they are given, with approximate percentage errors, in Table 4.7.

The complex substrate refractive indices corresponding to different degrees of triangular ridge rough surfaces were calculated and are given in Table 4.6. The thicknesses of water films on these (apparently absorbing) smooth surfaces corresponding to the values Δ and ψ which would be measured, are given in parentheses in Table 4.7 for comparison.

From Table 4.7 it is apparent that the two analyses of the Δ and ψ values, which would be measured on model rough surfaces, with and without films, give almost identical errors. These errors are large if the surface roughness is comparable with the water film thickness. By comparison, in Table 4.7, between square-based pyramid and triangular—ridge surfaces it may also be observed that the <u>form</u> of the surface roughness is relevant although not as

Table 4.3 Results of calculation for 1.332 film thickness for rough triangular ridge substrate with contoured film.

D(Å)	Y(Å)	X(Å)	T_{cal}(Å)	N_{cal}	tan ψ. exp (iΔ)	D_i(Å)
25	50	500	54.82	1.3945	0.05330+0.007724i	43.6
25	100	500	90.01	1.3895	0.05385+0.01298i	73.7
25	200	500	164.55	1.3802	0.05591+0.02465i	140.0
25	300	500	241.00	1.3765	0.05929+0.03651i	207.25
25	500	500	395.91	1.3738	0.07033+0.05976i	339.40
25	50	2000	54.41	1.3945	0.05330+0.007665i	43.6

$\lambda = 632.8$ nm., $\phi_1 = 59.0°$

Table 4.4 Results of calculation for 1.330 film thickness for square-based pyramid model with and without the contoured water film. ($n_3 = 1.51$ in this case, otherwise same condit.)

D(Å)	Y(Å)	X(Å)	T_{cal}(Å)	N_{cal}	tan ψ. exp (iΔ)	D_i (Å)
0	100	300	53.84	1.298	0.06895+i0.009216	58.5
25	100	300	73.61	1.358	0.06924+i0.01041	66.3

$\lambda = 632.8$ nm, $\phi_1 = 59.0°$

Table 4.5 Results of calculation for 1.332 film thickness for small roughness squared-based pyramid.

ZL(Å)	ZH(Å)	T_{cal}(Å)	N_{cal}	$\tan\psi . \exp(i\Delta)$	D_i(Å)
5	100	99.4	1.339	0.05397+i0.01718	97.6
10	100	98.9	1.346	0.05398+i0.01676	95.6
25	100	97.9	1.346	0.05400+i0.01554	88.2
30	100	97.5	1.372	0.05400+i0.01514	86.0
50	100	97.0	1.395	0.05400+i0.01361	77.3
70	100	97.14	1.416	0.05397+i0.01215	69.0
90	100	97.68	1.435	0.05393+i0.01074	60.9

$\lambda = 632.8nm.,\ \phi_1 = 59.0^\circ$

Table 4.6 Results of calculation of complex substrate refractive indices (N_s^*) ellipsometrically equivalent to surface rough triangular-ridge quartz.

Y(Å)	N_s^*
5	1.5430-i0.001306
10	1.5430-i0.002613
15	1.5430-i0.003920
20	1.5429-i0.005225
25	1.5429-i0.006530
50	1.5426-i0.01306
100	1.5414-i0.02645
200	1.5367-i0.05186
300	1.5287-i0.07707
500	1.5035-i0.1245

Table 4.7 Comparison of apparent film thickness deduced by ellipsometry with actual film thickness (Compiled from Tables 4.2 - 4.6)

Type of surface and film	Peak-peak height (A)	Real-film thickness (A)	Measured value (Å)	± % Error
Low roughness	5	97.5	94.1	- 3
triangular ridge	10	95	88.3 (88.2)	- 7
substrate	25	87.5	70.9	-19
	50	75	42.8 (42.6)	-43
High roughness	50	25	9.1 (9.2)	-64
triangular ridge	100	25	4.3 (3.5)	-84
substrate with contoured film	500	25	-ve	-
Square-based pyramid substrate with contoured film.	100	25	7.8	-69

important as the peak-to-peak height. These results, of course, apply only to thin water films on quartz or glass.

Thus it appears that for accurate measurement of thin water films on quartz very smooth surfaces are required. These surfaces must be smooth down to 5 nm. The production of such smooth surfaces of quartz has been investigated in Chapter 5.

The effect of roughness (e.g from different degrees of etching) on the ellipsometric measurement of quartz surfaces has not previously been properly investigated (4.2). Thus no thorough test of the Fenstermaker-McCrakin treatment for glass-like surfaces has been reported. A comparison using electron microscopy and ellipsometric measurement of differently etched quartz plates has been carried out in this work and is discussed in Chapter 7.

B EXPERIMENTAL SECTION

CHAPTER 5

CHARACTERISATION OF CRYSTALLINE QUARTZ SURFACES

Introduction

Perhaps the best method of producing a crystalline, clean and well-defined surface is cleavage of a pure crystal under clean conditions. Mica is a mineral amenable to this method of preparation. However, this is not possible for crystalline quartz, because it has no strong cleavage planes. Therefore, for this present work quartz plates were cut, polished and mildly etched.

Both synthetic crystalline quartz (supplied by Messrs. Gooch and Housego Ltd.) and natural quartz (Brazilian) were used in this work. The quartz specimens were z-cut plates i.e. cut with the surface perpendicular to the optical axis. This plane was chosen because the important ultra-violet data used in the van der Waals force calculations were for z-cut crystals; also, the ordinary and extra-ordinary refractive indices are the same parallel to the optical axis. Thus an accurately defined surface was used, its surface was then further characterised.

Polishing and etching of quartz plates

Introduction

The mechanism of the polishing process is a function of such properties as the melting point and hardness of the surface to be polished and those of the polishing material. Plates for ellipsometric work must be free from strain and disturbed layers

and scratches and must be optically flat and very smooth (e.g at the electron-optical level). Attention had, therefore, to be given to polishing and etching techniques.

Vitreous silica surfaces polished using a hard material such as diamond paste show substantial deviations from expected values of Δ and Ψ , for a smooth surface, due to compression of the surface layer (5.1, 5.2). Silica surfaces polished with a softer material such as cerium oxide powder show very little deviation from expected values. The values of hardness (on the Moh scale) for the materials of interest are: diamond 10, crystalline quartz 7, cerium oxide 5 and vitreous silica 4.9. It is to be expected therefore that polishing powder based on cerium oxide should cause negligible surface disturbance on crystalline quartz. Hodgkinson (5.3) reported a r.m.s. roughness obtained from analysis of fringes of equal chromatic order (FECO) for polished fused silica of about 0.25 nm after polishing with "cerirouge", followed by polishing with water addition only, for long periods. Such smooth surfaces probably have very little surface disturbance, requiring only a light etching treatment.

Results

Both natural and synthetic quartz crystals (z-cut) were polished first using carborundum powder (9-10 on Moh's scale) followed by finer and finer diamond paste (10 - 0.5 μm) and finally polished using 150 Regipole (a cerium oxide based polishing powder, of 2.8 μm average particle size, kindly provided by London and Scandinavian Ltd) as an aqueous slurry on a Pellon pad base (Hyprocel Pellon, English Ltd.). Surfaces so prepared showed no scratches under an optical microscope (200 x magnification).

However, uniform scratches appeared after etching in 1.5% ammonium hydrogen difluoride solution (a convenient source of dilute hydrofluoric acid) for about 15 hours at room temperature. These scratches were up to about 5 μm wide.

The etched surfaces were then repolished using only the cerirouge slurry until the plate was again optically scratch-free. On etching a second time no scratches appeared. Thus either the carborundum or diamond powder (or both) produce lines of disturbance or compression in smooth quartz plates. The softer cerium oxide based powder causes no such latent features.

All the plates used for water vapour adsorption studies were etched and repolished with the cerium oxide powder (finishing with long periods of polishing with water addition only) and then finally very mildly etched to remove any amorphous surface layers and inorganic ions. This latter etching was carried out so that a crystalline quartz surface was used in the adsorption experiments. The plates were polished for a total of about 24 hours using the cerium oxide powder and with water addition only.

Electron microscopy

Introduction

Although interference microscopy is sometimes used to investigate roughness of surfaces, the technique is limited in its discrimination of features in the plane of the surface by the resolution of optical microscopes (i.e. $\sim$0·2 μm). Therefore information on the microstructure of surfaces cannot be obtained by this method. The roughness theory discussed earlier (in Chapter 4) indicates that the substrate surface must either be very smooth or its structure must be known to very fine detail (i.e. $\sim$ 5 nm). To

obtain this information the technique of shadowed-replica-transmission electron microscopy was used.

Method and results

Polished and polished-and-etched plates were shadowed with platinum at an angle of 20° in a vacuum of 10^{-4} Torr (using C/Pt rods). A thin carbon film ($\sim$ 25 nm thick) was then evaporated on to the plate at 90° to act as support replica. The plate and coating film was then held just above a hydrofluoric acid solution (NH_4HF_2 solution was not used for this method because such solutions left crystals on the carbon film on evaporation of droplets of solution). The plate was fixed at about 30° to the horizontal and the solution was slowly raised by adding additional solution from a reservoir. Within a few minutes the platinum/carbon film was pulled by surface tension on to the surface of the solution and was caught on fine copper grids. These were then carefully dried on Velin (fluff-less) tissue. Dilute HF solution easily pulled off films from smooth plates; however, for rough plates (e.g. plates etched for 24 h in 1.5% NH_4HF_2) a 10% HF solution had to be used.

Great care was taken to avoid crinkling of the thin film (see Fig. 5.1a) which could occur both on drying and on subsequent handling. This crinkling could easily be seen by using a reflected light microscope. However, when transmitted light was used (or a T.E.M.) the films appeared perfectly flat (see Fig. 5.1b). Obviously measurements from electron microscope photographs would be in error if the region of the film studied was not at right angles to the electron beam. Since the electron microscope has a complicated image-focus relation, differences in focus on scanning

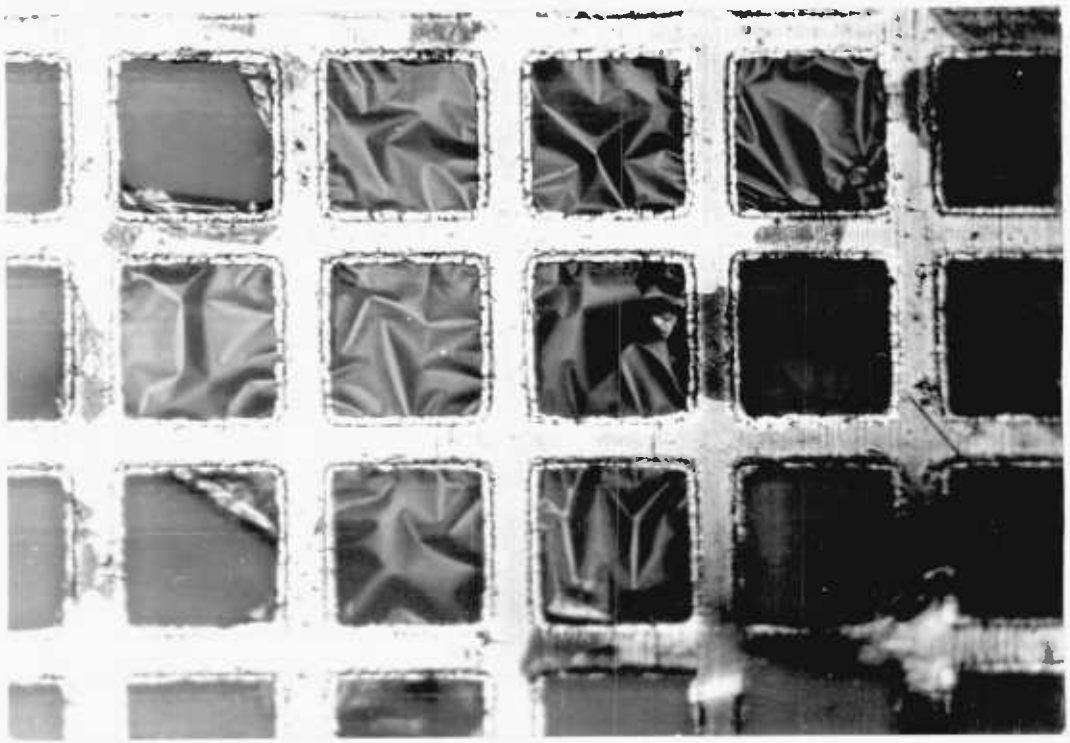

Figure 5.1a. Crinkled carbon film held on copper grid as seen with a reflected-light microscope. (200 x mag.)

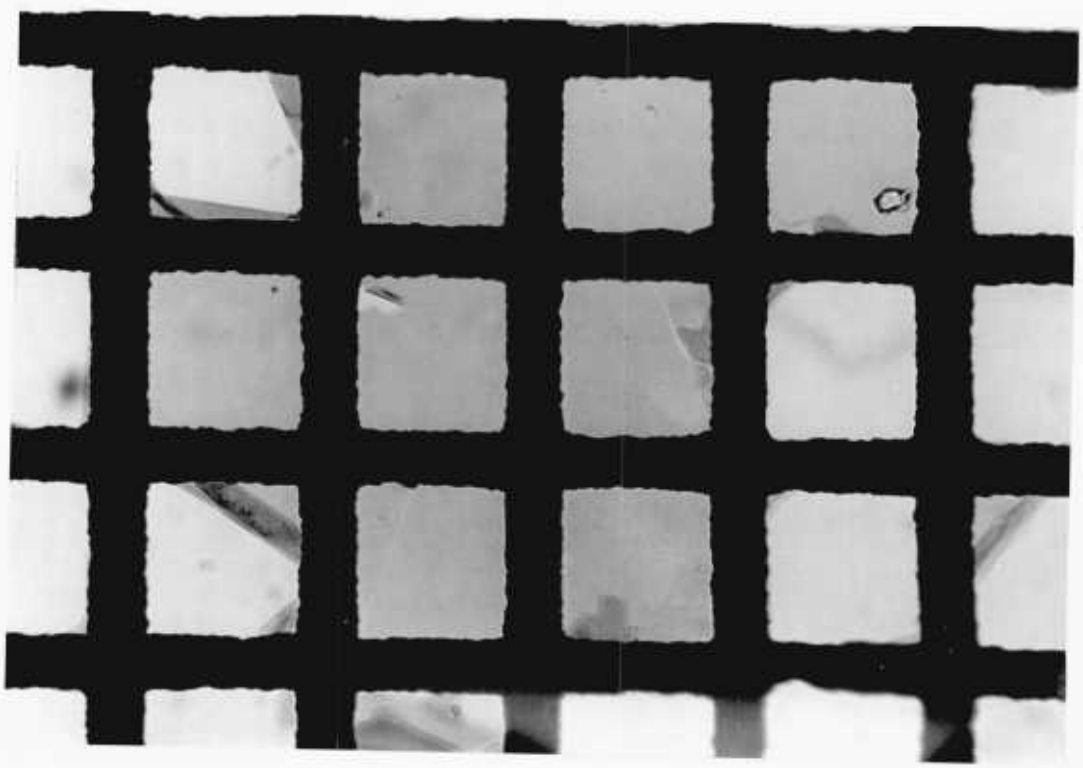

Figure 5.1b. Same as above but seen with a transmitted-light microscope. (200 x mag.)

across a crinkled film are not easily detected. Films similar to that shown in Fig. 5.1c were therefore used.

Figs. 5.2a and 5.2b show photographs obtained using a JEOL (Japan Electron Optics Lab. Co. Ltd.) "JEM-100B" microscope for crystalline quartz plates polished as previously described. From these results it is apparent that extremely smooth surfaces can be obtained after polishing for long periods with water addition only, on a Regipole impregnated polishing pad. The random (i.e. not shadowed in the same direction) microstructure observed on these photographs is apparently that of the carbon film itself and hence represents the resolution of the technique (i.e. about 2-4 nm). To this resolution the surfaces are perfectly smooth. The image expected from the replica of a rough surface is illustrated in Fig. 5.3. The carbon microstructure observed varies with focus of the microscope; this can be seen from comparison of Fig. 5.2a and 5.2b.

The affects of various degrees of hydrofluoric acid etching are shown in Figs. 5.4, 5.5. 5.6 and 5.7. The dark regions on the photographs correspond to those regions which have most platinum deposit. Plates which have been etched in 5% HF for a long time, Figs. 5.6 and 5.7, are very rough and tend to show what are apparently diamond-shaped etch-pits.

The effect of insufficient polishing of an initially very rough quartz plate is shown in Fig. 5.8. The surface was probably covered with pits, which can be removed on further polishing. This plate was polished for only about 3 hrs using the cerium oxide powder.

It is apparent from Fig. 5.4 that highly polished quartz plates etched for 2 hours (in 1.5% NH_4HF_2) show a negligible increase

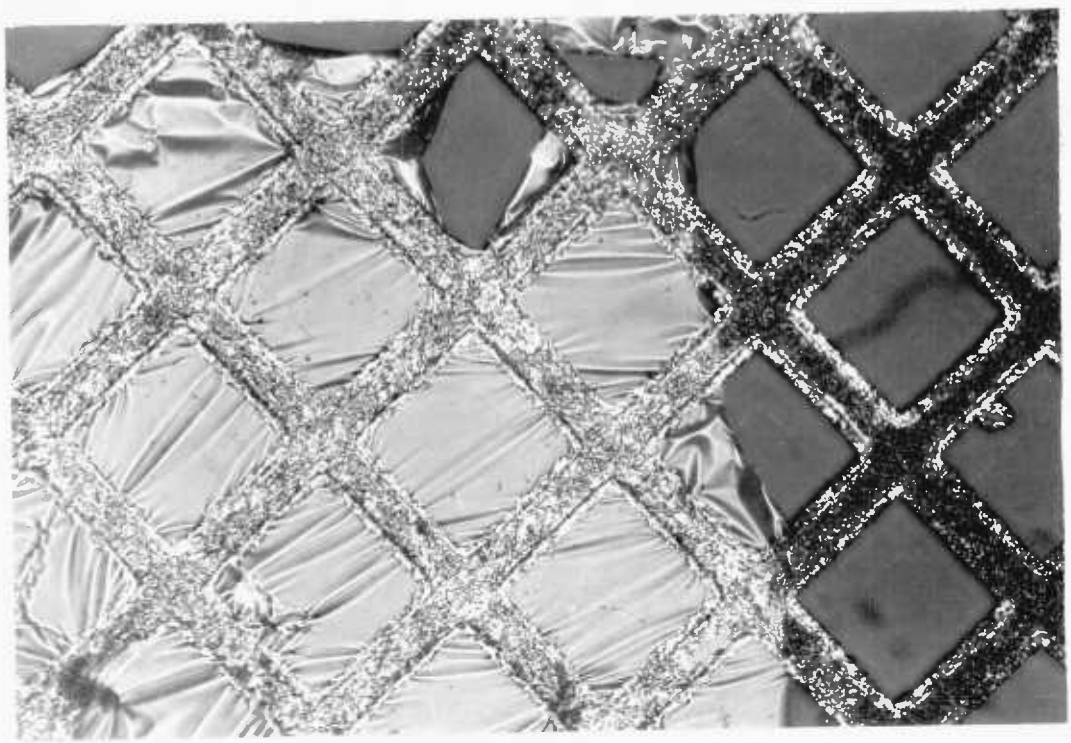

Figure 5.1c. Not so badly crinkled film as seen with reflected-light microscope. (200× mag.)

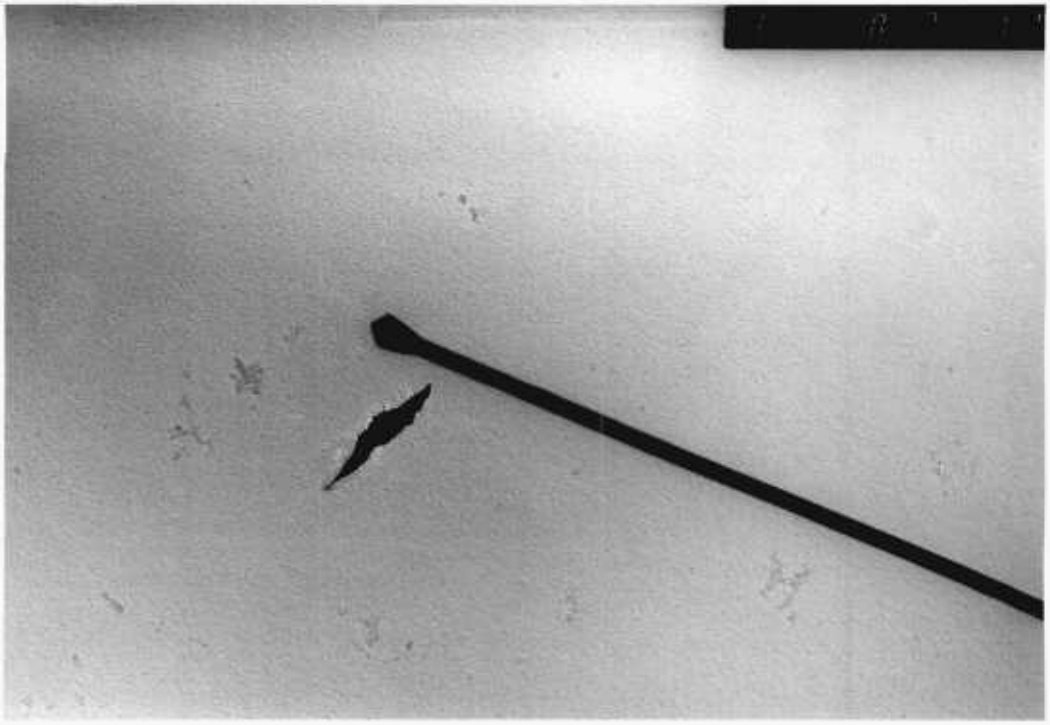

Figure 5.2a. Highly polished crystalline quartz plate platinum shadowed at 20°.

magnification: 96,000 x

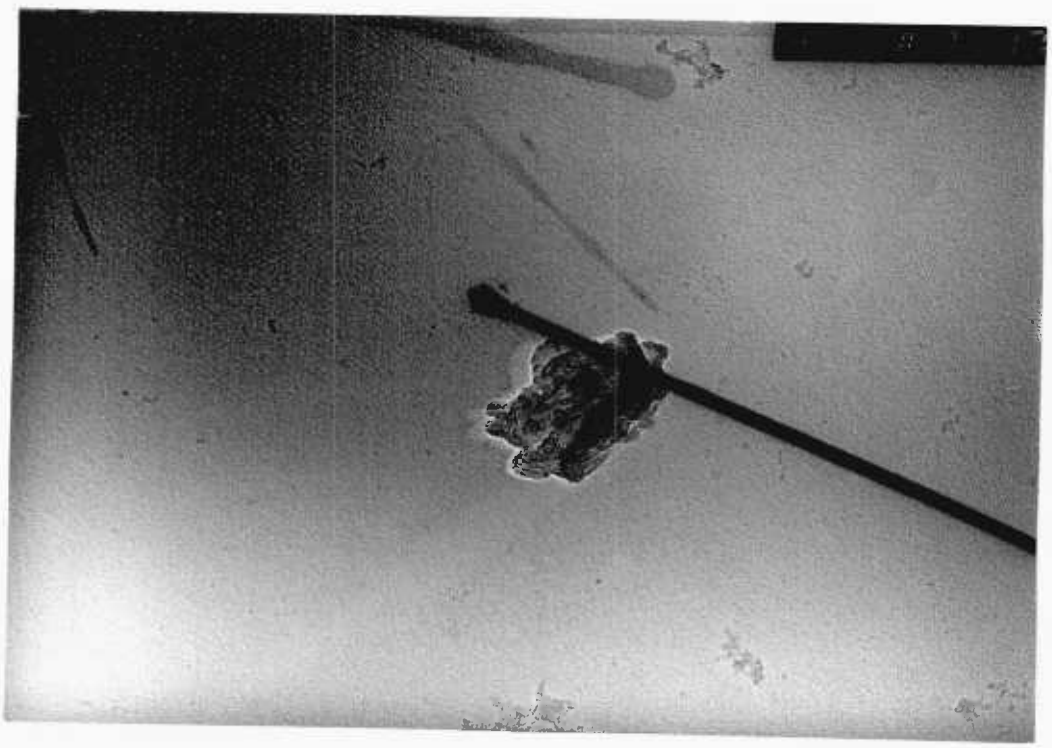

Figure 5.2b. Highly polished crystalline quartz plate.

magnification: 96,000 x

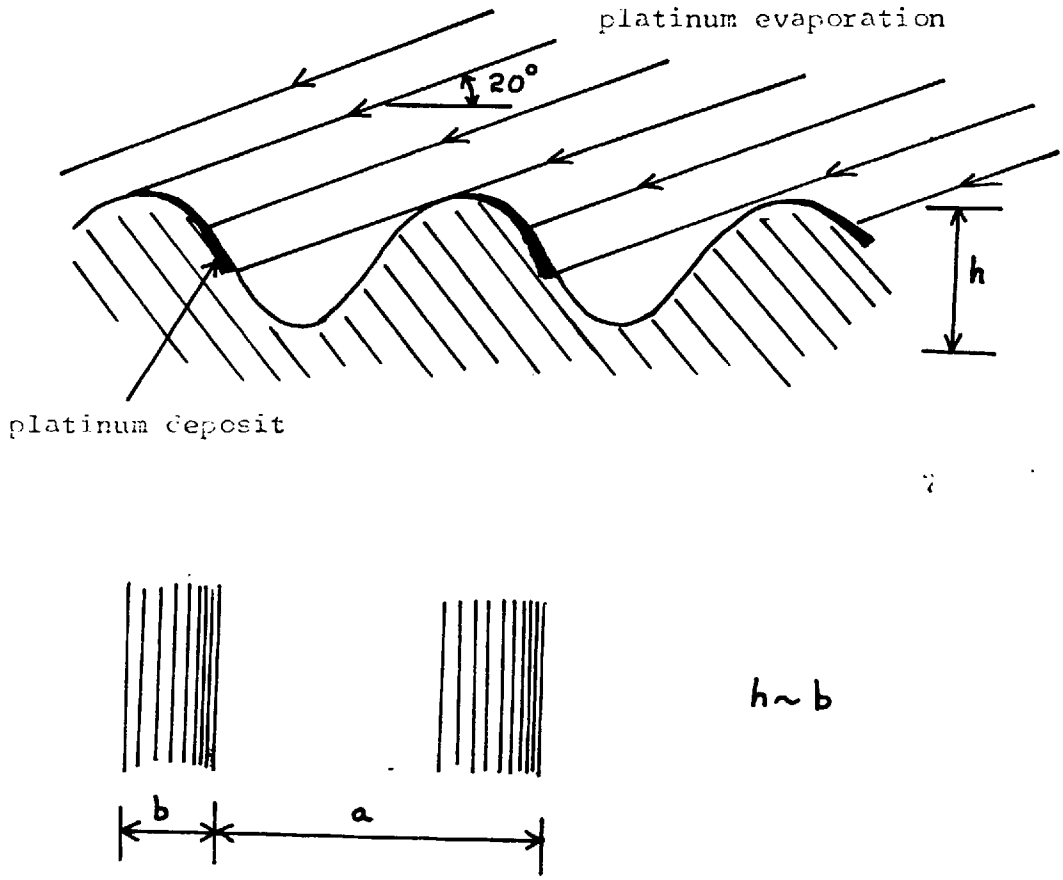

Fig. 5.2. Side-view and plan of platinum shadowing on a sinsusoidal type model surface roughness

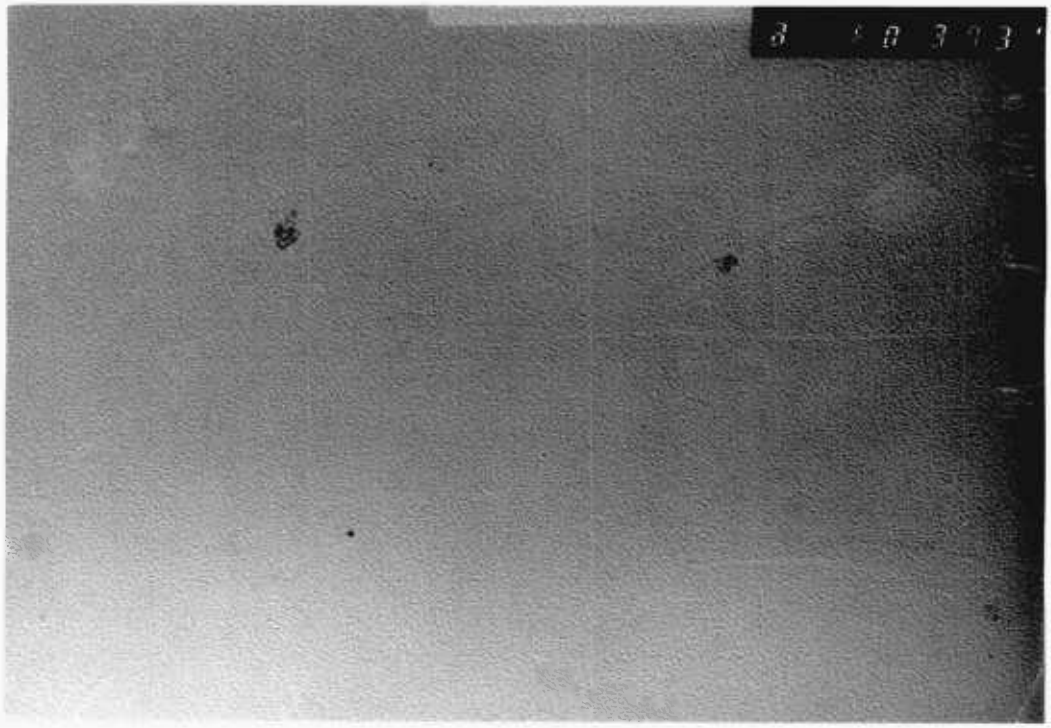

Figure 5.4. Highly polished crystalline quartz plate etched for 2 hours, at room temperature, in 0.5% hydrofluoric acid.

magnification: 96,000 x

Figure 5.5. Highly polished crystalline quartz plate etched for 17 hours, at room temperature, in 0.5% hydrofluoric acid.

magnification: 96,000 x

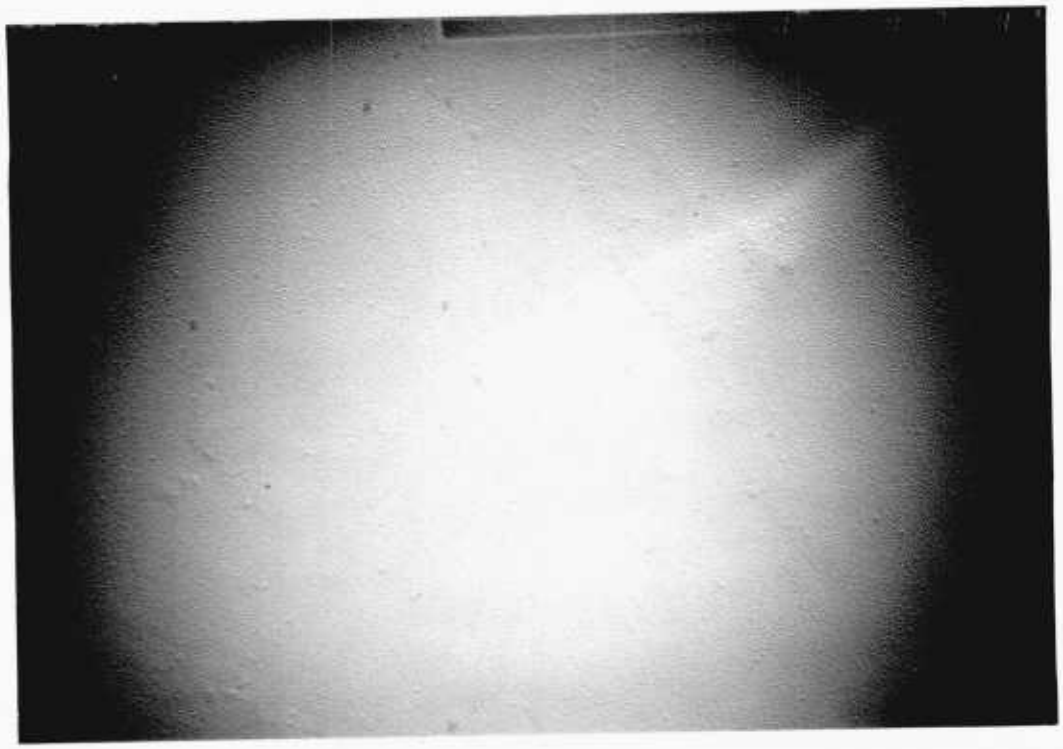

Figure 5.6. Highly polished crystalline quartz plate etched for 17 hours, at room temperature, in 0.5% hydrofluoric acid.

magnification: 48,000 x

Figure 5.7. Highly polished crystalline quartz plate etched for a long time in 5% hydrofluoric acid.

magnification: 24,000 x

Figure 5.8. Initially very rough crystalline quartz plate polished for 3 hours using the cerium oxide based polishing powder.

magnification: 30,000 x

in roughness from replica electron microscopy techniques. Carbon films are easily removed from such plates in dilute hydrofluoric acid. Plates etched for 17 hours, however, show a definite micro-roughness and evaporated carbon films are much more difficult to remove. In Fig. 5.5 the direction of shadowing is defined by the particles of dirt which were presumably present on the quartz surface before shadowing. The microstructure is now observed to be shadowed in this direction. From Fig. 5.5 and using the model assumed in Fig. 5.3 the peak-peak height of the surface roughness appears to be of the order of 2.5 nm (i.e. the dimension "b" $\triangleq$ 0.25 mm in Fig. 5.5, where at 100,000 x ,100 nm $\equiv$ 10 mm). The shadows produced behind the particles of dirt faintly show the carbon microstructure; the carbon was evaporated normal to the sample after platinum shadowing.

In Fig. 5.5 particles of dirt were used for focussing. Fig. 5.6 shows the same surface at lower magnification, but without the presence of dirt particles. That etching for 17 hours has so little effect on surface roughness (for quartz) is important in the understanding of ellipsometric measurements on such surfaces. These are discussed in Chapter 7.

Gold decoration study

Introduction

In order to characterise the surface of crystalline quartz it is necessary to prove that the surface, after preparation, is, indeed, crystalline. Surface electron diffraction techniques such as L.E.E.D. give information from a minimum depth of about 1 nm for relatively low atomic number species such as SiO_2. For such layers the ellipsometer itself is a good monitor of crystallinity,

assuming that a disturbed region would have a refractive index-significantly different from that of crystalline quartz (for example that of vitreous silica is 1.46, compared with 1.54 for quartz).

Gold "decoration" has been successfully applied to mica and kaolinite (5.4) to reveal monatomic steps providing evidence of surface crystallinity. Apparently no regular decoration patterns have been reported for crystalline quartz. A gold decoration study on quartz was therefore carried out in this work.

The gold decoration technique uses the principle that hot metal atoms will collide with a surface and travel either a random distance, before colliding and sticking to other gold atoms, or will travel to a step or fault where they are more strongly adsorbed than on a molecularly smooth surface. Gold nucleii are thus built-up along steps and faults of atomic height and are subsequently easily observed by the T.E.M. (when lifted off the surface with evaporated carbon films). The steps are seen as lines of gold spheres, whereas smooth areas have random arrangements of these spheres (5.5).

Method

The procedure followed here was that used by Mrs. P.M. Soper (English Clays Lovering Pochin & Co. Ltd) for successful decoration of kaolinite particles. Gold, cleaned by heating in air to 600°C, was evaporated from a molybdenum dish (electrically heated) under vacuum of $2 - 4 \times 10^{-5}$ Torr on to a quartz plate (previously heated under vacuum). The plate was held 13 cm away from the molybdenum dish and was positioned with its surface perpendicular to the gold source. Sufficient gold was evaporated, over 10 secs. to give a layer of about 1 nm thickness on the quartz plate

(5.5, 5.6). The degree of etching and amount of pre-heating of the quartz sample (to expose adsorption edges) was varied

The thin carbon film evaporated on to the gold decorated surface was removed together with the gold deposit by the method previously described for shadowed films. The same T.E.M. was used.

Results and Discussion

The results obtained for different conditions are shown in Figs. 5.9, 5.10 and 5.11. It is clear from these results that for all the conditions studied the gold nucleii are randomly spaced over the surface. The size and spacing of the nucleii was very similar to those observed by Gritsaenko and Samotoyin (5.4) for the decoration of clay minerals; showing that a suitable quantity of gold had been deposited.

Thus it appears that z-cut crystalline quartz plates which have been polished and etched do not show any regular surface features. A plate which was not etched at all showed a similar random distribution of gold. Information on surface morphology and crystallinity could therefore not be obtained from the gold decoration technique.

The observation that crystalline quartz plates do not "decorate" could be explained by the fact that there are no strong cleavage planes in the quartz lattice. Thus, attack by hydrofluoric acid would be essentially random and hence a uniformly rough surface would be produced which would show no steps or preferential etching. That etching of crystalline quartz (z-cut) is indeed a uniform process was apparent from the small increase in surface roughness observed in the previous section.

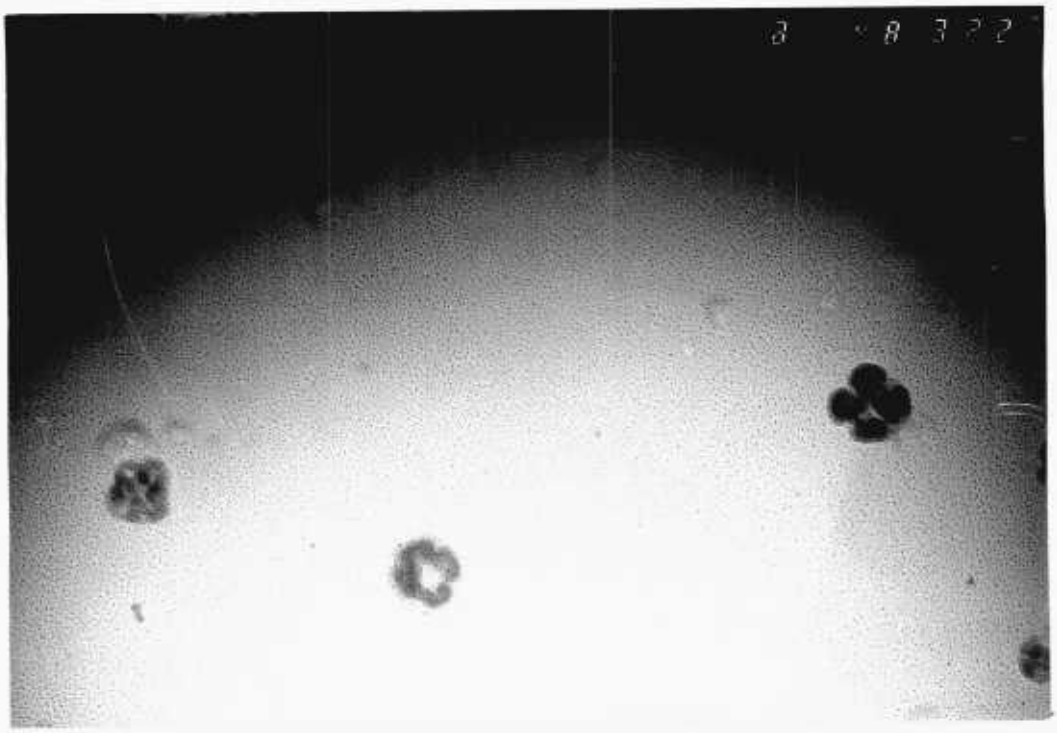

Figure 5.9. Gold decoration of a mildly etched, initially highly polished, crystalline quartz plate.

magnification: 76,000 x

Conditions: highly polished plate etched for 1 hour, at room temperature, in 0.5% hydrofluoric acid. Plate then pre-heated to 245°C for $\frac{3}{4}$ hour in 2 x 10^{-5} Torr. Then gold evaporated on to plate in same vacuum. Sufficient gold to deposit a 0.5 nm layer was evaporated over about 10 seconds.

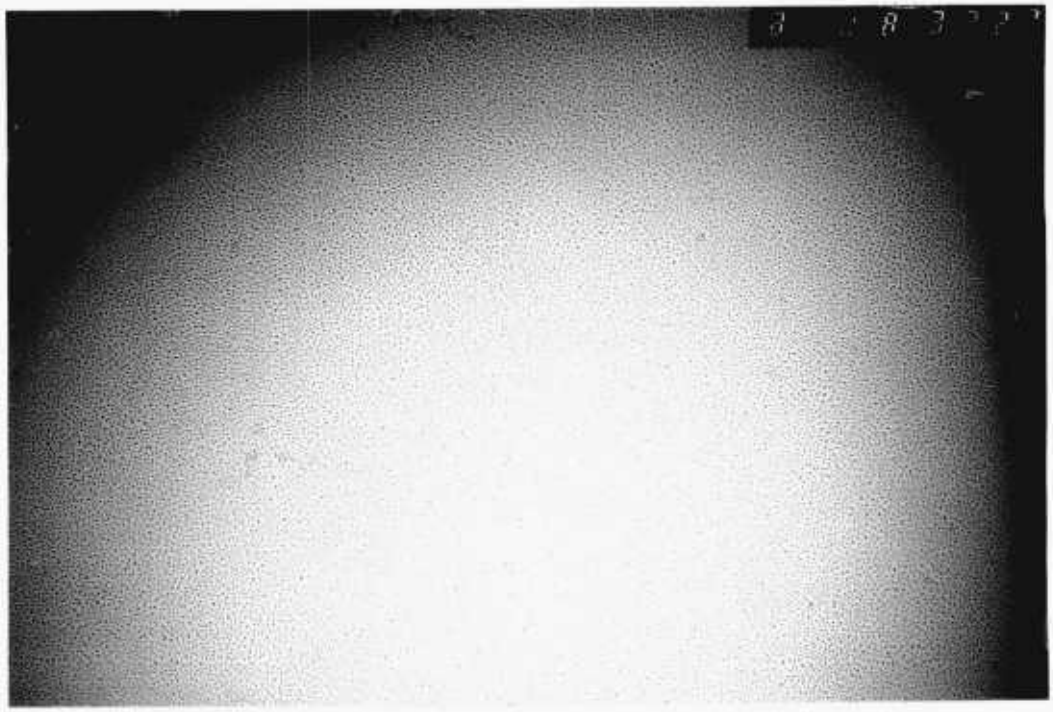

Figure 5.10. Gold decoration of a mildly etched crystalline quartz plate.

magnification: 76,000 x

Conditions: Highly polished crystalline quartz plate etched, at room temperature, in 0.5% hydrofluoric acid for 20 minutes. Plate pre-heated under 2 x 10^{-5} Torr vacuum at 200°C for 1 hour before evaporation of sufficient gold to give a layer of 0.5 nm thickness on the plate.

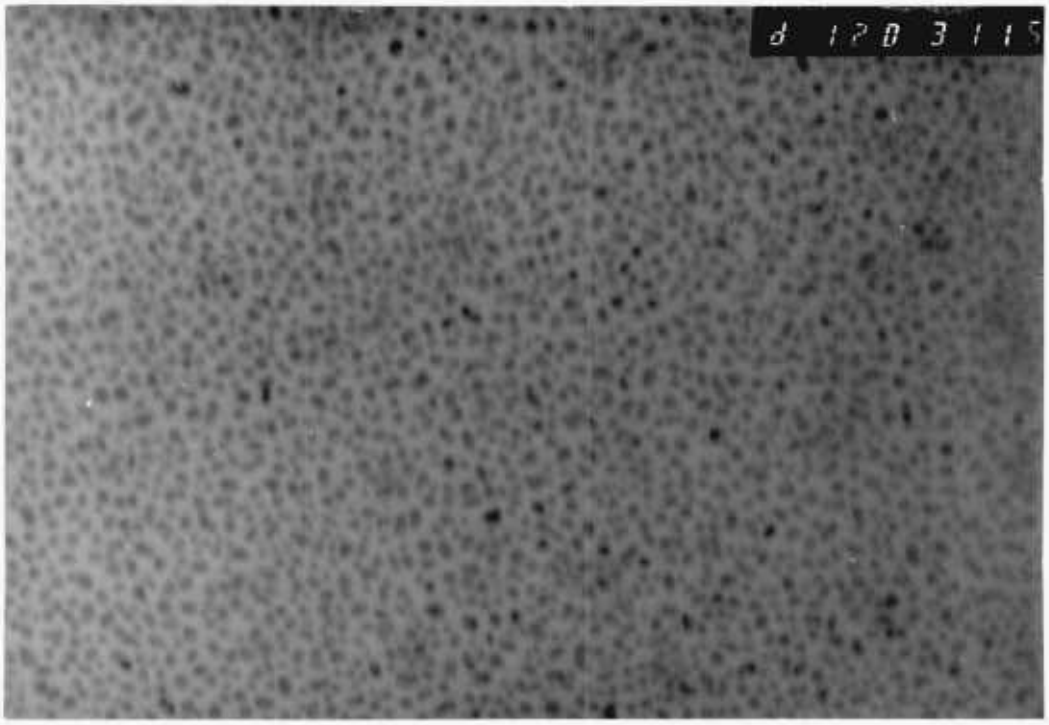

Figure 5.11. Gold decoration of a mildly etched crystalline quartz plate.

magnification: 192,000 x

Conditions: Highly polished crystalline quartz plate etched, at room temperature, in 0.5% hydrofluoric acid for 5 minutes. Plate then pre-heated under 4 x 10^{-5} Torr vacuum for 2 hours at 170^{o}C before evaporation of sufficient gold to give a layer of 1.0 nm thickness on the plate.

Frederick and Hruska (5.7) have recently suggested that contamination, present in the vacuum evaporation system, is necessary to obtain decoration. Lack of contamination could therefore not be ruled out in explaining the results obtained here.

Cleaning of silica and quartz surfaces

Introduction

The effect of hydrophobic molecules adsorbed on to the surface of fully hydroxylated silica (and quartz) is to increase the contact angle of water droplets on the surface. This effect has been known and used in the process of froth flotation for many years (5.8). Clean (hydroxylated) quartz is not floatable. However, quartz in the presence of flotation collectors (e.g. alkylamines or carboxylic acids in the presence of inorganic cations) is readily floatable. This is due to the adsorption of hydrophobic molecules and hence the formation of a large contact angle with water. The treatment of any silanol surface (e.g. of quartz and silica) with methylating agents such as trimethyl-chlorosilane produces a surface of essentially close-packed trimethyl (hydrophobic) groups (5.9). Such a surface has a water contact angle of about 90^{o} (5.10).

The effect of contamination is likely to be similar for both vitreous silica and crystalline quartz both possess fully hydroxylated silanol surfaces when cleaned.

Thus it is apparent that the wetting properties of quartz/silica are very sensitive to hydrophobic (organic) contamination. It is therefore necessary to be able to produce and store clean surfaces of quartz for use in the study of its wetting properties.

Main methods of cleaning quartz surfaces

Organic surface contamination can be removed by oxidative and non-oxidative processes. For oxidation to be effective very strong oxidising processes are necessary such as heating in air, chemical oxidation and exposure to atomic oxygen. The use of heat oxidation for quartz is severely limited because of loss of surface hydroxyl groups and hence the formation of siloxane bridges (which are hydrophobic and slow to rehydrate (see later).

Non-oxidative processes are mainly those which actually remove surface material from the substrate. Ion bombardment has been used to clean surfaces (5.11) by such a stripping process. However, the ions used penetrate into the sample and cause surface structural damage (as well as constituting an impurity). The simplest cleaning process is mild etching of the substrate. Etching can be used only if surface residues or complexes of the etching agent can be easily removed from the surface.

Thus chemical and atomic oxidation and etch-cleaning appear to be possibilities for quartz cleaning.

Methods of measuring surface cleanliness

Once a clean surface is produced, however, it is necessary to measure its cleanliness in some way. Surface analysis methods such as E.S.C.A. and Auger spectroscopy, although sufficiently sensitive, are difficult to apply because of the necessity of handling and mounting the samples, which are thereby exposed to contamination. The complexity of these techniques also makes them unsuitable for easy monitoring of cleanliness.

In 1959 Feder and Koontz (5.12) described the use of the "atomiser test" for wettability. On a hydrophilic surface (free

from hydrophobic contamination) the micro-droplets of water sprayed on to the surface spread and cause the build up of thick films which produce uniform coloured fringes (e.g. uniform films of about 150 nm thickness). Using this test, those authors were able to easily monitor the effects of cleaning and contamination on metals. On a markedly hydrophobic surface the micro-droplets do not spread and hence an opaque mist is clearly observed.

This simple test was refined by White (5.13), who used the condensation of steam (from a beaker of warm water) on to quartz oscillator plates. Uniform coloured fringes (indicating smooth water films of considerable thickness) were obtained only after certain initial cleaning treatments.

Freshly cleaved mica is hydrophilic with a water contact angle of no more than 2-4^{o} and is reported to always give excellent fringes in the steam test. Mica can therefore be used as a standard for comparison, and it has been used for checking the cleanliness of storage conditions, etc.

Vig et al (5.14) compared observations from the steam test for differently cleaned quartz plates with both Auger analysis (with a sensitivity of 1% of a monolayer of carbon) and measured contact angles. The observed condensation behaviour and corresponding contact angles are shown in Table 5.1. If fog was observed, it was found to correspond to a monolayer or more of contamination. An "orange-peel" result indicated approximately 0.1 to 1.0 monolayer, whereas coloured fringes indicated less than 0.1 monolayer of contamination. These results very clearly indicate that perfectly clean crystalline quartz has a contact angle of not more than 4^{o} with water.

Table 5.1. Results of steam test related to contact angle according to Vig et al (5.14).

Result	Appearance on condensation on polished quartz	Contact angle ($\pm 2^{\circ}$)
1. Excellent fringes	uniform rainbow-like fringes during both condensation and evaporation	4°
2. Good fringes	uniform fringes during condensation, irregular fringes during evaporation	4°
3. Poor fringes	irregular fringes during condensation	4°
4. "Orange peel"	no colours, micro-droplets visible, transparent	$5 - 10^{\circ}$
5. Fog	translucent due to large number of small droplets	$> 10^{\circ}$

Previously recommended methods of cleaning glass, silica and quartz

A frequently recommended method for cleaning quartz is treatment with the oxidising mixture ammoniacal hydrogen peroxide (5.12, 5.15, 5.16). The process involves heating a 30% H_2O_2 solution to 60 - 80°C and adding 1/10 th its volume of concentrated ammonia solution. The peroxide then vigorously decomposes over several minutes. The rapid evolution of oxygen "scrubs" the substrate, partially oxidises organic contamination and the raised pH has a dispersing action. The products from the decomposition are materials which are either water-soluble or volatile. It is also possible that the ammonia complexes some insoluble materials and hence makes them more susceptible to oxidation.

Chromic acid solutions are also often used to clean silica and glassware; however, it has been shown that chromic acid leaves inorganic residues which are difficult to remove (5.16).

A more recently favoured method of producing clean quartz plates for electronic oscillator crystals is the use of ultra-violet irradiation cleaning. Bolon and Kunz (5.17) studied the depolymerisation and removal of polymer films from quartz substrates under a powerful medium-pressure mercury arc lamp. Typical polymer films of 1 μm thickness could be completely removed in less than 1 hour, leaving no detectable trace of carbon on AES analysis.

Vig et al (5.11, 5.14, 5.15) used a low pressure mercury lamp to clean and store quartz crystals. Such crystals gave excellent fringes in the steam test and negligible carbon was detected from AES. The wavelengths important for cleaning were found to be 185 nm and 254 nm, the former producing ozone and the latter being absorbed by most hydrocarbons and hence activating

them for reaction with ozone.

Methods and results of cleaning tests on silica

Various methods of cleaning were tested on polished, transparent silica (and quartz) plates which were grossly contaminated with skin fats. This type of contamination is expected to be most commonly encountered and is known to be particularly difficult to remove (5.14).

After each of the cleaning processes, the plates were rinsed in double-distilled water (which had been passed through ion exchange resin and activated charcoal columns between distillations) and immediately dried by a jet of clean nitrogen, to prevent evaporation and hence deposition of any non-volatile contamination. Compressed air filtered through a membrane filter and "white spot" cylinder nitrogen were tried and no difference between them was observed.

The steam test, as previously described, was used to monitor the efficiency of cleaning. Warm doubly distilled water was used as source of vapour so as to avoid contamination from the test itself. Using this water the test could be repeated at least ten times without contamination from the atmosphere or the water used.

The results obtained from various treatments are given in Table 5.2.

Discussion of results

Freshly made up chromic acid (prepared by the method recommended in the Rubber Handbook 1961/62) at room temperature was found incapable of cleaning the grossly contaminated plates even after many days of immersion. Very hot acid, however, does clean but

Table 5.2. Results of various cleaning techniques applied to artificially contaminated smooth silica plates (followed by thorough rinsing, drying in air jet and testing with "steam")

	Initial contamination of plate	Cleaning procedure
Unsuccessful cleaning (mist formed in steam test)	A or B	freshly made up chromic acid (F.C.A.)* room temp. -14 days
	A	EtOH/HNO_3 "bomb" repeated several times
	A or B	45 W u.v. lamp (185 and 254 nm, ozone producing) 24 h exposure
	A	conc. HCl, hot, 2 h.
	A	conc. HNO_3, room temp. 24 h.
	A	conc. NH_3, hot, 1 h.
	A	3% NaOH, boiling, 5 min.
	A	4 g EDTA, 80 ml H_2O adjusted to pH = 3.4, 85°C, 22 h.
Successful cleaning (good fringes obtained:)	C	F.C.A., 115°C, 6 h**
	C	F.C.A., 150°C, 3 h
	B	F.C.A., 120°C, 5 days
	B	F.C.A.. 140°C, 1-3 days
	A	30% H_2O_2/NH_3 hot, 4 min (***)
	A or B	30% NaOH hot, 20 sec (***)
	A or B	1.5% NH_4HF_2, room temp., 2 min.
	A or B	scrubbing in hot EtOH/ultrasonically clean (hot); 45 W u.v. lamp. 5 min
	B	4 g of EDTA in 90 ml H_2O adjusted to pH 7 with NaOH, 80°C, 7-22 h.
	A or B	C.HNO_3, 80-90°C, 4 h (***)

Notes

* F.C.A.:- 6 g $Na_2Cr_2O_7.2H_2O$ dissolved in small amount of H_2O + 100 ml conc. H_2SO_4.

** chromic acid decomposes when heated > 100°C for more than 24 h

Contamination

A. rubbing plate in hands, using small amount of EtOH to wet.

B. rubbing plate in dry hands.

C. new plate - stored in sealed polythene bag.

Note: crystalline quartz plates were also tested by several of the methods (***) and these were found to be similarly successful.

still takes a few days! Chromic acid decomposes when heated giving off oxygen, and changing colour:

$$\underset{\text{(orange)}}{2Cr_2O_7^{2-}} + 16H^+ \xrightarrow{\text{heat}} \underset{\text{(green)}}{4Cr^{3+}} + 8H_2O + 3O_2\uparrow$$

The normal oxidising action is:

$$Cr_2O_7^{2-} + 14H^+ + 6e^- \rightleftharpoons 2Cr^{3+} + 7H_2O \qquad E = +1.33v.$$

Thus it appears that decomposition and production of nascent oxygen is required before efficient oxidation of organic contamination occurs. Certainly, chromic acid at room temperature is incapable of oxidizing carboxylic acids or alkanes.

Ultra-violet irradiation in air from a low pressure mercury lamp of 45 watt total input power was found to clean plates only when they had been pre-scrubbed in hot ethanol. The latter washing removes gross contamination but still leaves sufficient to produce an opaque mist in the steam test. Vig et al (5.14) recommended the use of ultrasonic scrubbing; however, damage to optical surfaces can occur due to the ultrasonic treatment (5.18). For effective cleaning of quartz apparatus a much more powerful lamp than was available would be required. The probable cleaning process is of complete oxidation of organic materials, any inorganic residue being washed off in the final rinse and blow-drying.

Hot dilute (pH = 0.85) or concentrated hydrochloric acid did not clean the contaminated plates. If the contamination were attached by a cationic charge to a negative surface on the silica, at pH = 0.85 the latter charge should reverse. However, it appears unlikely that contamination already present can be removed in this way. Hot concentrated HCl acid very slowly dissolves silica, but

the rate of dissolution is apparently too slow for effective etch-cleaning.

Concentrated nitric acid can clean contaminated plates only when hot (80 - 90°C). It was found to be a much more effective cleaning agent than chromic acid. On heating, nitric acid decomposes and produces nascent oxygen:

$$2HNO_3 \xrightarrow[\text{heat}]{h\nu \text{ or}} 2NO_2\uparrow + H_2O + \tfrac{1}{2}O_2\uparrow$$

Nitric acid may also nitrate organic compounds via the nitronium ion (NO_2^+) (as well as oxidise) and hence increase their stability in water.

Hot concentrated sodium hydroxide solution cleaned contaminated plates very quickly. This action is most likely due to a rapid etch-cleaning process; but it may also enhance the solubility of the contaminants. for example by saponifying lipids.

A similarly efficient etch-cleaning action was obtained from dilute ammonium hydrogen difluoride (NH_4HF_2) solutions at room temperature. Crystals of this material are a convenient source of hydrofluoric acid when dissolved in water:

$$NH_4HF_2 \xrightleftharpoons{H_2O} NH_4^+ + F^- + HF$$

An ESCA analysis (kindly provided by courtesy of Dr D. Chadwick at Dept. Chem. Eng., Imperial College) was carried out on a typically polished (CeO_2-based powder) and cleaned (using NH_4HF_2) and washed crystalline quartz plate. The analysis showed no detectable traces of Al, Fe or Ce in the surface layers and less than 1% of a monolayer of fluorine. Thus it appears that fluoride was easily washed from

the quartz surface after HF etching which is in agreement with the findings of Warren and Kitchener (5.19) on the hydrolysis of fluorosilicate complexes. Fluoride groups retained in the surface would be expected to make the surface less hydrophilic (5.20).

Decomposing ammoniacal hydrogen peroxide solution was found to be a very effective cleaning agent. The main cleaning action is probably the vigorous production of oxygen which both oxidises organic contamination and scrubs the surface, while ammonia is a good dispersant for fats.

Hot concentrated ammonia solutions alone have little cleaning action. Hot hydrogen peroxide solutions rapidly decompose on addition of ammonia.

A hot solution of E.D.T.A. in sodium hydroxide at pH = 3.4 did not clean contaminated plates after 22 hours. However, at pH = 7 the plates were cleaned in 7 - 22 hours. Since the chelating power of E.D.T.A. for metal ions is much greater at higher pH it seems most likely that the cleaning action is due to surface metal ion removal. This strongly suggests that the contamination on the surface is associated with metal ions.

Cations such as Ca^{2+}, Mg^{2+}, Al^{3+} and Fe^{3+}, are known to activate quartz for flotation with carboxylic acid collectors such as oleic acid. Only very small amounts of these cations are required to activate the quartz for adsorption of the collector and hence induce hydrophobicity and flotation. Indeed, flotation can be prevented by addition of E.D.T.A. (5.21). Polyvalent cations may be adsorbed on silica and provide positively charged sites for attachment of anionic surfactants. These metal bridging properties are sometimes represented by diagrams such as:

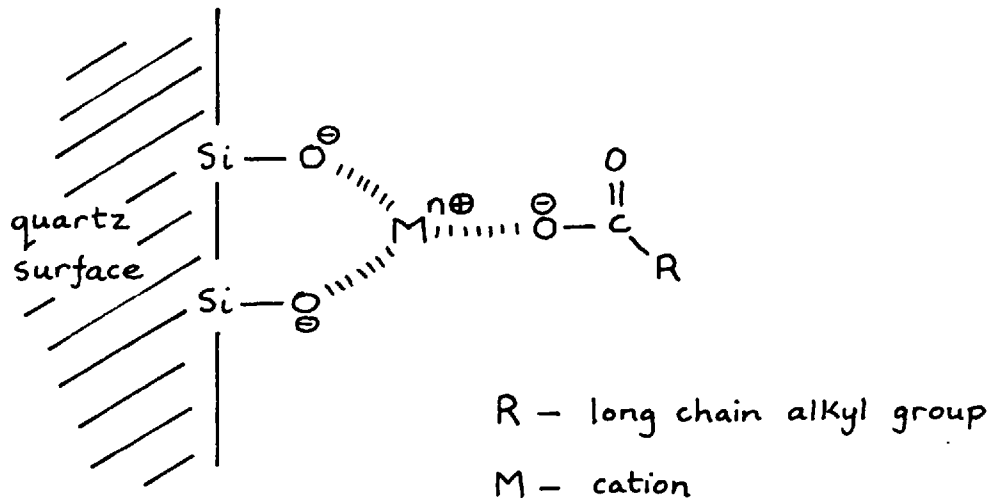

though the precise structure of adsorbed materials is not well known.

Contamination of this nature would explain the ineffectiveness of mild oxidation, since carboxylic acids are themselves at the end of an oxidation chain (i.e. alcohol ⟶ aldehyde ⟶ carboxylic acid). It would also explain the tenacity with which the last layer of contamination is held.

Long-chain carboxylic acids are likely to be common contaminants since they are one of the main constituents of skin fats (5.22).

From this cleaning study it is apparent that several entirely different methods produce silica or quartz surfaces which are perfectly hydrophilic and are apparently free from almost all contamination. The use of mild etching techniques appears to be the best method of producing clean, crystalline surfaces.

From reported values of the rate of dissolution of vitreous silica in 20% hot sodium hydroxide solution (5.23) it is possible to estimate the amount of crystalline quartz dissolved. Assuming crystalline quartz dissolves at one tenth the rate of amorphous material, in 10 sec. a layer of about 5 nm should be dissolved. Similarly, from work reported by Smit et al (5.24) the amount

dissolved in 0.5% HF at room temperature can be estimated as approximately 2 nm in 10 mins. Thus the amounts removed in successful cleaning are similar and are not sufficient to produce rough surfaces.

Pyrex glass flasks cleaned by NaOH etching could be kept clean (as indicated by the presence of uniform coloured fringes when sealed by ground glass joints with a small amount of clean water) for up to at least 2 weeks.

It thus appears possible to produce and store clean, hydrophilic quartz surfaces.

The affect of heating on clean quartz with respect to the zeta-potential and contact angle with water is considered in the following sections.

Measurement of the zeta-potential on hydroxylated and de-hydroxylated quartz surfaces

Method and results

Ground Brazilian quartz ($< 30\mu m$) of optical grade was washed in concentrated hydrochloric acid at 60°C for 24 h to remove surface inorganic contamination and then washed and separated (by centrifugation) several times. The final pH value of this suspension was 5.8. One portion of the powder was placed in a platinum vessel and heated to 1050°C (in air in an electric furnace) and then allowed to slowly cool for 24 h to 300°C. It was then removed and suspended in 0.01 N KCl solution, of pH = 5.9. The average electrophoretic mobility (U) of these particles was measured at 25°C immediately and after one week in a Rank Bros. MK2 microelectrophoresis apparatus.

A second portion of the washed quartz was stored as a suspension

in water in 'Pyrex' glass sealed vessels at pH = 5.8 - 5.9. Portions from this suspension were measured in the electrophoresis apparatus at different pH values in 0.01 N KCl solution.

A third portion was stored in water in a platinum crucible at pH = 5.9 for comparison.

The zeta-potential (ζ) of these suspensions were estimated from the electrophoretic mobility assuming the validity of the Smoluckowski equation (i.e. large κa):

$$\zeta = \frac{\eta u}{\epsilon} \qquad 5.1$$

where η = viscosity of the suspension

and ϵ = permittivity of the electrolyte medium

The results obtained for the zeta-potentials of the particles in the various media are given in Figure 5. 12.

Discussion

The zeta-potentials measured here are expected to be somewhat lower than the absolute values because of the lack of a correction for surface conductivity (which can be accounted for in streaming potential measurements (5.25). Bergman and Langrish (5.26) reported the observation that the zeta-potential on quartz was very sensitive to the pretreatment of the powder. Li and De Bruyn (5.27) , however, report a value of -55 mV for the zeta-potential of quartz in 10^{-2} M sodium chloride. This value agrees very well with the value measured here. The form of the curve in Figure 5.12 agrees very well with that measured by Fujii (5.28) for similar HCl-leached quartz powder measured in a solution of ionic strength 5×10^{-4} N.

The results obtained show that the quartz surfaces dehydroxylated by heating have only a slightly lowered zeta-potential, though there

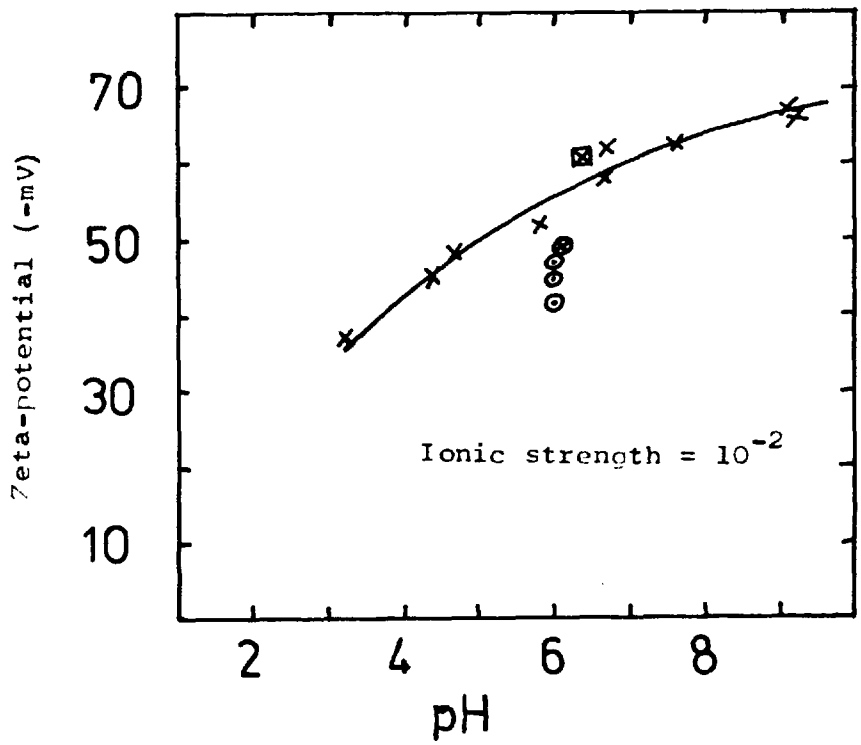

Figure 5.12. Zeta-potential as a function of pH for variously treated crystalline quartz powders.

X - hydrochloric acid washed powder, stored in distilled water at pH = 6, in a sealed Pyrex vessel

⊠ - as previously but stored in a platinum vessel

⊙ - hydrochloric acid washed powder, treated to 1050°C in air and rapidly measured

⊗ - heated powder re-measured after 1 week in water

are only about (0.2 - 0.7) OH groups per nm^2 after heating to 1000°C, compared with an original density of about 4.6 ± 0.2 OH/nm^2 at room temperature (5.29). This effect has been considered for the case of partially methylated surfaces by Laskowski and Kitchener (5.30), where methylation was observed to affect the contact angle against water but not the zeta-potential. (The affect of such heat-treatment on contact angles is considered in the following section).

The zeta-potential measured on the suspension stored in a platinum crucible was indistinguishable from that of suspensions stored in Pyrex vessels. Thus there appeared to be no deposition of silicic acid layers from the more soluble Pyrex vessels onto the crystalline quartz surface during the experiment.

Contact angles related to dehydroxylation of silica by heat

Methods and results

A vitreous silica plate was heated in a tube furnace (see Figure 5.13) to 875°C. After 24 h the tube was slowly withdrawn so as to allow the bulk of the silica tube to cool while the narrow tube remained hot. In this way, any air drawn into the tube on cooling was cleaned (by oxidation) by passage along a section of narrow bore tubing at 875°C. The end of the narrow tube was then completely sealed.

After cooling the plate was rapidly removed from the tube and a drop of clean water was placed on the plate in a closed vessel which already contained saturated water-vapour. The contact angles were quickly measured (approximately) from the drop profile projected on to a screen. The advancing and receding angles measured were:

$$\theta_A = 35\text{-}40^\circ \text{ and } \theta_R \simeq 17^\circ.$$

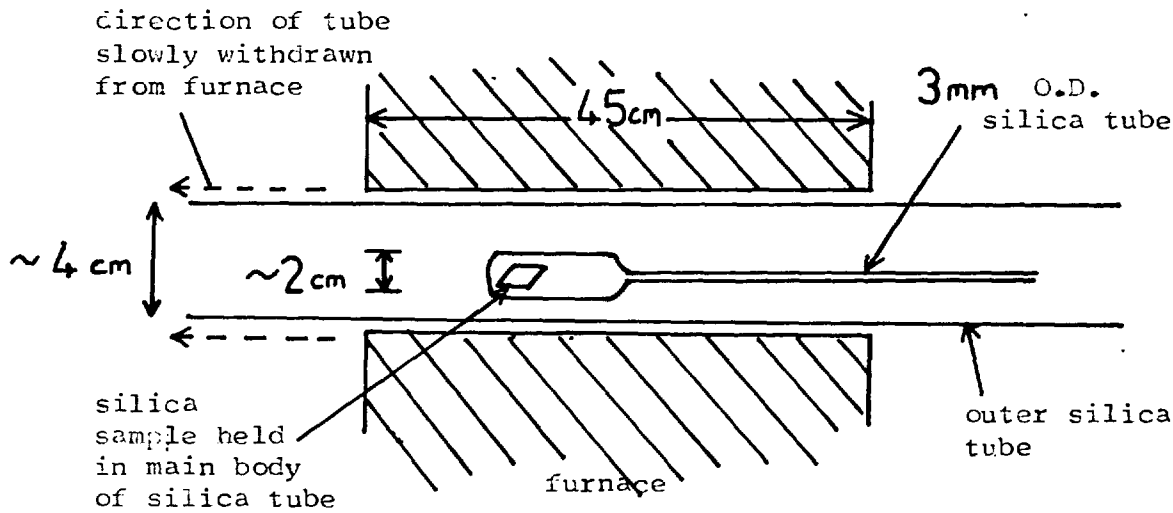

Fig. 5.13. Tube furnace used to heat dehydroxylate silica plates without contamination.

The experiment was then repeated with an empty vitreous silica tube only. This was sealed on cooling and opened in order to place a drop of clean water in the tube. The tube was then resealed. The droplet had a contact angle of $\sim 35^{\circ}$ and mist was produced when one end of the tube was warmed and another section cooled. After storage for 8 weeks at room temperature, droplets were still present in the tube. The tube was then irradiated with ultra-violet light from the lamp previously described. After 10 min coloured fringes were clearly visible on mild heating and cooling of different regions of the tube. No droplets were observed in this tube after a further period 6 weeks at room temperature (i.e. the tube remained hydrophilic). A heat dehydroxylated tube containing a few drops of clean water became completely wettable on heating to $85^{\circ}C$ for 24 h.

Discussion

The water contact angle observed on silica after heating agrees well with that reported by White (5.31). The large hysteresis was probably due to surface heterogeneity i.e. micro-areas of different silanol density. At room temperature and in a saturated water vapour environment, the rate of rehydroxylation is slow. This phenomenon was also observed by De Boer et al (5.32) for silica powders heated up to $700^{\circ}C$. Both wet heating (up to $100^{\circ}C$) and ultra-violet irradiation accelerate the rehydration process.

Since care was taken in these experiments to prevent contamination of the heated surfaces, the increased water contact angle must be due to loss of surface hydroxyl groups only. The surface process

involved for a vicinal silanol system is shown below:

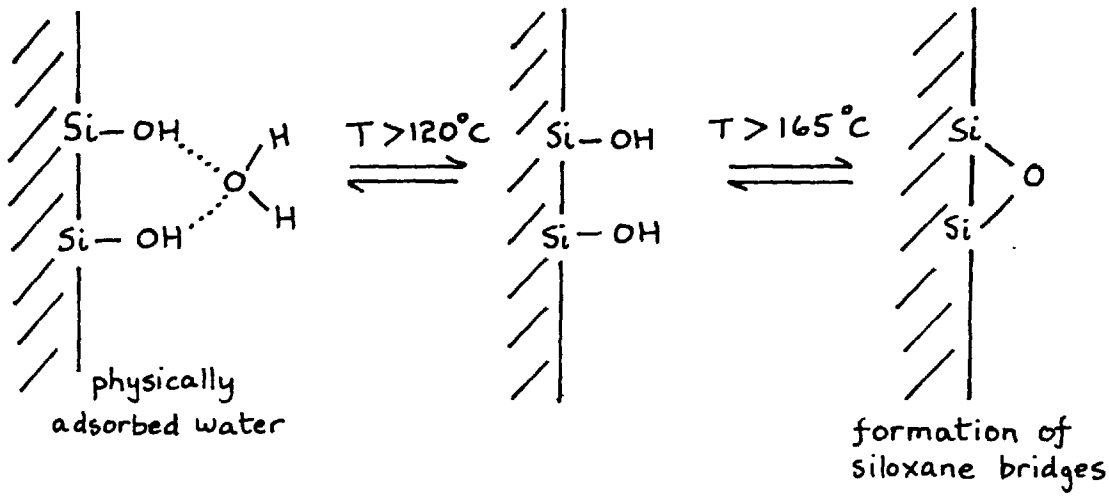

Hair (5.33) states that up to 400°C the hydroxyl groups thermally removed can be replaced by exposure to water; but above 400°C a decreasing number of groups can be re-formed. Hair reported that at 800°C addition of water is futile and the dehydration process is "irreversible". However, from the work reported here irreversible means very slow at room temperature, but fairly rapid reversibility at 85°C (for plates heated to 875°C).

Since the main wavelengths emitted by the u.v. lamp are not absorbed by either water or quartz, it is likely that the ozone or atomic oxygen produced by the lamp catalyses the rehydration process. The mechanism may possibly involve the formation of hydroxyl radicals:

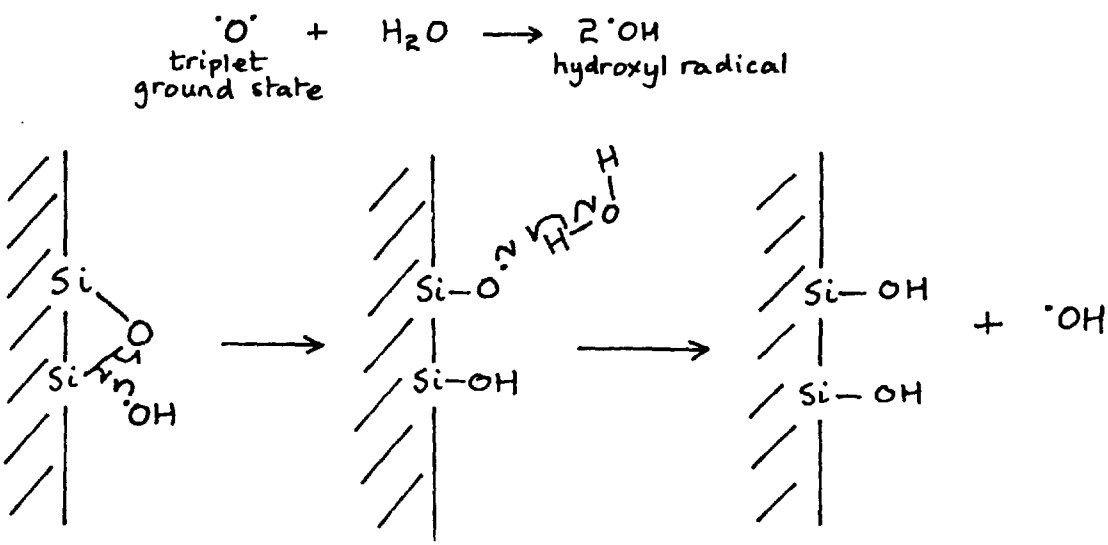

heat alone presumably catalyses the reaction:

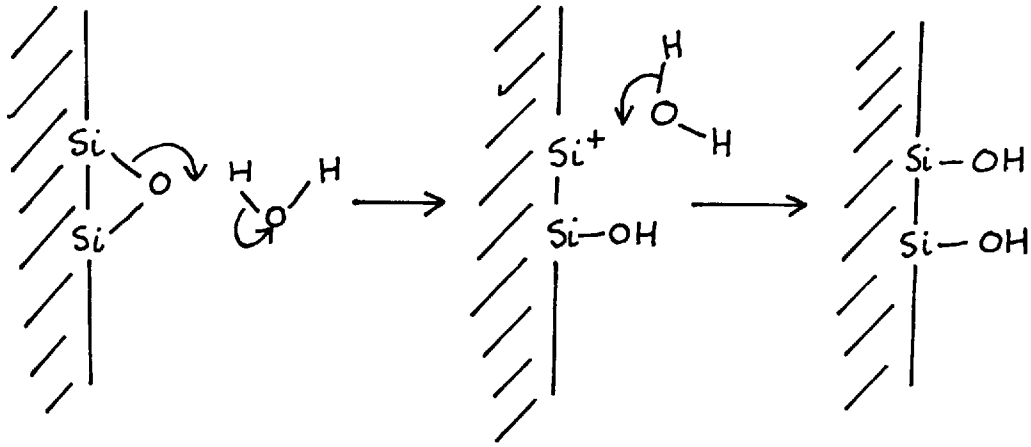

or possibly by a concerted reaction with the same water molecule.

Thus from the results obtained it appears possible to produce a dehydroxylated surface which will remain stable for hours or even days in contact with water at room temperature.

The large increase in contact angle caused by dehydroxylation of the silanol surface must be due primarily to a reduced short range interaction with water molecules via hydrogen bonds. The silicon-oxygen bond in the siloxane bridges formed is expected to be very strong due to $d_{\pi} - P_{\pi}$ bonding (5.29). Hence there is little tendency for the oxygen atom to be basic in nature, a character which is important for the formation of hydrogen bonds.

The surface of silica, after chemisorption of water, is believed (from i.r. spectroscopic evidence) to consist of three main types of silanol group (5.34) which may interact with water molecules via hydrogen bonds in the ways shown:

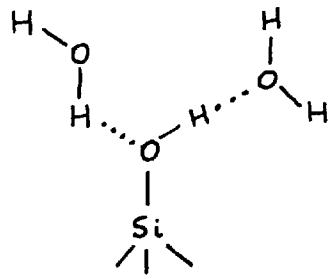

isolated silanol
group (a)

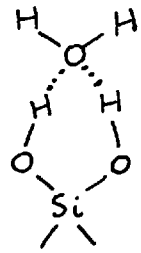

geminal silanol
group (b)

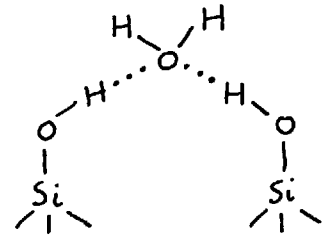

vicinal silanol
group (c)

It is now generally agreed (5.29) that water molecules adsorb preferentially on to -OH pairs of type (b) or (c) and only onto type (a) at low Si-OH surface density (i.e. partially dehydroxylated surfaces).

The Si-OH density on fully hydroxylated silica surfaces is about the same as the Si surface density expected from the rhombohedral face of β tridymite i.e. $4.6 \pm 0.2/nm^2$ (5.29). However, the surface probably consists of a variety of different crystallographic faces. The surface of fully hydroxylated crystalline quartz plates (z-cut), after polishing and etching, probably also contain various crystallographic faces, since no preferential etching was observed. Such a surface should have a similar silanol density to that of silica.

CHAPTER 6

THE PRODUCTION AND TESTING OF SURFACTANT-FREE WATER

Introduction

Since water has a high surface energy organic contaminants are liable to be concentrated at the surface. Thus even if bulk water has only about 0.01 p.p.b. contamination, if the material is strongly surface active, adsorption at the surface could markedly affect surface chemical properties (6.1). To remove levels of bulk contamination of this order poses many problems. Exposure of purified water to air for even a short time can cause sufficient contamination to alter surface properties (6.2).

Supposing pure water has been obtained, however, it is another problem to prove that it is pure and to do so without contaminating it. Purity with respect to ionised solutes is easy to measure by bulk conductivity (6.3). Since very small bulk concentrations can correspond to measurable surface contamination, it is the surface properties of the water which are often used as a monitor of cleanliness with respect to surfactant. In principle a fundamental approach is to measure the surface tension. However, the absolute value of the surface tension of water is still in dispute with reported values in the region 72.0 ± 0.2 dyn cm^{-1} at $25^{\circ}C$ (6.1). The variations are probably due to differences in cleanliness. Absolute surface tension measurements are difficult to perform with high accuracy and, in any case, surface tension is not a very sensitive criterion; also, the actual process of measurement is liable to cause contamination.

In the following sections methods of producing and monitoring surfactant-free water are reviewed and two methods are reported which were investigated in this work.

Methods of producing surfactant-free water

The most commonly used method of producing pure water is distillation. However, volatile organic species are distilled over with the steam, and unless very effective baffles are used microdroplets (1-100 nm size) of contaminated water may also be transferred in the vapour (6.3). Distilling alternately from oxidising acid and alkaline media (i.e. chromic acid and alkaline potassium permanganate solutions) should be more effective (6.6). The oxidising action may produce more soluble organic species which are retained in the residue. Also, the acid process will retain basic organic species (e.g. amines) whereas the alkaline solution will retain the volatile acidic species (e.g. carboxylic acids).

Distillation accompanied by mixed-bed (i.e. anionic and cationic) ion-exchange resins followed by activated charcoal should produce water that is free from both organic and inorganic contamination. Polyelectrolyte material may be leached from the resin (6.4) so an activated charcoal column must be placed after it.

Activated charcoal adsorbs organic compounds due mainly to the presence of a distribution of pores from 0.2 to at least 100 nm diameter (6.5). The charcoal surface contains various carboxyl groups since the surface must be oxidised in order to be an efficient adsorbent. Both chemical and physical adsorption are thought to occur; electrolytes are also adsorbed. Charcoal adsorbs 10 to 50% its own weight of aromatic organic compounds. Used charcoal is reactivated by strong heating under nitrogen.

Croll (6.6) has used a gas flow CuO furnace (at 900°C) to completely oxidise organic contamination in water. The CO_2 produced was then reduced (by a H_2/Ni catalyst, 450°C) to CH_4 which was then measured using a flame ionisation detector. The total organic carbon (TOC) in water could be measured to a sensitivity of about 0.1 p.p.m. Alkaline/acid distilled water did not contain detectable levels of organic carbon. This method of detection might also be used as a method of purifying water by oxidation of organic contamination in the CuO - packed furnace, although Croll (6.6) found it less satisfactory than triple distillation.

Using this analysis technique, it was found that storage of purified water in plastic vessels produced water containing $>$ 5 p.p.m carbon. The detrimental effect of exposure of "blank" (i.e. pure water) samples to laboratory air has also been reported. In all the methods considered here it is essential to eliminate any possibility of contact with air. This is probably best achieved by maintaining a positive pressure of filtered nitrogen in all apparatus.

The surface-active properties of the contamination were used recently by Scott (6.7) to purify water by a microflotation process. Bubbles were produced in a salt solution from a glass sinter at the base of a long narrow glass column; a froth was thereby formed at the top of the column and was continually run off. The froth contained surfactant material and the cleaned solution was drawn from the base of the column and distilled. The feed to the column was 4% NaCl solution; the electrolyte prevented the coalesence of bubbles produced at the sinter. Water obtained from this system produced bubbles which burst

immediately ($\sim 10^{-2}$ sec) (see bubble persistence test in next section).

The principle of this method is that surfactant material will be adsorbed at the bubble surface (especially when "salted out") and will therefore be carried to the top of the column where it can be removed. The degree of cleaning should depend on the gas and water flow-rates.

The method used to obtain organic-free water will depend on the amount of water required. Small amounts of very pure water may be obtained by combustion of H_2 and O_2 produced from the electrolysis of clean water, to which a little high purity salt is added. Water of crystallisation might also be used as a source of relatively small amounts of pure water. Organic impurities are unlikely to accompany water of crystallisation. Chemical decomposition. upon heating, with release of water could also be used.

Surfactant-free water can be stored in sealed glass vessels indefinitely. However, glass vessels with ground joints may be used only for short periods i.e. of the order of several days. Plastic vessels are best avoided due to the difficulty of thorough cleaning and the possibility of leaching of plastisizer, anti-oxidants and unreacted monomer from the moulded material. Where plastics must be used Teflon is the most inert and easily cleaned material. Smith (6.3) recommends leaching for 48 h in 30% NaOH solution before use.

Leakage of laboratory air into the storage vessels is usually the greatest source of contamination. Storage vessels should either be very well sealed or kept under filtered nitrogen. Storage under u.v. irradiation is effective (see Chapter 5) but is more inconvenient than storage under nitrogen.

Methods of testing water for freedom from surfactants

As already discussed, absolute surface tension measurements are not a very useful monitor of surface cleanliness. The sensitivity of this method may, however, be increased by rapidly reducing the surface area available to the contamination in a Langmuir trough. The effect of the contamination is thus increased and a much greater lowering in surface tension can be measured. However great care must be taken in this process to prevent contamination during measurement. Detection levels of about 0.5 p.p.m surfactant have been reported using this method (6.8).

A much simpler monitor is the "bubble persistance test" (6.9). Agitation of a sealed vessel containing water produces bubbles that are un-stable (bursting in less than 0.25 sec) in water which contains no surface-active contamination. Addition of less than 0.1 p.p.m of surfactant causes measurable bubble persistence. For relatively pure water the test is less sensitive because of the subjective nature of the measurement. However, the method is very useful as a rough monitor of water purity.

Total bulk carbon analysis, as described previously, is useful down to about 0.1 p.p.m carbon; however, much lower levels of contamination can be important in surface chemistry.

The effect of immersion in water on the steam test with a freshly cleaved mica sheet can be used as a simple monitor of water purity. It must be assumed however, that the surfactant contamination is of a nature to be adsorbed on to the negatively charged mica surface.

For many years water was thought to be anomalous in that air bubbles (of about 1 mm diameter) were found to rise in water at a rate corresponding to that expected for a solid sphere of equal

density. However, it is now known that this effect is caused by the adsorption of surface-active contamination on to the bubble surface (6.10, 6.11). The adsorbed material reduces the flow of the bulk fluid around the bubble, causing increased resistance and hence reducing rise velocity. Recent measurements on the rise velocities of bubbles immediately after formation (6.12) (i.e. before they become contaminated) gave higher values than those measured over a longer time in doubly distilled water (6.13). The difference in surface tension between doubly distilled water and pure water may only be about 1% but the difference in rise velocity appears to be about 100%. Hence bubble rise velocity should be a sensitive monitor of surfactant cleanliness and should not itself contaminate the water, given proper experimental conditions.

Production and measurement of surfactant-free water

Introduction

Following the previous review, two types of high purity water were investigated; distilled/ion-exchange/activated charcoal treated and micro-flotation cleaned water. Bubble-rise velocity was used as a monitor of purity of the water produced. This method is described in the following section.

Measurement of bubble rise velocity

A Pyrex column was constructed as shown in Fig. 6.1. The system was placed in-line for continuous water monitoring. A small bubble was formed on each rotation of the glass key containing a small cavity made by a diamond stylus. A thin water film was held between the glass key and the socket. When the cavity faces downwards the water in the cavity drained, presumably to a thin

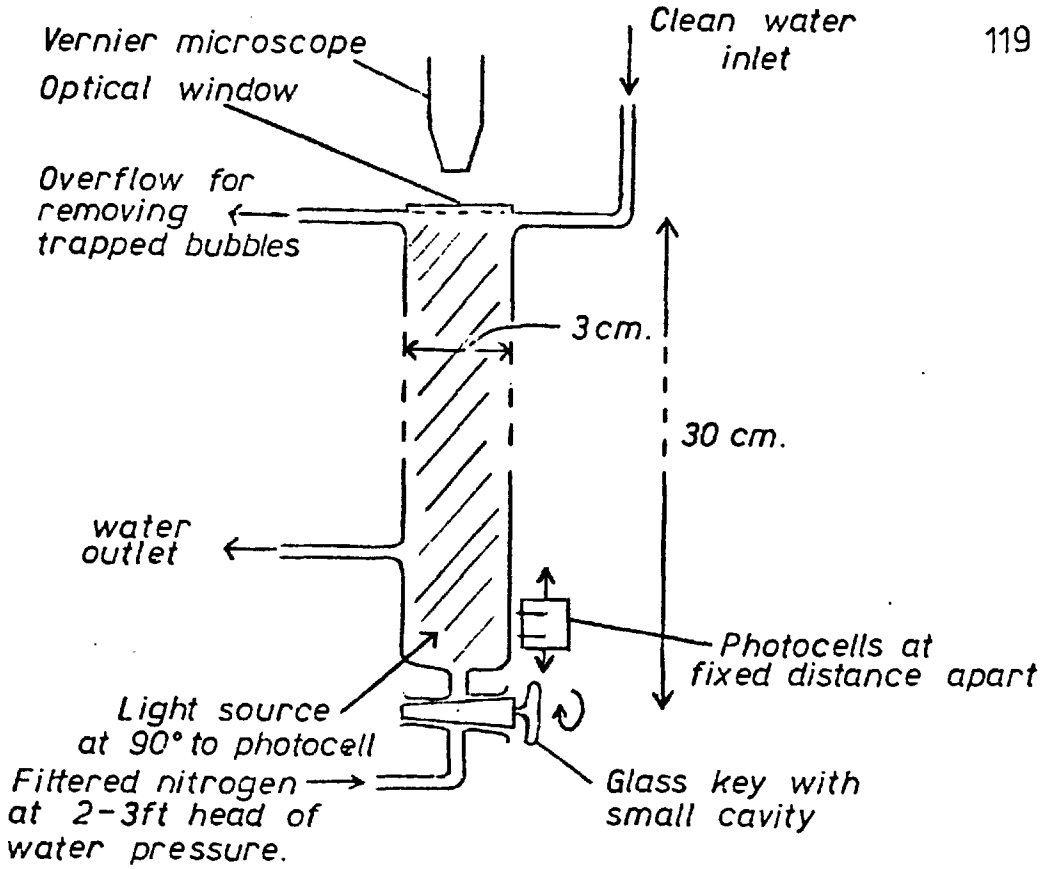

Figure 6.1. Apparatus used to measure velocity of rising bubbles

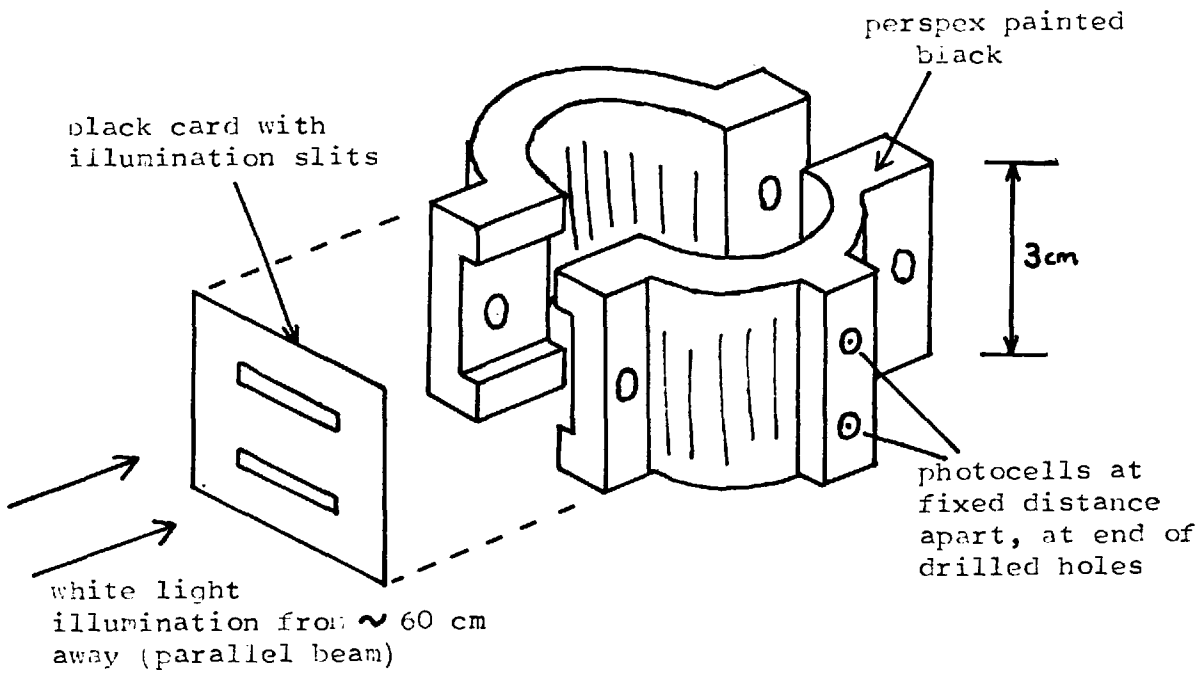

Figure 6.2. Photocell mounting

film. As the key was rotated this nitrogen cavity was trapped and then released into the column of water. The pressure of the filtered (activated charcoal) nitrogen was found to be important. If it were too low the cavity did not drain but was refilled by water from the column. If the pressure was too high the nitrogen forced water out from the film and many bubbles were released on rotation of the tap. The head of water from the column steadily forced water out through the film so that this film of water was continually replaced. If the water in the column became contaminated (with surfactant) the film on the key de-wetted and many bubbles were again released making measurement impossible. A Teflon tap was also tested but it was found that the bubbles formed were not released from a rotating Teflon key, because of the high contact angle of water on Teflon.

The bubbles generated rose in the centre of the vertical glass column which had an internal diameter 60 x the diameter of the bubbles, to avoid any wall effects. On reaching the top of the column the bubbles were caught on an optical plate where the diameters were measured using a venier microscope. The accuracy of this measurement was about 1-2%. The bubbles collected on the plate were removed by a water overflow. The diameter of the bubbles should not alter (within the accuracy of the measurement) over the height of the column, since the difference in pressure experienced by the bubbles was almost negligible.

The bubble velocity was measured with two photocells which were attached to the column as shown in Fig. 6.2.

(Unfortunately, the photocells could not be brought nearer than about 5 cm from the point of generation of the bubbles). The bubbles should have reached terminal velocity in 0.1 sec assuming

no adsorption (6.14). Even in contaminated water, according to Collins and Jameson (6.15), equilibrium adsorption should be reached typically within about 0.2 sec. Thus only terminal velocities could be measured using this equipment. (A more complicated cinematographic procedure would have to be used for measuring velocities very soon after bubble generation). For convenience, therefore, the photocells were situated 17.5 cm from the point of generation. Thus the bubbles measured were in contact with the water for about 3 sec. and a direct comparison could therefore be obtained between different quality waters.

An electronic timer accurate to 1 m sec was switched on and off by the photocells on decrease in light intensity (after initial increase) from bubbles passing the two illumination slits. The illumination source was a parallel beam of white light from a microscope lamp positioned 2 ft away from the slits. The glass column was partially covered in black paper to exclude strong light and so increase the sensitivity of the photocells. The affect of the width of the illumination slits was measured and the results obtained are given in Table 6.1. The slit width had negligible effect on the measured velocity so a width of 2 mm was chosen for these measurements. Consistent results were obtained for similar size bubbles, the limiting factor being the measurement of the diameter of the bubbles.

A. Microflotation cleaning

Method

The apparatus shown in Fig. 6.3 was constructed using only Pyrex glass and Teflon. The water flow rate used was about one tenth that used by Scott (6.7) so that better cleaning could be

Table 6.1 Effect of slit width on bubble velocity

(a) Slit width = 2 mm; distance apart 1.36 cm
time = 280 m sec; vel = 4.86 cm/sec; dia. = 0.53 mm
time = 275 m sec; vel = 4.94 cm/sec; dia = 0.53 mm
(b) Slit width = 0.5 mm; distance apart 1.38 cm
time = 274 m sec; vel = 5.04 cm/sec; dia. = 0.55 mm
time = 275 m sec; vel = 5.02 cm/sec; dia. = 0.53 mm

Table 6.2 Bubble rise velocity in flotation-cleaned water at two distances from the point of generation

at 15 cm distance:										
Velocity (cm/sec)	8.19	7.47	8.83	7.82	7.27	7.64				
diameter (mm)	0.50	0.48	0.49	0.50	0.46	0.50				
at 5 cm distance:										
Velocity (cm/sec)	6.51	5.57	4.56	4.46	6.36	5.00	7.27	4.35	4.74	7.86
diameter (mm)	0.45	0.42	0.36	0.33	0.43	0.39	0.54	0.33	0.43	0.52

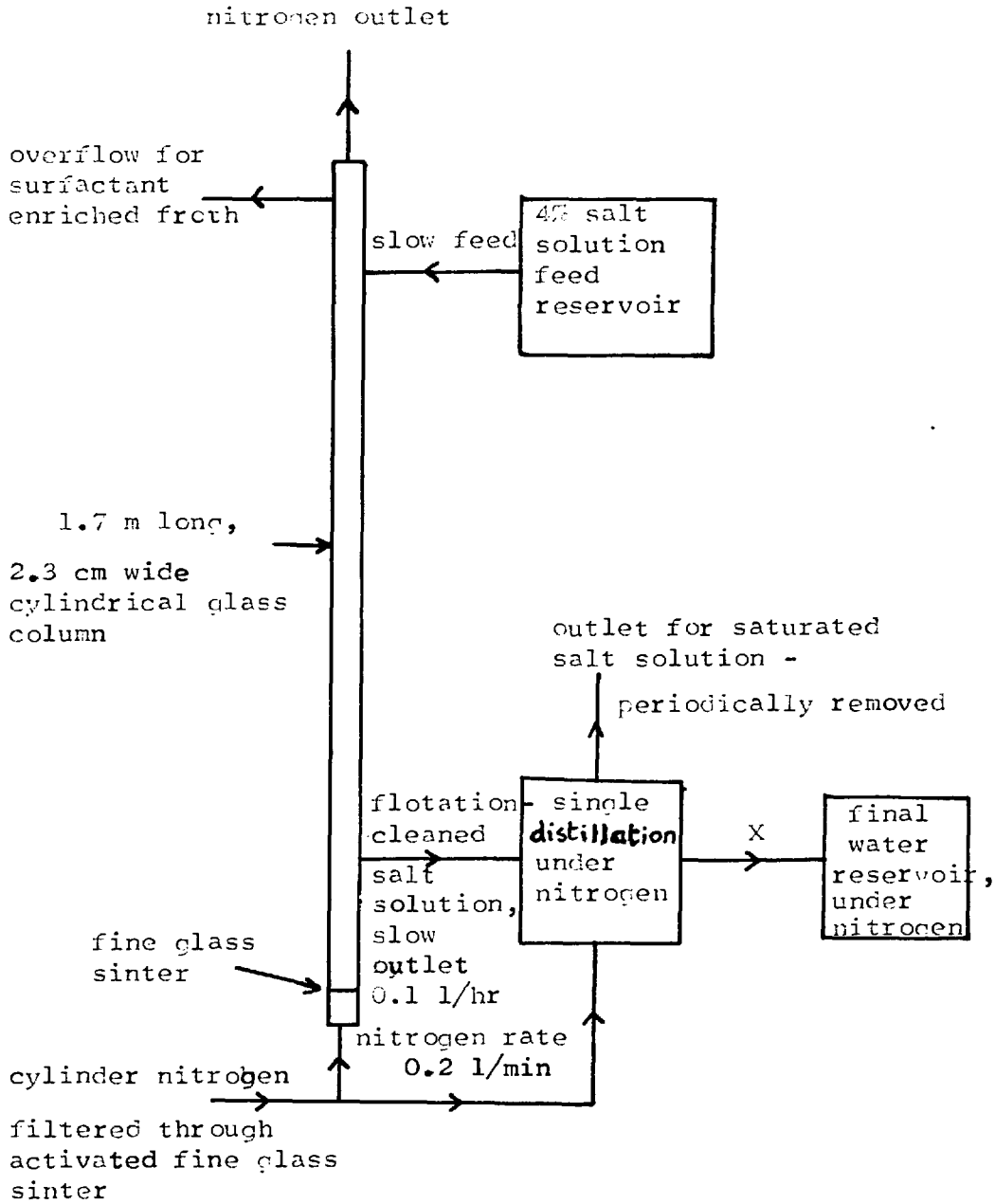

Figure 6.3. Microflotation cleaning apparatus

Note: Bubble velocity rise apparatus was fitted in-line as part of the system at point X

obtained. A 4% solution of NaCl made up in once-distilled water was used as feed. Small bubbles formed at the sinter coalesce in once-distilled water, producing very large bubbles; but addition of 4% salt causes the column to become opaque, at the same gas flow rate, due to the formation of many more, smaller, bubbles. The effect of electrolyte on prevention of bubble coalescence has recently been investigated (6.16, 6.17). NaCl solutions of greater than about 4% concentration produced no further decrease in bubble size. Obviously for efficient flotation cleaning a large transient air/water interface is required, and this is obtained by the production of very small bubbles in salt solutions. Since salt solution had to be used the feed water was probably further contaminated from organic materials present in the salt. The cleaned product from the column was once distilled (under N_2) to remove the sodium chloride. Hence the conductivity of the product should be relatively high, because of traces of salt carried over as spray.

The froth from the column was continuously run-off during operation of the apparatus. Due to the complexity of the apparatus the system could not be thoroughly cleaned after construction. Water cleaned by the system was continually washed through the system to remove possible contamination. The cleanliness of this water was monitored until no further improvement was obtained.

Results

The bubble rise velocities under different conditions were measured as described in the previous section, Figs. 6.4 and 6.5 show the measurements in water obtained under different conditions. The corresponding measurements by Bachhuber and Sanford (6.12)

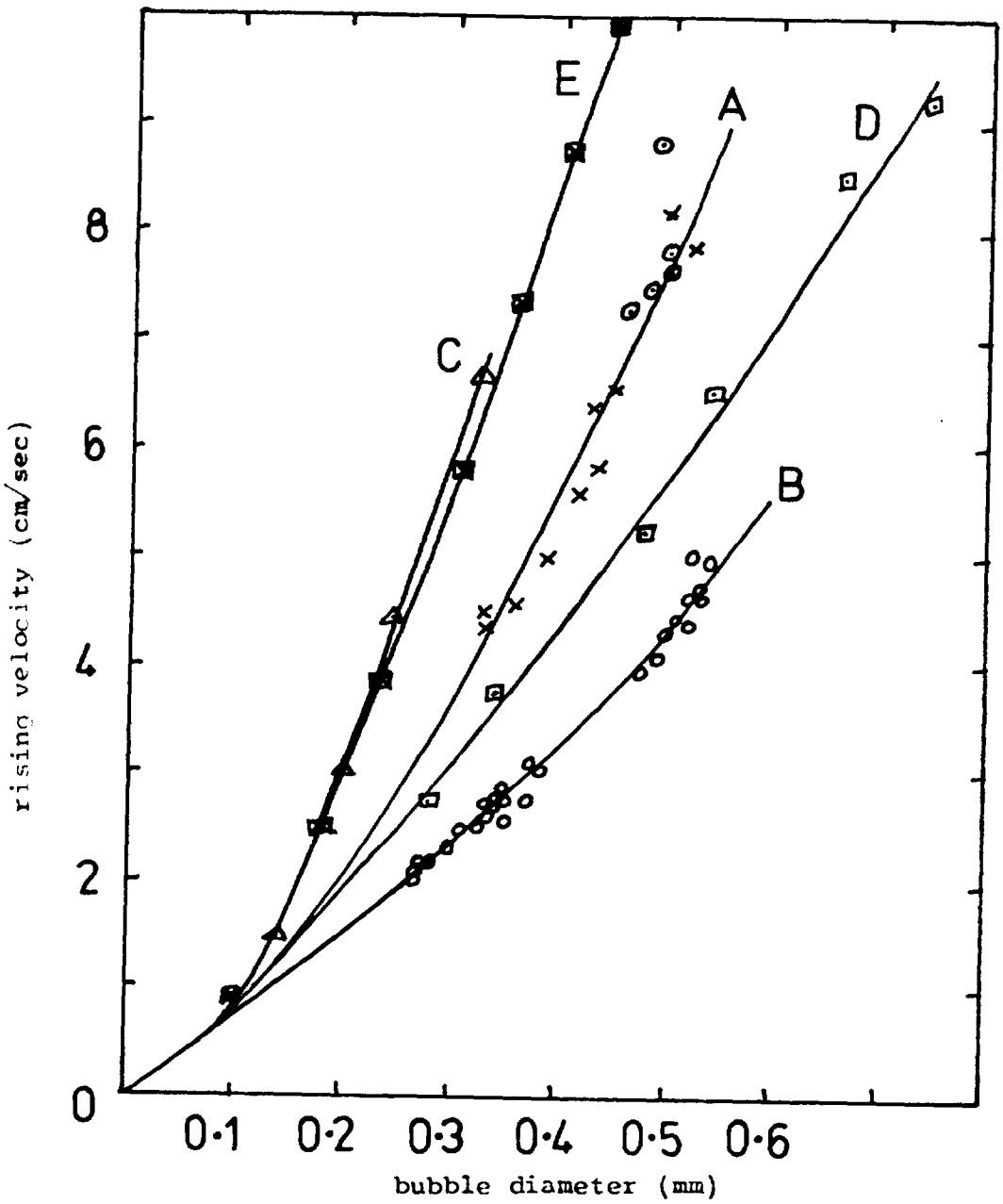

Figure 6.4. Rate of rise of small bubbles in water

A - rate of rise after initial 10 l passed through

B - rate of rise measured for same feed but without flotation cleaning

C - Bachhuber and Sanford's measurements very close to the bubble generation point, with not particularly well cleaned water.

D - Gorodetskaya's results for doubly-distilled water

E - experimental envelope curve for ideal behaviour

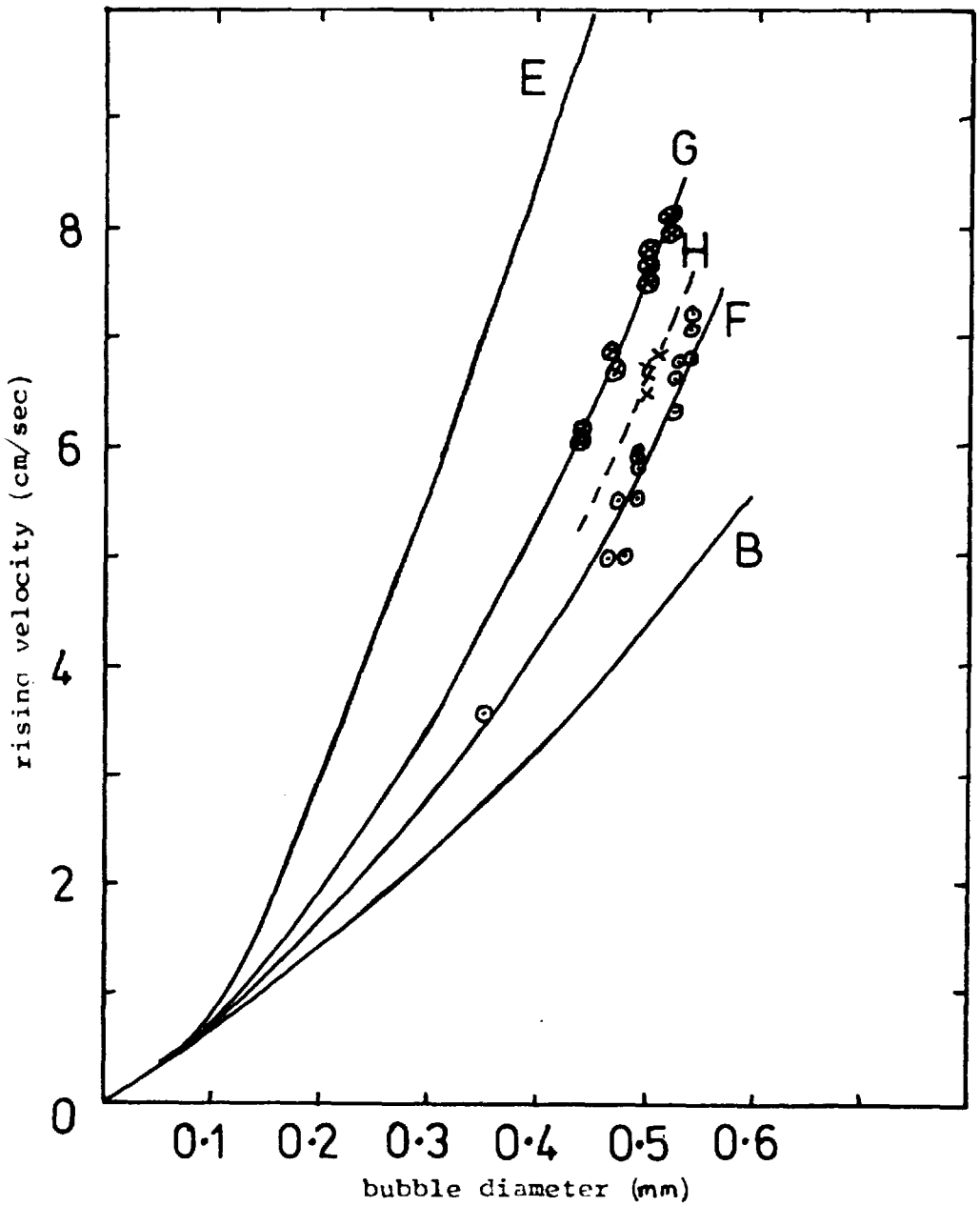

Figure 6.5. Rate of rise of small bubbles in water

F - rate after 4 l of flotation-cleaned water was passed through contaminated system

G - after addition of activated charcoal filter to F

H - laboratory-distilled water

and Gorodetskaya (6.13) are also plotted for comparison. The theoretical envelope curve obtained from non-aqueous systems, where surfactant contamination is negligible, is also shown.

The results in Fig. 6.4 show that the flotation column has a substantial cleaning effect. When the same feed was used, but without flotation-cleaning (distillation only) the rise velocity dropped by about 50% (curves A and B). The flotation system must therefore be removing steam-volatile surfactants.

After contamination of the measuring system by water B, 4 l of flotation-cleaned water were passed through the system. The measured rise velocities were then intermediate between A and B (Fig 6.5., curve F). Fresh activated charcoal was then placed in the system just prior to the velocity measuring column (Position X in Fig 6.3). After several more litres were run through, the velocities were measured and are plotted as curve G in Fig. 6.5. This curve is almost identical to that obtained from water which had been flotation-cleaned only (i.e. curve A, Fig. 6.4).

Curve A shows the results obtained for the best water obtained here from both flotation-cleaning and with activated charcoal washing. The velocities were measured both 5 cm and 15 cm from the point of generation (see Table 6.2) no difference between the results from the two positions was detected.

It was found impractical to further reduce the feed flow-rate in order to get still better cleaning. The rate used here was already one tenth that used by Scott for a similar size column and similar gas flow rate.

On leaving the bubble column stagnant for about 2 weeks initial nitrogen bubbling did not produce a significant froth at the top of the column. After about 2 hr of bubbling, however, a thick froth

was formed. Thus it appears that the surfactants diffused throughout the column are relatively rapidly transferred to the top of the column, where they can be run off. The effect of salt solution on prevention of bubble coalescence does not decrease on bubbling nitrogen through the column for several hours. Thus the prevention of coalescence does not appear to be due to surfactant present as contaminant in the sodium chloride, since this contaminant should be removed by flotation.

The specific resistivity of the final water, stored under nitrogen, was 0.4 M ohm. cm. This is very near the value expected for single distilled water (6.3). Absolutely pure water should have a resistivity of 18.3 M ohm. cm. The low value of the resistivity must be due to the carry over of microdroplets of water containing salt during distillation. Vey little CO_2 gas should be present in the water since the entire system was kept under a positive pressure of filtered nitrogen.

Conclusions and discussion

The main conclusions from this work are that the flotation-cleaning method does remove steam-volatile surfactants from water but does not produce water in which bubbles rise at the maximum expected speed. Treatment with activated charcoal does not further improve the water quality. The water obtained from this method was, however, cleaner than that obtained from double-distillation.

The ideal fluid behaviour expected in perfectly clean water (Fig 6.4, curves C and E) has been reported, for not particularly clean water, for bubbles which have had only a very short time in contact with the water (6.12). These measurements are substantiated

by agreement with the envelope curve obtained from a series of measurements on non-aqueous systems where surfactant contamination has little effect (6.10).

The bubbles measured here were in contact with the water for at least 3 seconds and therefore would give rise velocities which were dependent only on the quality of the water (see Fig 6.4., curve A). The difference in surface tension between doubly-distilled water and the water obtained from, the flotation-cleaning system should be of the order of about 1%. However, the difference in rise velocity (for a 0.5 mm diameter bubble) was about 25 - 30%.

For relatively clean water therefore bubble rise velocity is a much more sensitive monitor of surface cleanliness than is absolute surface tension measurement.

The effect of salt on the bubble size produced was most likely due to prevention of bubble coalescence after formation at the glass sinter. However, addition of electrolyte will reduce any double-layer repulsion between charged bubble surfaces. Melville and Matijevic (6.16) suggested that the effect is due to structuring of water in the interlayer between approaching bubbles. Small highly charged species such as Na^+ will thus have a larger influence on prevention of coalescence than K^+, as has been observed (6.16).

From Fig. 6.3 it is apparent that bubbles smaller than 0.1 mm diameter behave as solid spheres independent of water quality. Bubbles much larger than 1 mm are slower to become contaminated (6.14) and eventually become non-spherical.

B. Distillation - ion-exchange and activated charcoal washing

This system designed for general laboratory use (i.e $\sim$ 10 l

used per day) is shown diagrammatically below.

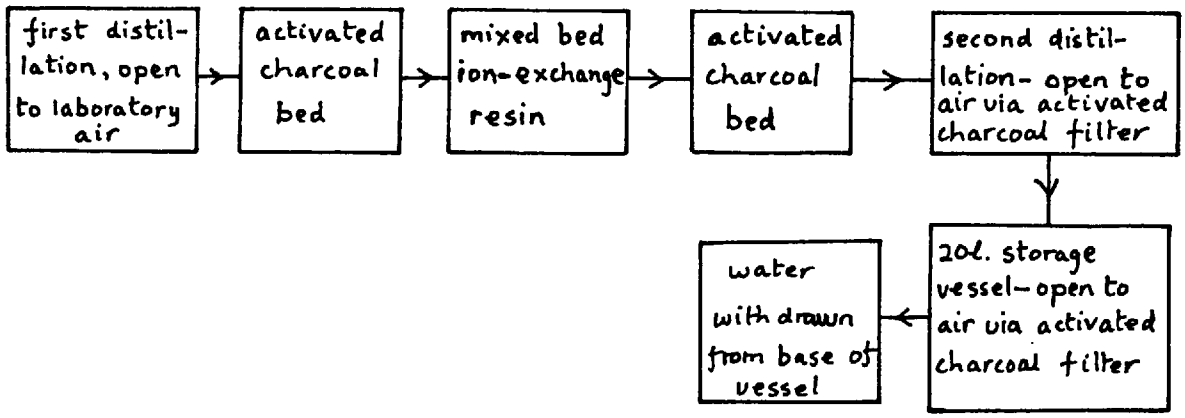

Figure 6.6. Preparation of general laboratory high-purity water

All the apparatus was constructed from Pyrex glass and was connected by glass tubes joined by short lengths of Teflon tubing. The first activated charcoal filter removed contamination from the air, present in the first distillation storage vessel. The second filter adsorbed polyelectrolytes leached from the ion-exchange resin. The ion exchange resin was an anionic/cationic mixture containing a coloured indicator. The second distillation system and final storage vessel were open to laboratory atmosphere via an activated charcoal filter. Water was withdrawn from the base of the 20 l vessel since any surfactant materials ought to concentrate on the surface of the large volume of liquid (6.2).

The main source of contamination in this system was most probably that from leakage to air. Ideally, the system should be sealed in a positive pressure of nitrogen but this proved difficult for such a complicated system. The specific resistivity of this water was about 10 M ohm cm. and its bubble persistence was < 0.25 sec. The bubble velocity apparatus was cleaned, rinsed and filled with this water. The bubble persistence of the water

sealed inside the test column was also < 0.25 sec. The bubble velocities measured in this water are given in Fig. 6.5, curve H.

The bubble velocities were approximately midway between Gorodetskaya's doubly-distilled water values and those measured in microflotation-cleaned water. It therefore appears that the flotation-cleaning process produces water containing less surfactant than distilled/ion-exchange/activated charcoal treated water.

Discussion

The water produced by the two methods appears not to be perfectly surfactant-free with respect to the sensitive bubble rise criteria. However, with regard to the wetting properties of quartz/silica the criteria will be that the water should not contaminate (and hence alters the properties of) a clean quartz surface over a reasonable length of time. Clean silica plates (see Chapter 5) which were stored in distilled/ion-exchange/activated charcoal treated water, were still clean (using the steam test) after at least four days. Quartz plates could be kept clean in saturated water vapour (using this water) in Teflon/glass sealed vessels for at least two weeks.

Water obtained from the distillation system was therefore considered sufficiently surfactant-free for use in wetting experiments on quartz and silica surfaces.

CHAPTER 7

ELLIPSOMETRIC MEASUREMENT OF THIN WATER FILMS ON QUARTZ

Methods of measuring the thickness of thin water films on quartz

Several methods are available for the measurement of the thickness of water films on quartz. The variation in the resonance frequency of quartz oscillator crystals due to water adsorption can be used (7.1, 2 and 3). Detection limits of 10^{-12} g cm^{-2} have been reported (7.2), corresponding to a fraction of a monolayer of water. However, the crystal housing and use of gold electrodes is likely to prevent adequate cleaning of the quartz plates.

Optical methods generally allow greater control over the samples used. Reflectivity measurements from "Newton's rings" interference patterns have been used to measure the thickness of alkane films down to 20 nm (7.4). Much thinner films (e.g. to 0.1 nm) can be measured by the use of multiple beam interferometry (7.5). However, two plates are required and both sides of the plates have to be highly polished, and the outer surfaces must also be silvered. These difficulties are not encountered in ellipsometry. In ellipsometric measurement only a single highly polished reflecting surface is required. The sample can be supported inside a sealed, clean, environment with two optical windows for the incident and reflected polarised beams. Very thin water films can be measured even with a relatively simple (manual) ellipsometer. Ellipsometry was therefore chosen for the investigation of water films on quartz crystals. Details of the ellipsometer constructed and results of the measurements obtained are given in the following sections.

Introduction

A historical review of the developments in ellipsometric measurement and theory has been published by Rothen (7.6).

The accuracy of ellipsometry is mainly due to the fact that the parameters measured are angles of rotation of optical components which can be measured very accurately. The best available research instruments can give Δ and Ψ (parameters measured - see later) to about $\pm 0.01^{\circ}$, corresponding to fractions of a monolayer (4.6). Automatic ellipsometers (i.e. with automatic rotation of optical components to find the null point) can be used to measure rapid changes with time. A manual ellipsometer was constructed for the present work, as rapid kinetic studies were not required.

Polarised light when reflected from a dielectric substrate with a transparent film is converted to elliptically polarised light. Degrees of ellipticity can be produced by means of a quarter - wave compensator (e.g. a mica plate of a certain thickness). The latter alters the relative phase of the orthogonal components in the plane polarised light. Hence, the ellipticity produced by reflection from a surface can be converted back to plane polarisation by the use of the $\frac{1}{4}\lambda$ plate. The orientation of the final polarised beam can then be measured with a second polarising prism. The degree of ellipticity produced by reflection also depends on the plane of polarisation of the incident beam. The parameters Δ and Ψ are determined from the orientation of the two polarising prisms and of the $\frac{1}{4}\lambda$ plate. These orientations are measured with respect to the fixed sample surface.

Conversely, the incident beam can be elliptically polarised such that the reflected beam becomes plane polarised. These two arrangements are illustrated in Figure 7.1. The $\frac{1}{4}\lambda$ plate

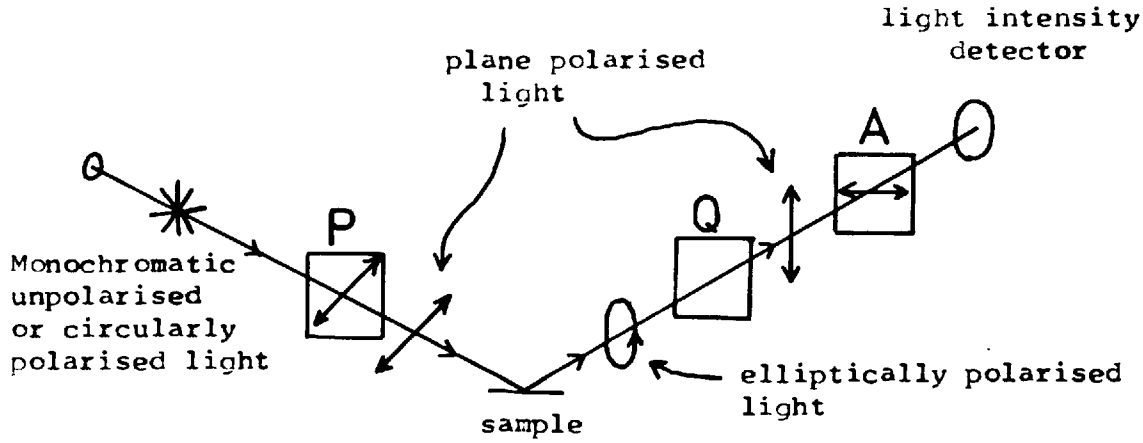

(a) plane-polarised light incident on the sample

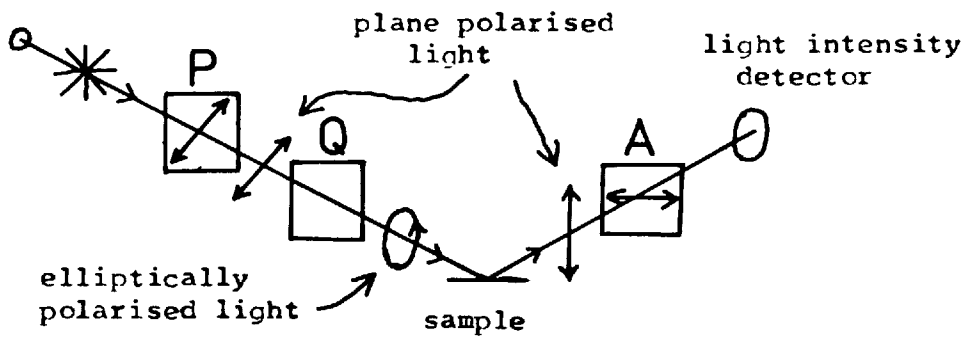

(b) elliptically polarised light incident on the sample

Figure 7.1. Common ellipsometer arrangements

produces a relative phase change of 90^{o} in the two orthogonal components when the plane of incident polarisation is at 45^{o} to either the 'fast' or 'slow' axis of the optically anisotropic mica plate (for a particular wavelength). The resultant beam then becomes circularly polarised (see Chapter 7).

The null position, i.e. where the P, Q and A components are rotated such that no light passes through the analysing prism (A), is determined by a photomultiplier device, which does not need to be calibrated for absolute sensitivity.

Variable retardation plates (e.g. the Babinet-Soleil compensator) are sometimes used to produce degrees of retardation in ellipsometry. More commonly, however, fixed $\frac{1}{4}\lambda$ compensators are used.

The orientation of the compensator is kept constant and the P and A components are rotated to produce extinction. For the case of linear polarisation incident on the sample any error in the position of the azimuth of the polariser results in a proportionate displacement of the analyser azimuth for minimum intensity. P and A therefore hunt each other in a search for the deepest minimum. With elliptically polarised light incident on the sample the position of P (assuming it is near to its final value i.e. within a few degrees) does not alter the position of A for minimum intensity. The minimum for A is not as deep (as it is when P = P min) but it is in the same position (4.4). The errors are thus not propagated and the minimum is relatively easy to locate.

Ellipsometer and sample cell construction

The manual ellipsometer constructed in the workshops of the Dept. of Mineral Resources Engineering, from variously supplied components, is shown in Figure 7.2. The instrument was designed with

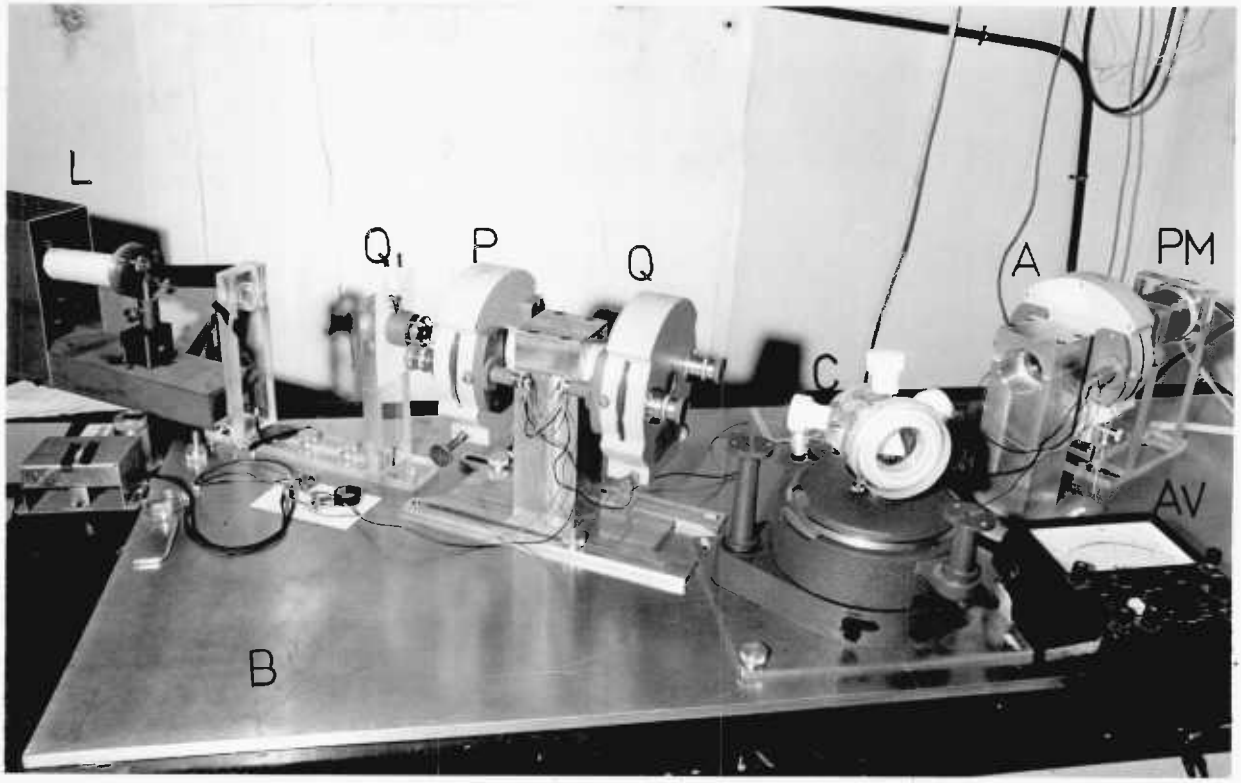

Figure 7.2. Ellipsometer constructed

L - laser: 632.8 nm, helium-neon [1]
Q_1 - mica $\frac{1}{4}$ wavelength plate [2] produces circularly polarised light from plane-polarised laser output.
P - Glan-Thompson polariser prism mounted in Bellingham and Stanley head [3] (scale to 0.01°)
Q - second mica $\frac{1}{4}$ wavelength pale mounted in "B and S" head.
C - sample cell positioned on spectrometer table.
A - Glan-Thompson analyser prism mounted in "B and S" head.
PM - photomultiplier tube [4] with stable voltage supply [5]
AV - avometer used to measure minimum current from photo-multiplier tube.
B - aluminium alloy base-plate to which components were fixed

[1] English Electric Value Co. Ltd., Chelmsford, Essex.

[2] Supplied by F. Wiggins & Sons. Ltd., London.

[3] Polarimeter heads supplied by Bellingham and Stanley Ltd., London

[4] Photomultiplier tube type 6094 B supplied by EMI Electronics Ltd. Hayes, Middlesex.

[5] E.H.T. supply type NE 5307 obtained from Nuclear Enterprises (G.B.) Ltd., Edinburgh.

the advice of Dr. B.T. Ingram and co-workers of Procter and Gamble Ltd. To simplify construction a fixed angle of incidence of about 60° was chosen (suitable for work on quartz plates) and the sample was held vertically so that all the components could be fixed to a large metal base-plate shown. The laser was tuned (by alteration of the position of the end mirrors) to achieve maximum output. At each end of the laser tube vacuum sealed quartz windows, mounted at the Brewster angle, converted the laser output to light polarised approximately parallel to the base-plate. The beam intensity was observed to be stable, as indicated on the red-sensitive photo-multiplier tube, for at least 10 minutes. Since the diameter of this laser beam was about 5 mm, no diffuser was required before the photocathode (a very narrow beam could otherwise burn out a small region of the cathode).

A mica $\frac{1}{4}\lambda$ plate was placed between the laser and a polarizing prism which was crossed (at 90°) to the laser polarisation (i.e. at minimum transmission intensity). The mica plate was then rotated until the intensity transmitted (as measured by the photomultiplier tube) was again minimum. The mica plate was then orientated with either the fast or slow axis in the plane of the laser polarisation (i.e. when the plane of polarisation lies along the fast or slow axis the retardation plate has no effect on the state of polarisation). The mica plate was then rotated through 45° and fixed. The resultant beam leaving the mica plate was then circularly polarised. This was checked by monitoring the intensity of light passing through the polariser prism, after the mica plate, on rotation of the prism; within 1% the intensity did not vary over a 360° rotation.

The position of the polariser (P, see Figure 7.2) then determined the plane of polarisation of the beam incident on the second quarter-

wave plate (Q). Following standard convention (7.7), the azimuths of the components were taken as positive counter-clockwise from the plane of incidence, when looking into the light beam.

As a laser was used as the source of polarised light no collimating systems or wavelength filters were required. A narrow band (3 nm) 632.8 nm filter was, however, inserted prior to the photo-multiplier cathode to reduce spurious room-light variations. The ellipsometer was housed in a constant temperature room with subdued light to minimize the background signal.

A sample cell was constructed out of Pyrex glass with highly polished (by means of cerium oxide polishing powder, see Chapter 5) glass flanges, containing Teflon washers, held together by both Perspex and Teflon screw caps (see Figures 7.3 and 7.5). The flange and washer joints were sufficient to hold a column of water at least 12 cm high. Two sets of three glass spikes were positioned in the base of the cell (Figure 7.3). These spikes were used to both locate the cell onto the spectrometer table (the cell being held down by a spring, see Figure 7.5) and to position the sample holder inside the cell. In both cases two of the spikes fitted into drilled holes while the third spike rested on a flat surface. This method of locating the components was found to be most convenient. The height of the spectrometer table could be adjusted, as well as its angle to the horizontal.

The Teflon sample holder can be seen inside the cell in Figure 7.5. A diagram of its construction is given in Figure 7.4. The reflecting surface of the sample was located against the three fixed Teflon spikes. The fourth spike (onto the back surface of the sample) was used to hold the sample in place. This spike was loosened when it was necessary to remove the sample. In this way, the front reflecting surfaces of the samples were always held in the same

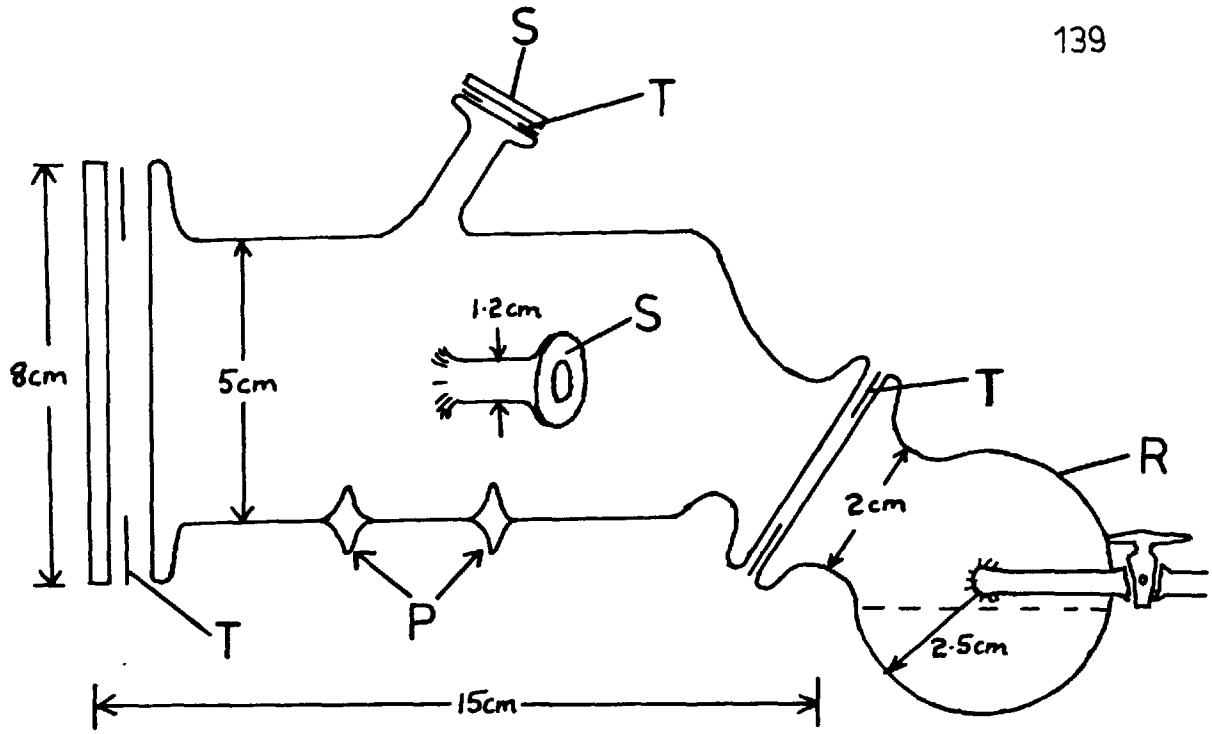

Figure 7.3. Pyrex glass sample cell

S = optical silica plate,
T = Teflon washer
R = reservoir
and P = positioning spikes

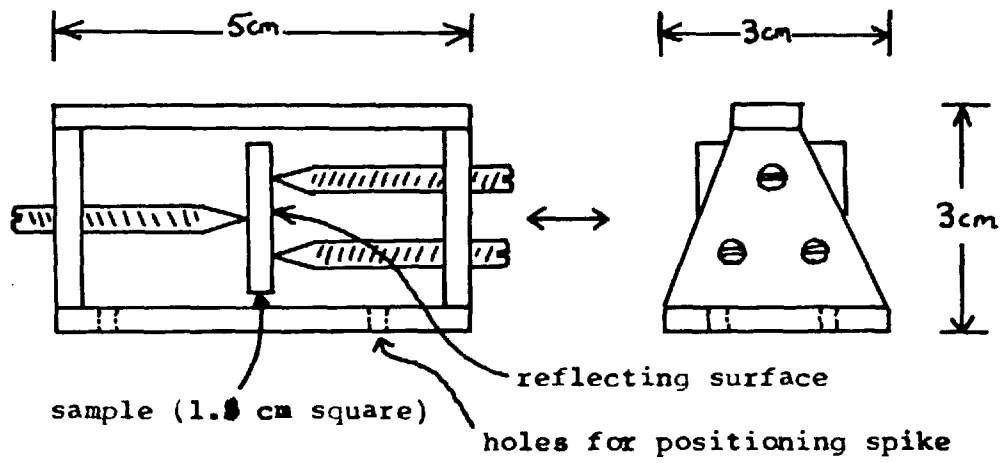

Figure 7.4. All Teflon sample holder.

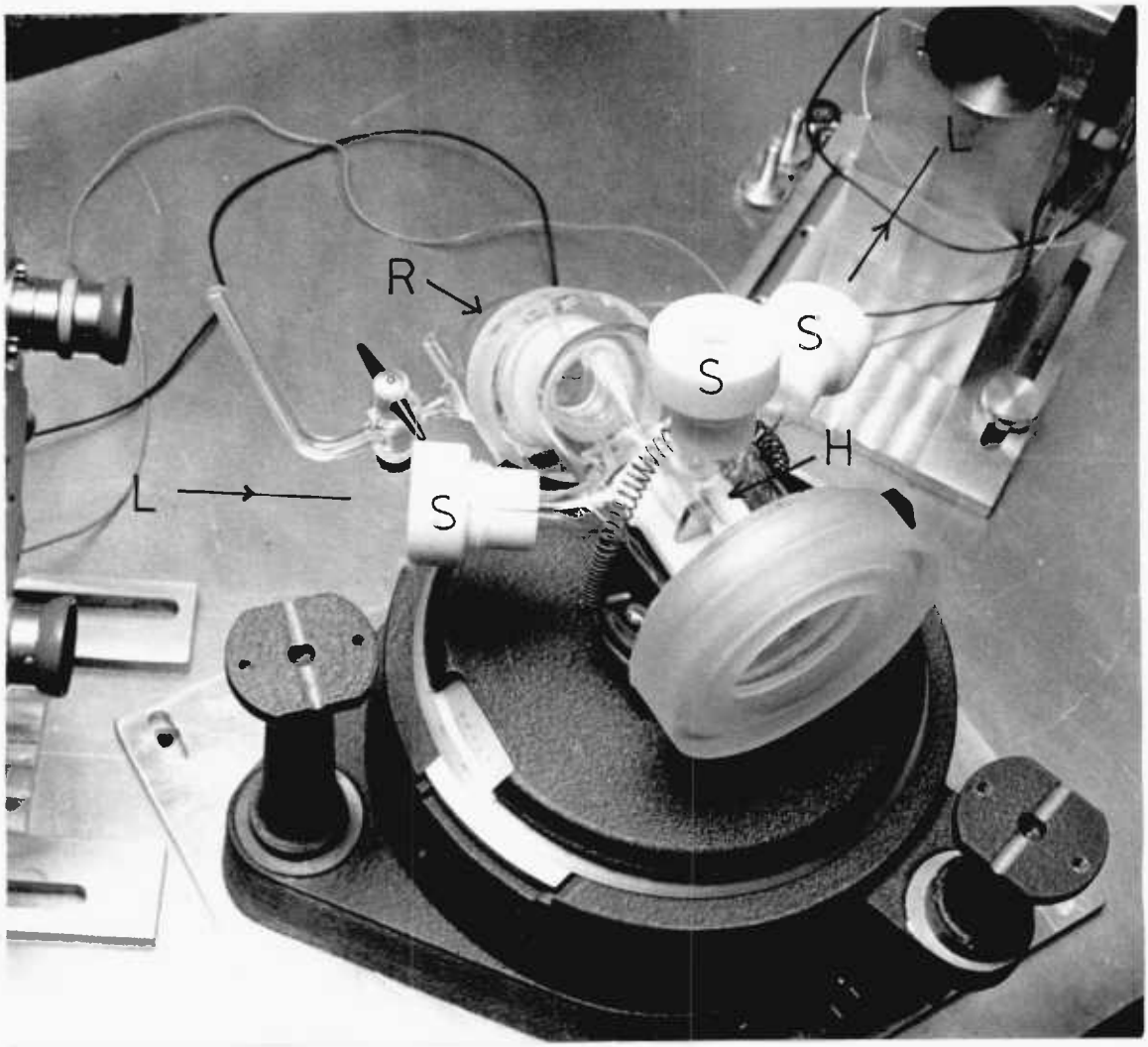

Figure 7.5. Sample cell and sample holder positioned on spectrometer table

S - optical silica windows held by Teflon caps.

H - Teflon sample holder

L - direction of laser beam

R - liquid reservoir

position independent of the thickness, shape or roughness of the back surface of the samples used.

As the laser produced an intense parallel beam, the components were easily aligned with respect to the direction of the beam. Thus if any component were not perpendicular to the beam the reflected light did not coincide with the incident beam, but gave an image beside the source. By using this procedure, the vitreous silica optical windows were positioned to within 1 - 2° perpendicular to the beam. This is within the commonly accepted tolerance angle for windows used in ellipsometry (4.4). (The state of polarisation of transmitted light is altered by deviation from normal incidence, even for a perfectly isotropic window).

A stainless steel plate was polished to give a mirror-like finish (with very few pits detectable at 200 X magnification with an optical microscope) using 1 μm size diamond paste followed by hand polishing with fine alumina powder. The plate was cleaned by washing in hot ethanol followed by thorough rinsing in hot clean water. This plate was then held in the sample holder and used as a reflecting surface to align the optical components of the ellipsometer with respect to the direction of the beam.

Alignment of the ellipsometer with respect to a reflecting surface

The alignment procedure used here was that described by McCrackin et al (7.7). This method uses the fact that pure "s" or "p" polarisation (see Chapter 4) remains linearly polarised on reflection from a metal surface, and remains unaffected by transmission through a compensator when the polarisation is parallel either to the slow or fast axis.

The quarter-wave plate (Q) and spectrometer table were removed

and the analyser (A) and photomultiplier detector were moved into a straight line with the laser source and polariser. The beam reflected from each optical component was again used to position the components perpendicular to the laser beam. The polariser (P) scale was then set to zero and the A scale was adjusted for minimum transmission. Since the scales were not exactly 90° apart the A prism was rotated in its holder so that the minimum value of $A = P + 90^{\circ}$. The P and A scales tracked each other within $\pm 0.05^{\circ}$ on full rotation.

The spectrometer table (which was positioned onto the base plate) sample cell and holder were replaced and the analyser and photomultiplier were moved back for reflection. The highly polished stainless steel plate was used for alignment since, for 60° angle of incidence, the reflected intensity of the "s" component (in the plane of sample) is substantially higher than for the "p" component (7.8). The alignment procedure is therefore sensitive to any "s" component reflected from the sample (i.e. any mis-alignment).

The plane of transmission of A was set approximately to the plane of the surface. P was then adjusted for P_{min} (value of P corresponding to minimum intensity). The P and A scale measurements were noted. The A scale was moved by about 0.2° and P_{min} was measured. If the minimum intensity meter reading was higher than before, then the A scale was rotated in the opposite direction. Thus the P and A values so measured pass through the point of minimum transmitted intensity. P and A values over a range of approximately 2° about this minimum intensity position were measured. Typical values of P is A are plotted in Figure 7.6. At the point where $P = A - 90^{\circ}$ the plane of transmission of the P prism is in the plane of incidence and the plane of transmission of A prism is in the plane of the surface. For the example shown in Figure 7.6 the scales were 0.13° out. Both

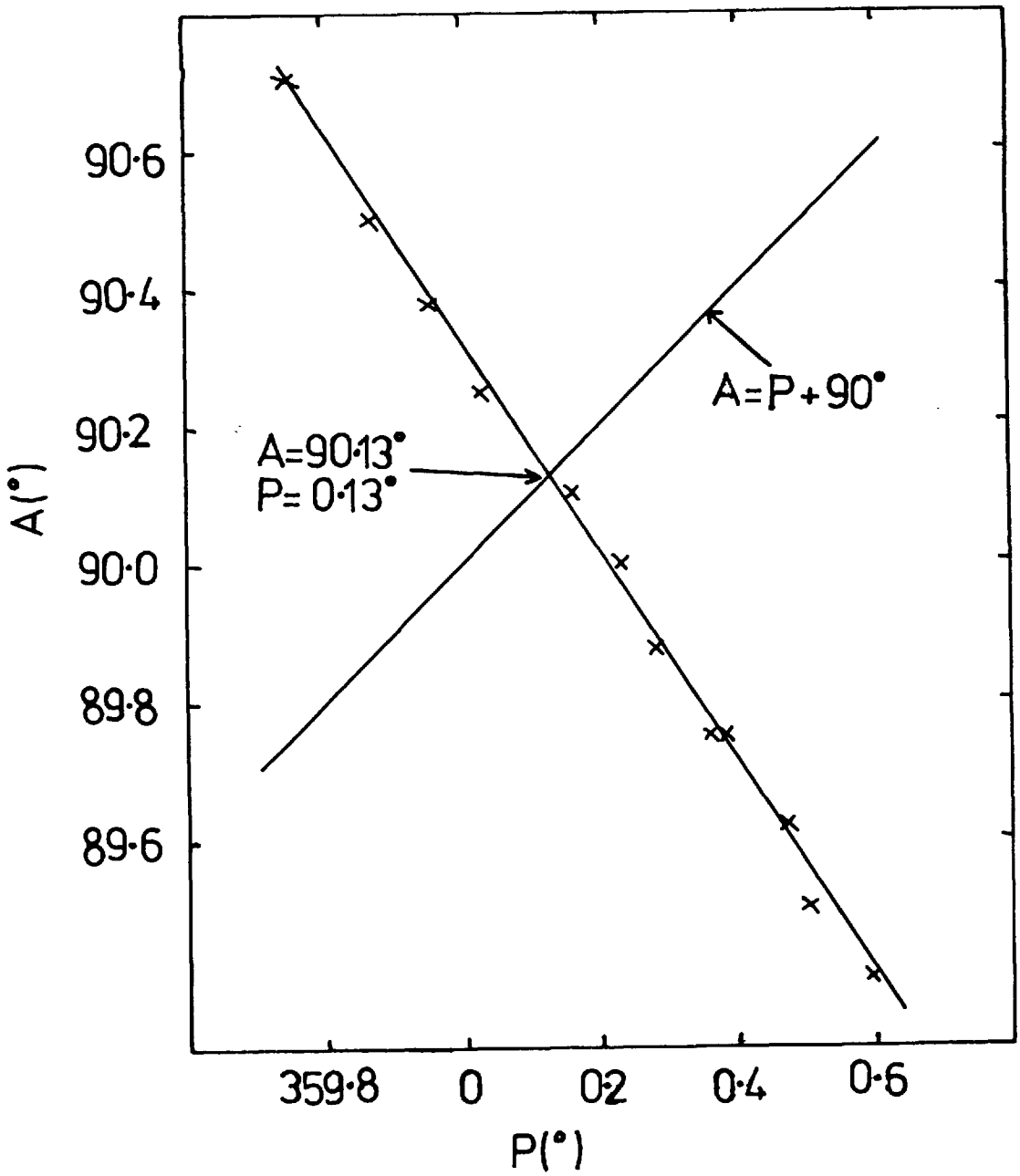

Figure 7.6. Ellipsometer alignment plot

scales were therefore 0.13° away from the true 0° and 90° azimuths. The A scale was then set at 90.13° and the P prism was rotated in its holder until the scale measured 0° for the minimum reflected intensity (with A = 90.13°).

The reflecting surface was then removed and the analyser and photomultiplier again moved to the straight-through position. The P scale was then set at 0° and the A scale was adjusted for minimum transmitted intensity. The A prism was then adjusted in its holder so that A min = 90°. The quarter-wave plate was next replaced between P and A and was rotated until the intensity transmitted was again at a minimum. In any one rotation there are 4 position, 90° apart, corresponding to two each when P is parallel to the fast and slow axis of the plate. The quarter-wave plate was rotated in its holder so that when Q = 0 (or 90°, 180°, 270°) the plate had no effect on the polarisation when P = 0°.

Table 7.1 gives typical measured results for the various combinations of P, Q and A for light reflected at 60° from a stainless steel plate, aligned using this procedure. This sample was replaced by a second polished stainless steel plate but having a thick gold film evaporated on to its surface. The results obtained with this plate are given in Table 7.2; they are in close agreement. Since the sample was changed between these measurements it is apparent that the sample holder can be removed and replaced (as well as the sample) without significantly altering the alignment.

The alignment procedure used eliminated errors due to ellipticity produced by the polariser. The effect of ellipticity of the analyser should be small, since the latter is used only for extinction of the light.

All the angles for intensity minimum values in these results

Table 7.1. Ellipsometer alignment check using highly polished stainless steel plate

polariser setting P (°)	quarter-wave plate setting, Q (°)	average of three measurements of minimum analyser setting A_{min} (°)
0.00	0.00	90.04
"	90.00	89.85
"	180.00	90.08
"	270.00	89.83
90.00	0.00	0.03
"	90.00	0.01
"	180.00	0.02
"	270.00	359.98
180.00	0.00	90.00
"	90.00	89.83
"	180.00	90.03
"	270.00	89.81
270.00	0.00	359.99
"	90.00	0.00
"	180.00	0.05
"	270.00	359.99

Total mean error $= -0.03^{\circ}$

Note: typical variation in A_{min} for set values of P and Q $= \pm 0.01^{\circ}$

Table 7.2. Ellipsometer alignment check using gold evaporated stainless steel plate

polariser setting, P(°)	quarter-wave setting, Q(°)	average of two measurements of minimum analyser setting, A_{min} (°)
90.00	0.00	0.16
0.00	90.00	359.83
0.00	0.00	0.03
90.00	90.00	0.03

Total mean error = + 0.02°

were measured by taking the average value of two measurements either side of the minimum at points of equal intensity. As the graphs of intensity minimum versus azimuth are symmetrical and have a flat base, this is the most sensitive method of locating the minimum (4.1, 4.4).

The alignment procedure was checked periodically during the course of subsequent measurements. The system was always re-aligned after the cell windows had been tightened since over-tightening was found to produce gross effects on the phase change difference between zones (see later in this chapter). This effect was due to strain induced in the optical windows.

Ellipsometric measurements on bare quartz substrates

Introduction

Crystalline quartz specimens used in this work were typically square plates 3 mm thick and of 1.8 cm side length. The polished surface was prepared as explained in Chapter 5. To avoid the use of collimators (which would be needed to separate the beams reflected from the front and back surface of the sample) the back surface of each plate was uniformly roughened. The light passing through the plate to the back surface was therefore scattered in all directions and so did not significantly affect the beam reflected from the front polished surface (since no difference, in blank measurement, was observed with a wedge-shaped plate polished on both sides where the back surface reflection was separated from the front).

Method

For a fixed retardation plate (quarter-wave plate in this case) there are 4 usual positions of the plate with respect to the surface;

these are 45°, 135°, 225° and 315°. For each of these positions there are 8 possible combinations of P and A values which will give minimum intensity transmission. The quarter-wave positions 180° apart should be identical, so only the positions 45° and 315° (or + $\pi/4$ and - $\pi/4$) are usually considered (7.7). For these two positions there are 16 combinations of P and A which will give a minimum. These combinations are split into four zones.

Since the angle of incidence and refractive index for the system considered here are approximately known the values of Δ and ψ for the bare substrate can be easily estimated i.e. $\Delta = 0^{\circ}$ (for any bare, smooth dielectric surface) and $\psi \simeq 4^{\circ}$ (corresponds to the angle of incidence chosen). From these values the possible combinations of P and A were calculated and are given in zones in Table 7.3.

Thus, from the measured values of P and A for particular settings of Q, the average value of Δ and ψ can be calculated using the equations given in Table 7.3.

Results and discussion : A. Highly polished quartz plates

For manual measurement approximately 1 h was required to determine all these values. However, McCrackin (7.7) states that measurements in only two zones (1 and 3 or 2 and 4) are necessary. Mean values of either of these pairs of zones have been reported to be very near to the values for the total average. Full zone measurements were carried out in this work to test the validity of this assumption with regard to measurements on quartz plates. Two typical sets of results are given in Tables 7.4 and 7.5.

The results obtained show that the 1/3 and 2/4 zone averages are within about 0.25° of the true mean value. For a 5 nm water film this error would correspond to about 0.2 nm. This is within

Table 7.3. Polariser and analyser settings, of the ellipsometer, expected for minimum transmitted intensity for quartz plates set at about 60° angle of incidence.

plate characteristics are assumed to be:

$$\Delta \simeq 0^\circ \; ; \quad \Psi \simeq 4^\circ$$

zone	quarter-wave compensator, $\Omega(^\circ)$	$P(^\circ)$	$A(^\circ)$
1	$(315^\circ)-45^\circ$	315 (p) 135 $(p+\pi)$ 315 (p) 135 $(p+\pi)$	4 (a_p) 4 (a_p) 184 $(a_p+\pi)$ 184 $(a_p+\pi)$
3	$(315^\circ)-45^\circ$	45 $(p+\pi/2)$ 225 $(p+3\pi/2)$ 45 $(p+\pi/2)$ 225 $(p+3\pi/2)$	176 $(\pi-a_s)$ 176 $(\pi-a_s)$ 356 $(2\pi-a_s)$ 356 $(2\pi-a_s)$
2	$+45^\circ$	135 $(\pi/2-p)$ 315 $(3\pi/2-p)$ 135 $(\pi/2-p)$ 315 $(3\pi/2-p)$	4 (a_s) 4 (a_s) 184 $(a_s+\pi)$ 184 $(a_s+\pi)$
4	$+45^\circ$	225 $(\pi-p)$ 45 $(2\pi-p)$ 225 $(\pi-p)$ 45 $(2\pi-p)$	176 $(\pi-a_p)$ 176 $(\pi-a_p)$ 356 $(2\pi-a_p)$ 356 $(2\pi-a_p)$

where $\Delta = \pi/2 + 2p$

$\Psi = a_p = a_s$

(Note: may also have corresponding values for $\Omega = 135^\circ$ and 225°).

Table 7.4. Full zone ellipsometric measurements on a bare, clean, highly polished quartz plate (in nitrogen)

set value of A or P (°)	corresponding (measured) minimum intensity value of P or A (°)	corresponding value of Δ or Ψ (°) (see Table 7.3)
Zone 1		
P = 315°	A_m = 184.06	Ψ = 4.06
"	A_m = 4.00	Ψ = 4.00
A = 4	P_m = 315.00	Δ = 0.00
"	P_m = 135.52	Δ = 1.04
A = 184	P_m = 135.50	Δ = 1.00
	P_m = 315.03	Δ = 0.06
mean values for zone 1 : Ψ_1 = 4.03°; Δ_1 = 0.53°		
Zone 3		
P = 45°	Am = 175.90	Ψ = 4.10
A = 176	P_m = 45.57	Δ = 1.14
"	P_m = 225.10	Δ = 0.20
A = 356	P_m = 225.17	Δ = 0.34
"	P_m = 45.50	Δ = 1.00
mean values for zone 3: Ψ_3 = 4.10°; Δ_3 = 0.67°		
Zone 2		
P = 135°	A_m = 4.08	Ψ = 4.08
A = 4	P_m = 135.39	Δ = -0.78
"	P_m = 314.94	Δ = +0.12
A = 184	P_m = 315.17	Δ = -0.34
"	P_m = 135.52	Δ = -1.04
mean values for zone 2: Ψ_2 = 4.08°; Δ_2 = -0.51°		

(cont.)

Table 7.4 continued.

set value of A or P ($^\circ$)	corresponding (measured) minimum intensity value of P or A ($^\circ$)	corresponding value of Δ or Ψ ($^\circ$) (see Table 7.3)
Zone 4		
P = 225	A_m = 175.87	Ψ = 4.13
A = 176	P_m = 223.46	Δ = 3.08
"	P_m = 43.52	Δ = 2.96
A = 356	P_m = 43.85	Δ = 2.34
"	P_m = 223.76	Δ = 2.48
mean values for zone 4: $\Psi_4 = 4.13^\circ$; $\Delta_4 = 2.72^\circ$		

mean values for zones 1 and 3: $\Delta = 0.60^\circ$; $\Psi = 4.07^\circ$

mean values for zones 2 and 4: $\Delta = 1.10^\circ$; $\Psi = 4.10^\circ$

Total mean values: $\overline{\Delta} = 0.85^\circ$; $\overline{\Psi} = 4.09^\circ$

Table 7.5. Full zone ellipsometric measurements on a bare, clean, highly polished quartz plate (in nitrogen)

set value of A or P (^{o})	corresponding (measured) minimum intensity value of P or A(^{o})	corresponding value of Δ or Ψ (^{o}) (see Table 7.3)
Zone 1		
P = 315	A_m = 184.04	Ψ = 4.04
A = 184	P_m = 315.19	Δ = 0.38
"	P_m = 135.72	Δ = 1.44
A = 4	P_m = 135.74	Δ = 1.48
"	P_m = 315.26	Δ = 0.52
mean values for zone 1: Ψ_1 = 4.04; Δ_1 = 0.96^{o}		
Zone 3		
P = 45^{o}	A_m = 355.78	Ψ = 4.22
A = 356	P_m = 45.50	Δ = 1.0
"	P_m = 225.14	Δ = 0.28
A = 176	P_m = 224.94	Δ = -0.12
"	P_m = 45.66	Δ = 1.32
mean values for zone 3: Ψ_3 = 4.22^{o}; Δ_3 = 0.62^{o}		
Zone 2		
A = 184	P_m = 135.56	Δ = -1.12
"	P_m = 315.19	Δ =-0.38
A = 4	P_m = 314.95	Δ =+0.10
"	P_m = 135.08	Δ =-0.16
mean value for zone 2: Δ_2 = -0.32^{o}		

(cont.)

Table 7.5. continued

set value of A or P (^{o})	corresponding (measured) minimum intensity value of P or A (^{o})	corresponding value of Δ or Ψ (^{o}) (see Table 7.3)
Zone 4		
A = 356	P_m = 44.00	Δ = 2.00
"	P_m = 223.85	Δ = 2.30
A = 176	P_m = 223.75	Δ = 2.50
"	P_m = 44.04	Δ = 1.92
mean value for zone 4: Δ_4 = 2.18^{o}		

mean value for zones 1 and 3: Δ = 0.79^{o} (Ψ = 4.13^{o})

mean value for zones 2 and 4: Δ = 0.93^{o}

Total mean value: $\overline{\Delta}$ = 0.86^{o} ($\overline{\Psi}$ = 4.13^{o})

the error limit required for adsorption isotherm measurements carried out here. For convenience, therefore, only zones 1 and 3 were measured. (A full zone measurement was also carried out for a thin water film on quartz and is reported later; very close agreement between zone averages was obtained). From the full zone measurements it was also concluded that rotation of either P or A by 180° did not significantly alter the minimum value obtained. For rapid measurements, therefore, one set of P and A values were measured for each of the two zones.

The results obtained on polished quartz plates which were cleaned by several different methods (e.g. 30% NaOH, hot conc. HNO_3 and NH_3/H_2O_2 washing - see Chapter 5) and dried in filtered nitrogen for about 1 h had phase changes of typically 0.5 - 0.9° (Ψ = 4.2 - 4.4). This would correspond to a residual water film of 0.4 - 0.7 nm thickness (i.e. about 2 monolayers) or, if due to roughness, a surface triangular ridge peak-peak height roughness of about 0.5 nm. Etching of these plates with dilute hydrofluoric acid (0.5%) did not further reduce the phase change but gradually increased it. If the phase change measured was due to the presence of a thin disturbed layer of material (of lower refractive index than quartz), mild etching ought to remove this layer and hence the phase change would fall to zero (4.3, 7.9).

It thus appears that typically produced quartz plates may have a tightly bound monolayer of water (held even in nitrogen atmosphere at room temperature) or have a slight surface micro-roughness of the order of 0.5 nm peak-peak height (or a contribution from both). For water films of 3 nm or more the error due to such blank values can be ignored.

B. Mildly polished quartz plates

A quartz plate which was opaque on both sides due to gross surface roughness was polished on one side for about 3 h using a cerium-oxide based polishing powder (see Chapter 5). This mildly polished surface was mirror-like but contained numerous pits which were clearly visible to the naked eye. The plate was cleaned in hot concentrated nitric acid and then rinsed in clean water, blown dry and stored in a nitrogen atmosphere. The phase change of this plate was then measured and found to be $+3.2^{\circ}$ (see Table 7.6).

The phase-change measured was not markedly different from that expected from a perfectly smooth surface ($\Delta = 0^{\circ}$). The phase-change would correspond to a water-film thickness of only 2.5 nm. That such a grossly pitted surface gives relatively little phase change is probably due to the almost total loss of the reflected light (by scattering) from the large pits. Thus the light detected is reflected almost entirely from the smooth, polished, regions between the pits. The phase-change observed would then correspond to that due to the micro-roughness of the polished (and hence reflecting) regions. Large roughness features (i.e. those with dimensions greater than the wavelength of the light) are therefore not detected by ellipsometry in these circumstances.

The absolute intensity of reflected light from such surfaces was, however, found to be markedly reduced relative to that for a highly polished plate.

Further polishing produced a decrease in phase change (see Table 7.6).

Table 7.6. Phase change (Δ) measured by ellipsometer for variously treated crystalline quartz plates

treatment of crystalline quartz surface	typical Δ measured
cerium oxide-based polishing followed by ultrasonic and hot concentrated nitric acid cleaning	$+0.50^{\circ}$ (0.38 nm)
as previously but with 2 hour etching in 1.5% NH_4HF_2 solution at room temperature	$+0.85^{\circ}$ (0.65 nm)
as previously but with 24 hour etching at room temperature	$+2.2^{\circ}$ (1.7 nm)
initially very rough plate (opaque) after only 3 hours polishing (producing mirror-like finish, but with many clearly visible pits)	$+ 3.2^{\circ}$
previous plate after further 6 hours polishing	$+ 1.4^{\circ}$
clean, highly polished plate pulled through a concentrated solution of cetyltrimethylammonium bromide - increase in Δ given.	$+ 3.1^{\circ}$

C. Mildly and grossly etched quartz plates

A highly polished crystalline quartz plate was cleaned in hot concentrated nitric acid and blown dry, as before. The phase change of this plate was measured dry after etching in 1.5% NH_4HF_2 solutions for 2 h and 24 h at room temperature. The results are given in Table 7.6.

The peak-peak surface roughnesses corresponding to these phase-changes (as calculated from the theory given in Chapter 4) are shown in parenthesis in Table 7.6. Thus even after 24 h etching in dilute hydrofluoric acid solution the phase charge, and hence the apparent surface roughness, were found to be only slightly increased. This observation has been reported by other researchers for the hydrofluoric acid etching of vitreous silica (4.2, 4.3, 7.9). The effect of such etching on surface roughness has not, however, been investigated. In Chapter 5 the shadow-replica electron micrographs of quartz plates etched for both 2 h and 17 h in the same concentration of NH_4HF_2 solution were given. Plates etched for 2 h showed negligible increase in surface roughness compared with highly polished plates. Plates etched for 17 h showed only slight, uniform, surface roughness of about 3 nm peak-peak height.

Considerable amounts of the surface should be removed after this length of time (see Chapter 5). However, the etching appears to be almost uniform and no great increase in roughness occurs. The peak-peak height estimated from ellipsometric measurements, using the theory explained in Chapter 4, agree very roughly with those obtained from electron microscopy.

The quartz surfaces after 17 - 24 h etching were still mirror-like, although again the absolute reflected light intensity was reduced by surface roughness.

D. Grossly contaminated quartz plates

A clean quartz plate was withdrawn through the surface of a strong solution of cetytrimethylammonium bromide, followed by drying and 15 min. storage in nitrogen. The phase change measured on this plate is given in Table 7.6. This phase change corresponds to a "grossly contaminated" quartz plate.

The sensitivity of the phase change with respect to surface cleanliness depends on the refractive index of the contaminating material. Thus any organic contamination which has a refractive index of about 1.54 would not be detected on the surface of quartz by ellipsometry. Typical fatty materials (common contaminants) have refractive indices around 1.45. Such materials would not be detected on the surface of vitreous silica but would be on quartz.

Cetyl bromide has a refractive index of 1.46 which should be near to that of the cetyltrimethyl ammonium bromide film measured. The thickness of this film would therefore be about 3 nm.

Ellipsometric measurement of water films on quartz

Method

The plates used in these measurements were polished, etched, cleaned and dried using the methods described in Chapter 5. The glass cell was also thoroughly cleaned before use. The vapour pressure inside the cell was varied by using different concentrations of sodium chloride solution. The salt was cleaned by heating to 600°C in an electric oven, open to air, followed by cooling under nitrogen.

The vapour pressure of such solutions has been accurately determined at 25°C (7.10, 7.11). Pure water was used to obtain saturated vapour pressure. Generally, the water used was that

obtained from the laboratory distillation system already described (Chapter 6). But water distilled from acid and alkaline solution was also used.

This method of controlling vapour pressures has been used by Ershova et al (1.11). Alternatively the vapour pressure can also be varied by applying a temperature differential between reservoir water and sample (1.11, 7.12) but this method is more difficult to arrange because two small but very accurate thermostats are needed. A suction technique via a porous plug has been recently used (1.12) to control vapour pressures near to the saturated region. In this method, however, the possibility of contaminating the sample is higher (because of the hydraulic connection with the reservoir) and the apparatus required is more complicated than that used here.

To preserve uniformity of temperature, the cell was surrounded by cotton wool and was placed inside a cardboard insulating box, in a constant temperature room. The temperature of the air inside the box was 25.0°C ± 0.1°C (monitored using a quartz oscillator thermometer to 0.01°C). a maximum drift of 0.2°C occurring over at least 24 hours. The variation in temperature inside the insulated cell was typically about 0.05°C over a period of 12 hours. Temperature differences between different positions inside the insulated glass cell (e.g. between water or solution immediately below the sample and the sample itself) should therefore be no more than about 0.02°C . The effect of small temperature differences on the partial pressure can be calculated from the following equation (which may be derived from the Clausius - Clapeyron equation):

$$\ln. \; P_2/P_1 = \frac{\Delta H_v^m}{R}\left(\frac{1}{T_1} - \frac{1}{T_2}\right) \qquad 7.1$$

where P_n is the vapour pressure at a position where the temperature is T_n, ΔH_v^m is the molar latent heat of vaporisation of the liquid (assumed to be independent of temperature) and R is the molar gas constant. In deriving equation 7.1 it was also assumed that the molar volume of the vapour is much greater than that of the liquid.

For the case of water equation 7.1 becomes:

$$\ln. P_2/P_1 = \frac{5.24 \times 10^3 \times \Delta T}{T_1 \times T_2} \qquad 7.2$$

using this equation, it can be calculated that if the temperature difference between sample and water vapour source were 0.05°C the error in P/P_o would be 0.003; if the difference were 0.02°C the error would be 0.001. Thus the maximum error in relative vapour pressure should be about 0.001.

Both the sample cell and solution and the sample itself were allowed to come to thermal equilibrium in the constant temperature room before sealing the sample in the cell. Filtered nitrogen was used to prevent the sample and interior of the cell coming into contact with laboratory air. The possibility of temporary supersaturation was thus kept to a minimum.

Results

A. Clean, highly polished quartz surfaces at saturated vapour pressure

In a series of preliminary experiments the initial film thickness measurements were made for clean plates sealed in the cell with water held in the reservoir (see Figure 7.3). The film thicknesses measured as a function of time after sealing the cell are given in Figure 7.7. (At the time of sealing, the cell was filled with

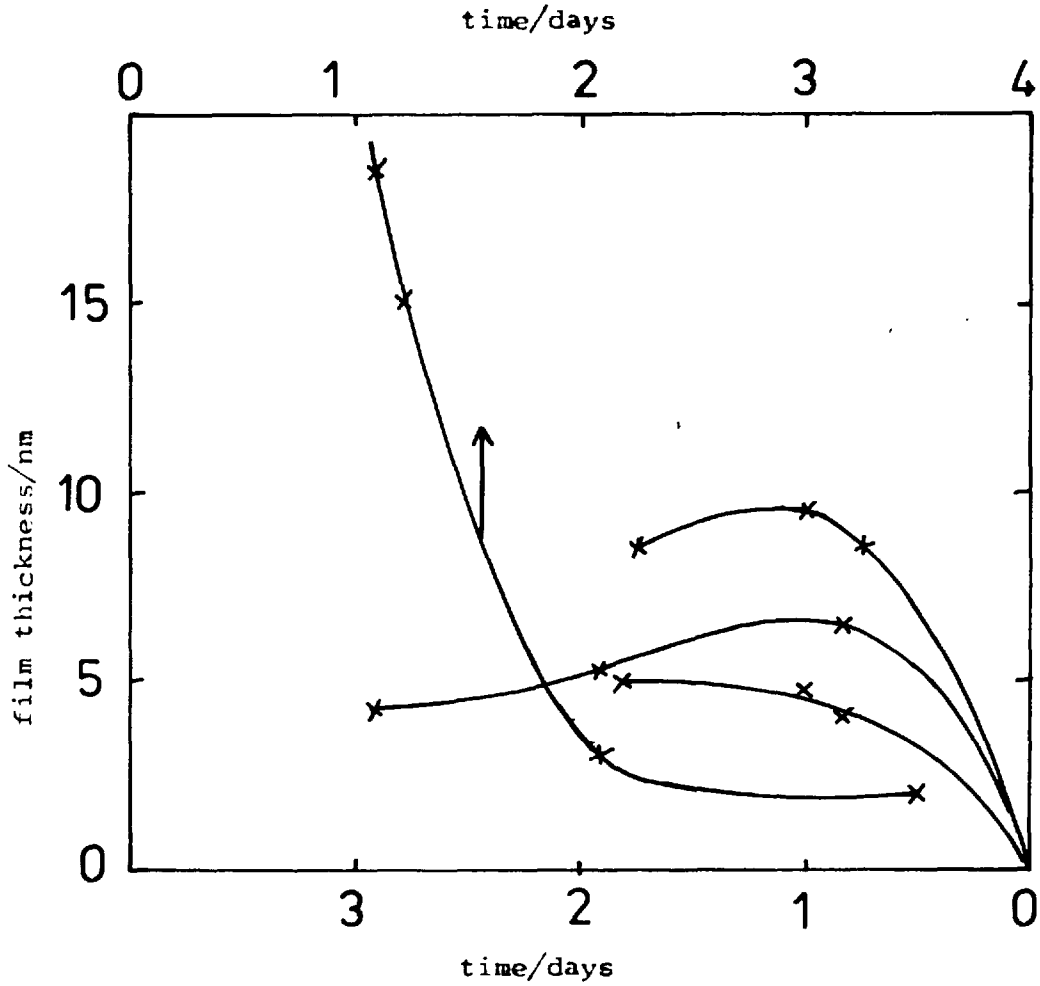

Figure 7.7. Water film thickness measured on clean quartz plates as a function of time when using reservoir as water vapour source.

filtered nitrogen gas, used to prevent contamination from laboratory air).

The "equilibrium" film obtained was about 5 nm thick whether the plate was initially wet or dry. When a small amount of clean water was placed in the sample cell, it was observed to distil into the reservoir. Thus the bulk of the cell was not at saturated vapour pressure. After a clean quartz plate had come to equilibrium with the reservoir water (after 24 h), further insulation was added (for a further 24 h). However, this had no affect on the film thickness. Reservoir water was then run into the main part of the cell by tilting the cell and reservoir. Within 6 h the film thickness had increased to 23 nm. It thus appeared that saturation was not obtained in the main part of the cell around the sample. This could have been due to very slow vapour diffusion transfer from reservoir to the bulk of the cell.

In order to obtain vapour equilibrium more rapidly, the reservoir was removed and the connecting orifice sealed with a silica plate. The water (or solution) used was then held in the base of the cell just below the sample holder. The surface area available for evaporation was thus increased and the distance from the sample to the solution was reduced from about 13 cm to 2 cm. There was no danger of the liquid creeping by capillarity on to the sample because it was insulated by its Teflon holder which was not wetted.

A clean quartz plate was sealed in this smaller cell with clean water in the base of the cell. The increase in film thickness, of the initially dry sample, with time is given in Table 7.7. Filtered nitrogen was then slowly blown onto the surface containing the thick film and the thickness of the film was monitored during thinning of the film. When the plate was again dry the cell was

Table 7.7. Variation of water film thickness with time for a clean crystalline quartz plate sealed, initially in a nitrogen atmosphere, with water.

time after initial sealing	Δ (°) (measured)	Ψ (°) (measured)	corresponding water film thickness (nm)
18 h	37.3	10.3	~ 43
20 h	38.1	9.0	~ 45
25 h	37.7	9.3	~ 45
3 days 18 h	1.5	15.4	~ 150*
time after slow rate of nitrogen blown into cell			
1 min	~ 20°	~ 14.5	~ 130
2 min	~ 25	~ 14.5	~ 125
5 min	~ 40	~ 13	~ 85
10 min	~ 44	~ 10	~ 70
20 min	~ 44	~ 8	~ 60
25 min	38.5	7.3	~ 45
1 h	35.2	7.3	~ 37
(increased N_2 flow rate):			
1 h 25 min	~ 2.3	~ 4	~ 1.8
resealed cell:			
35 min	28.3	5.6	26.5
4 h	31.5	5.7	30.0
21 h	35.9	8.0	~ 40

* Coloured fringes observed all over sample.

(Note: these measurements are plotted in Fig. 7.9 for comparison with theoretically calculated values).

resealed and the film thickness was again monitored with time.

That the water film corresponding to $\Delta \simeq 0^{\circ}$ and $\psi \simeq 15^{\circ}$ was about 150 nm thick was proved by the observation of coloured fringes which were clearly visible to the naked eye on the sample sealed in the cell for 3 - 4 days. Such thick films were stable for at least 3 days and were consistently formed on clean quartz surfaces sealed in equilibrium with surfactant-free water.

When the cell water became contaminated (i.e. after several days, judged by the bubble persistence test) the thickness of the film dropped to about 10 nm. The sample then gave either transparent mist or mist and fringes in the steam test. Great care had to be taken to obtain and transfer clean quartz plates and to keep the vapour source water clean. Many experiments were abandoned due to obvious contamination which was found to be very difficult to prevent.

When a clean quartz plate was stored dry in a sealed vessel next to the sample cell (itself sealed, containing clean water) in the constant temperature room for about 24 hours and then rapidly placed in the cell and sealed, the film thickness increased consistently to approximately 150 nm after about 1 hour. This thick film was stable for about 3 days depending on how quickly the cell became contaminated. The film thickness increased rapidly, presumably because the cell already contained saturated vapour when the sample was introduced. When the cell initially contained dry nitrogen, the film thickness increased more slowly. The rate of increase, however, also appeared to depend on the cleanliness of the water used as vapour source. Monolayers of surfactant are known to reduce the rate of water evaporation (7.13) and presumably traces of contamination caused the slower increase in film thickness. If the vapour-source

water was sufficiently contaminated, the contamination migrated to the plate and only a thin film could then be formed.

To prove that the thick film was not formed via supersaturation, a plate which was warmer by several degrees than the cell and water (which had been sealed for about 24 hours in the constant temperature room) was sealed in it. A thick film was still formed after several hours.

The Δ and ψ values measured by the ellipsometer for various water films from 1 to about 150 nm are given in Figures 7.8 and 7.9. Up to 30 nm agreement, within experimental error, with the theoretically calculated values (full line) was obtained. For films thicker than 30 nm the measured values deviate from the theoretical curve. At the point where $\Delta = 0$ again (i.e. for thick films of about 150 nm) the ψ values correspond to these for a film of refractive index 1.39. However, in the region of large Δ values the measured values correspond to those expected for a film of about 1.33 ± 0.05 refractive index (i.e. over the range 30 to 80 nm). The cause of the apparent deviation for thick films was not the build-up of thick water films on the window, because when the windows were removed immediately before a measurement, the values of Δ and ψ did not alter. A wedge-shaped plate, highly polished on both sides, was cleaned and sealed in the cell with water. After a similar length of time the same results were obtained. Thus the deviation was not due to the back-surface of the plate (which was opaque when dry) becoming a better reflecting surface when wet and hence interfering with the front-surface reflected beam. The reflection from the back-surface of the wedge shaped plate was easily separated from that of the front surface.

Since patterned coloured fringes were observed on the clean plate the film cannot be uniformly thick over areas of more than about 1 mm^2.

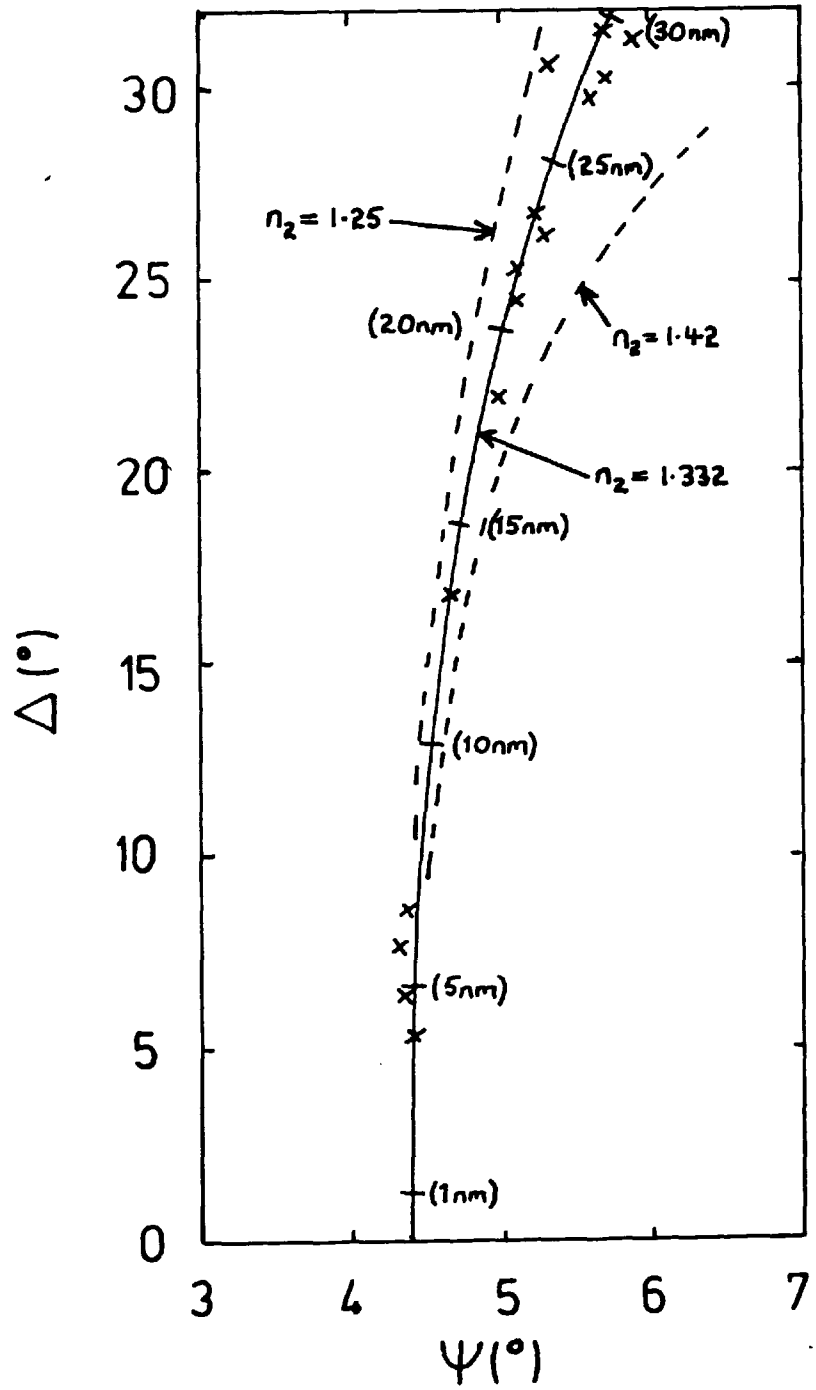

Figure 7.8. Theoretically calculated and experimentally measured values of Δ and Ψ asa function of film thickness

(where $\phi_1 = 59.85^\circ$, $n_3 = 1.543$ and $\lambda = 632.8$ nm)

X - experimentally measured values

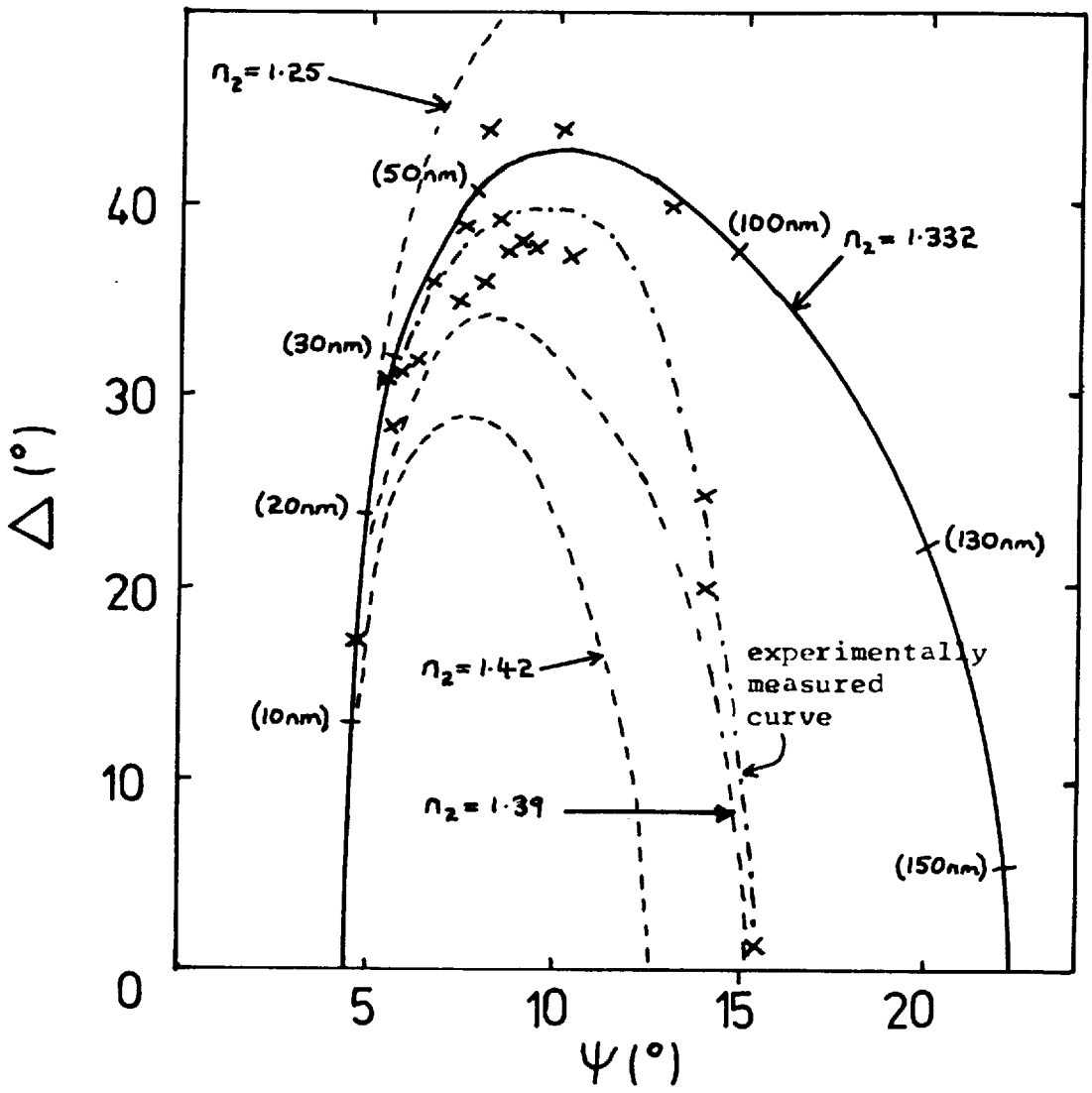

Figure 7.9. Theoretically calculated and experimentally measured values of Δ and Ψ as a function of film thickness

(where $\phi_1 = 59.85^\circ$, $n_3 = 1.543$ and $\lambda = 632.8\text{nm}$)

X = experimentally measured values

The effect of such a wavy-type film (of typically 1 mm wavelength) may be to cause deviations for Δ and ψ values for such relatively thick films. The Fenstermaker-McCrackin type treatment would not apply to such a system since the "film roughness" observed was much larger than the wavelength of light.

After up to 7 days sealed in the cell the quartz plate still gave excellent uniform fringes in the steam test.

For convenience, quartz plates were usually cleaned by washing for 20 seconds in hot 30% sodium hydroxide solution, followed by water washing and blow drying. Plates cleaned with hot concentrated nitric acid or hot ammoniacal hydrogen peroxide also gave fringes when sealed in the cell with clean water.

As explained previously, normally zones 1 and 3 only were measured, however, all 4 zones were measured on a quartz plate cleaned and dried and sealed in the cell with clean water for 2 hours. The phase change and azimuth values measured for the 4 zones are given in Table 7.8. From these results it is apparent that the zone averages (1/3 and 2/4) agree very well for films of this thickness. From Figure 7.8 the measured values of Δ and ψ accurately correspond to a water film of 20 nm thickness.

An optically polished vitreous silica plate was cleaned with sodium hydroxide solution and sealed dry in the cell with clean water. After about 24 hours the film thickness was found to be 43 nm. Thus, as observed in the steam test, clean vitreous silica behaves in an almost identical manner to crystalline quartz, with respect to its wetting properties with water.

A drop of clean water was placed at the base of a vertical clean quartz plate while held in the Teflon holder. Uniform fringes were formed above it and were stable for at least 5 hours (sealed

7.8. Four-zone ellipsometric measurements of thin water film on crystalline quartz (at $P/P_o = 0.98$).

set value of P or A	corresponding (measured) minimum value of A or P	corresponding value of Δ and Ψ (see Table 7.3)
Zone 1		
P = 147	$A_m = 4.7$	$\Psi_1 = 4.7^\circ$
A = 5	$P_m = 147.13$	$\Delta_1 = 24.3^\circ$
Zone 3		
P = 58	$A_m = 354.75$	$\Psi_3 = 5.25^\circ$
A = 355	$P_m = 57.5$	$\Delta_3 = 23.0^\circ$
Zone 2		
P = 124	$A_m = 4.93$	$\Psi_2 = 4.9^\circ$
A = 5	$P_m = 123.5$	$\Delta_2 = 23.0^\circ$
Zone 4		
P = 33	$A_m = 354.85$	$\Psi_4 = 5.15$
A = 355	$P_m = 32.93$	$\Delta_4 = 24.14$

mean values for zones 1 and 3: $\Delta = 23.6^\circ$; $\Psi = 4.85^\circ$

mean values for zones 2 and 4: $\Delta = 23.6^\circ$; $\Psi = 5.04$

Total mean values: $\overline{\Delta} = 23.6^\circ$; $\overline{\Psi} = 4.95^\circ$

These measured values of Δ and Ψ correspond (see Fig. 7.8) to a water film thickness of 19.8 nm.

in the cell, containing clean water). Thus clean water on the surface of clean quartz must have a zero or very low contact angle. The significance of these results, in relation to previously published work, will be considered later.

B. Clean quartz surfaces in equilibrium with solutions of relative vapour pressures below saturated

The sodium chloride solutions used in this part of the work gave relative vapour pressures (at 25°C), P/P_o = 0.90, 0.95, 0.965, 0.973 and 0.98. Equilibrium thickness of water films were assumed to have been obtained when the measured values were constant over about 24 hours. Typical variations of film thickness with salt solutions as the film approaches equilibrium thickness are given in Figures 7.10 and 7.11. In both cases about 3 days were required to reach equilibrium, even though the salt solutions were initially already at the same temperature as the cell.

The equilibrium film thicknesses measured at various vapour pressures are given in Figure 7.12, curve A, with the times required to come to equilibrium (as defined above). The results obtained clearly show that as the relative vapour pressure approaches the saturation value for pure water, the thickness of the film increases sharply. Where the thickness changes rapidly with relative vapour pressure the measured values are less precise. The curve does not intersect the axis for P/P_o = 1 except for films of about 150 nm thickness. The values of Δ and Ψ measured for water films formed in equilibrium with various relative vapour pressures are given in Table 7.9.

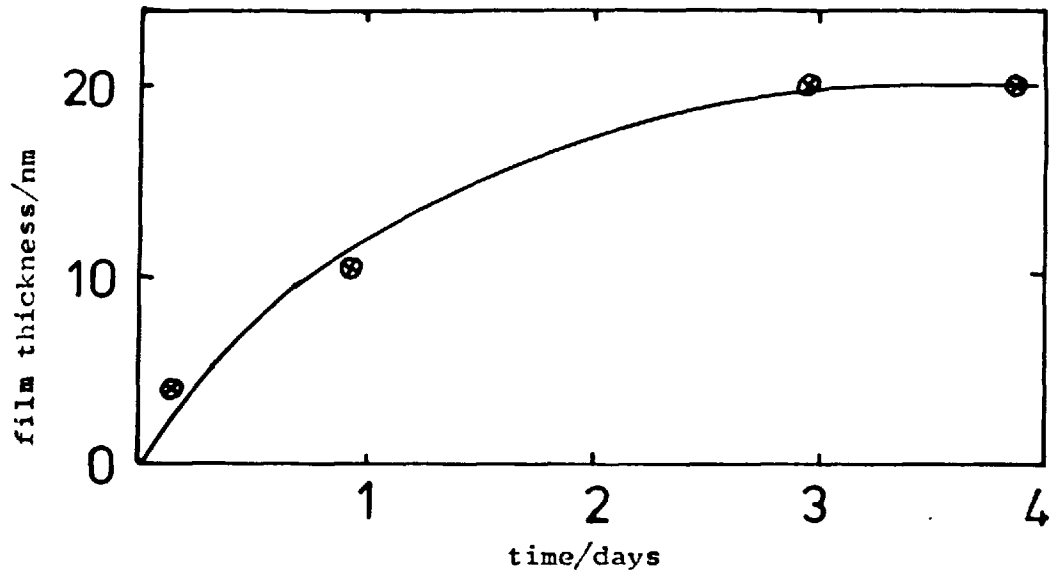

Figure 7.10. Thickening of water film on initially dry quartz surface $P/P_o = 0.98$

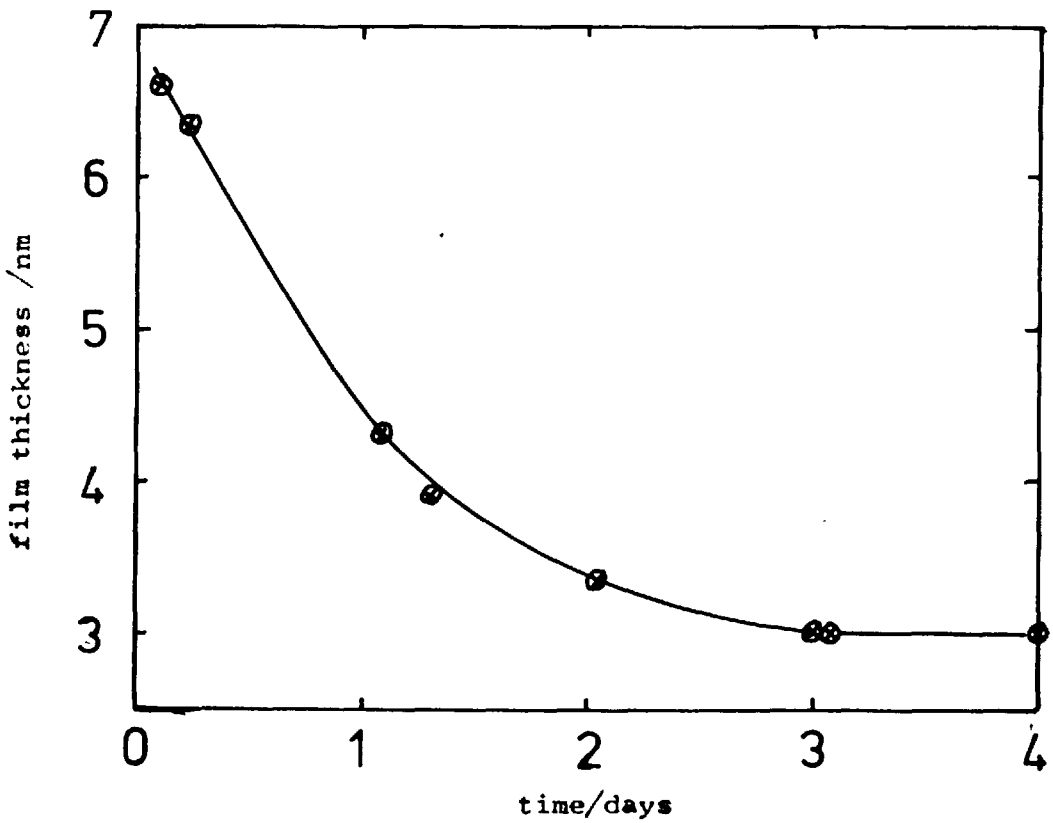

Figure 7.11. Thinning of initially thick water film on quartz to equilibrium value at $P/P_o = 0.90$

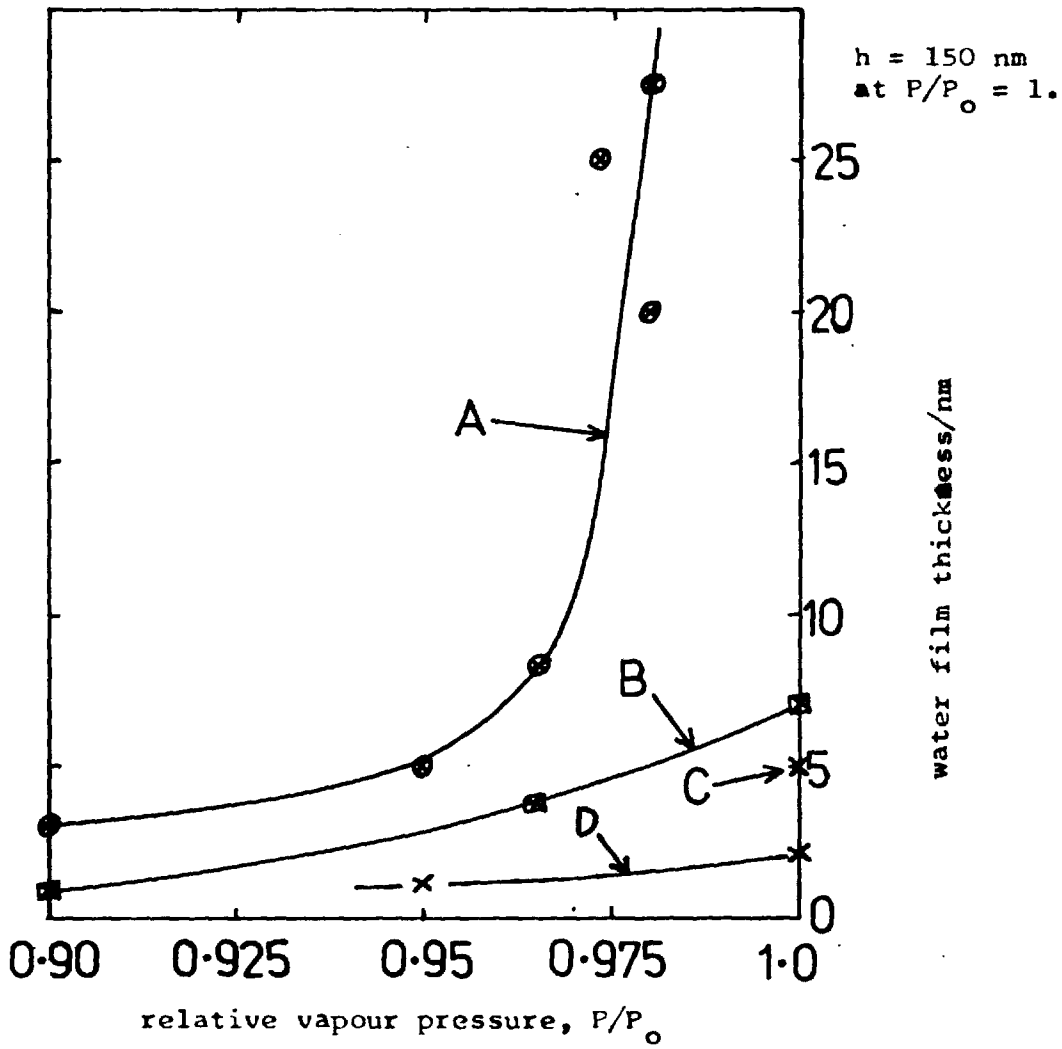

Figure. 7.12. Water adsorption isotherms measured on crystalline quartz plates, at 25°C

A - clean, fully hydroxylated quartz

B - heat de-hydroxylated (850°C) quartz

C - contaminated (by hydropbobic material

D - methylated quartz

Table 7.9. Ellipsometrically measured values of Δ and Ψ for water films on clean and heat de-hydroxylated quartz plates at various relative water vapour pressures.

relative vapour pressure, P/P_o	Δ (°)	Ψ (°)	corresponding water film thickness (nm)
clean plate:-			
0.980	29.7	5.6	27.3
0.980	23.6	4.95	19.8
0.973	28.1	5.8	25.0
0.965	10.7	4.91	8.3
0.950	6.3	4.22	5.0
0.90	3.95	4.20	3.0
heat de-hydroxylated plate (875°C):-			
1.0	9.2	4.4	7.0
0.965	5.18	4.4	3.9
0.90	1.4	4.2	1.1

C. Heat dehydroxylated, contaminated and methylated quartz surfaces in equilibrium with solutions of different relative vapour pressures

Heat dehydroxylated

A crystalline quartz plate was heated to 875°C in an electric furnace, in air. Heating and cooling through 573°C (the $\alpha - \beta$ transition temperature for quartz) was carried out very slowly. The quartz plate was held at 875°C for 2 hours before allowing it to slowly cool. When the plate had cooled to a temperature of 550°C, filtered nitrogen was slowly blown into the silica cell in which the quartz plate was housed. When the plate was cool it was transferred, in a nitrogen atmosphere, to the ellipsometer cell. The equilibrium water film thicknesses measured at three vapour pressures are given in Figure 7.12, curve B. The adsorption is greatly reduced, compared with that on a hydroxylated (non-heated) sample.

The reduction in film thickness with respect to the clean hydroxylated surface (curve A) must be due entirely to the loss of surface hydroxyl groups since precautions were taken to keep the plate isolated from contamination after heating.

For very thin water films (i.e. $\lesssim 3$ nm) all four zones were measured for greater accuracy. A typical four zone measurement is given in Table 7.10. Again there was found to be good agreement between the two zone averages.

For the heated quartz plate the maximum equilibrium thickness (at $P/P_o = 1$) was about 7 nm. After the heated plate had been used to measure these thicknesses the $P/P_o = 1$ value was again measured. The equilibrium thickness had increased to about 11 nm, indicating that the surface was slowly rehydroxylating due to the continual presence of a thin water film on its surface.

7.10. Four-zone ellipsometric measurements for a thin water film on crystalline quartz (at $P/P_o = 0.90$)

set value of P or A	corresponding (measured) minimum value of A or P	corresponding value of Δ and Ψ (see Table 7.3).
Zone 1		
P = 136	$A_m = 3.98$	$\Psi_1 = 3.98^\circ$
A = 4	$P_m = 136.1$	$\Delta_1 = 2.2^\circ$
Zone 3		
P = 48	$A_m = 355.65$	$\Psi_3 = 4.35^\circ$
A = 356	$P_m = 48.12$	$\Delta_3 = 6.2^\circ$
Zone 2		
P = 314	$A_m = 4.13$	$\Psi_2 = 4.13^\circ$
A = 4	$P_m = 314.35$	$\Delta_2 = 1.3^\circ$
Zone 4		
P = 222	$A_m = 355.65$	$\Psi_4 = 4.35$
A = 356	$P_m = 221.98^\circ$	$\Delta_4 = 6.04$

mean values for zones 1 and 3: $\Delta = 4.2^\circ$; $\Psi = 4.16^\circ$

mean values for zones 2 and 4: $\Delta = 3.7^\circ$; $\Psi = 4.24^\circ$

Total mean values: $\overline{\Delta} = 3.95^\circ$; $\overline{\Psi} = 4.20^\circ$

These measured values of Δ and Ψ correspond (see Figure 7.8) to a water film thickness of 3.0 nm.

The advancing water contact angle on this plate was measured after removal from the cell. The value of about 20° obtained was significantly smaller than observed with a freshly dehydroxylated silica plate.

Contaminated plate

A cleaned quartz plate (i.e. giving uniform fringes in the steam test) was placed in running London tap water for 30 sec; and then blown dry with nitrogen. It gave a uniform opaque mist in the steam test. This plate was then sealed in the ellipsometer cell and the equilibrium film thickness at $P/P_o = 1$ was measured. A constant value of about 5 nm was obtained.

Methylated quartz plate

A clean quartz plate was methylated with trimethylchlorosilane following the procedure of Laskowski and Kitchener (5.30). It was then allowed to come to thermal equilibrium in the constant temperature room before being sealed in the sample cell with clean water. After about 2 hours the thickness of the adsorbed water film became constant and remained so for 24 hours at 4.8 nm ($\pm$ 0.2 nm). After the specimen had been in the cell for about 4 days, the film thickness increased to about 9 nm. The contact angle of water on the methylated plate on removal from the cell was: $\theta_A \simeq \theta_R \simeq 70^{\circ}$ with little ($\sim 5^{\circ}$) hysteresis. The contact angle of water on a similar plate before wetting the surface was measured as: $\theta_A \simeq \theta_R \simeq 80^{\circ}$. These contact angle results agree well with those reported by Laskowski and Kitchener (5.30) and Blake and Kitchener (5.10) and also show that methylated quartz surfaces slowly become less hydrophobic on contact with only a thin water film.

A second, freshly methylated plate was sealed in the cell with salt solution corresponding to $P/P_o = 0.95$. After 24 h the thickness of the film was constant at about 3.5 nm (± 0.3).

This plate was then washed in Analar benzene and dried for 15 h at 110°C and was then immediately transferred, in a nitrogen atmosphere, and measured in the cell, containing dry nitrogen. The phase change and azimuth values measured are given in Table 7.11. These values, if interpreted as a nominal water film, would correspond to a thickness of 2.6 nm. The plate was then heated in a nitrogen atmosphere at 320°C for 15 hours and again measured in a dry nitrogen atmosphere (using all four zones, as a check). Exactly the same thickness was measured.

This "blank" measurement shows that the methylated quartz surface carried a layer of low refractive index. If it is assumed that the chemically attached species had a refractive index of about 1.33 then the thickness of the adsorbed layer would be ~ 2.6 nm. A suggested model for the methylated surface is given below since it has been estimated that methylation of silica with trimethylchlorsilane covers only about half the surface with methyl groups (5.30):-

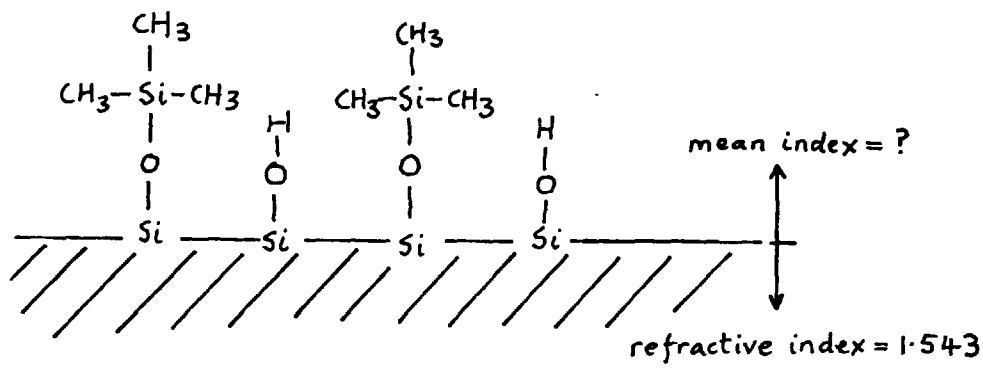

From the atomic radii given by Cotton and Wilkinson (7.14) the maximum length of the chain (i.e. assumed straight): - O - Si - C - H is about 0.6 nm. From the blank measurement, however, the layer appears to be much thicker. Even if it were assumed that the layer has a lower refractive index than water, due to an open structure, for example a refractive index of 1.25, then the corresponding film thickness would still be about 2.3 nm, which could not be accounted for by the theoretical structure shown above.

The layer attached could have been due to some other material present in the methylating reagent which was a sample supplied by BDH and not subjected to further purification. It may, conceivably, have contained some dimethyl dichlorsilane, which yields silicone resin on hydrolysis. Any benzene and water, possibly initially adsorbed on the methylated surface, should have been removed at 320°C. Since the refractive index of this very thin layer could not be determined it was estimated, for simplicity that the layer had a refractive index near to that of water. The water film subsequently adsorbed on this basic layer could then be roughly estimated (Table 7.11 and Figure 7.12).

Water adsorption isotherms on methylated and non-methylated crystalline quartz oscillator crystals (up to, about $P/P_o = 0.91$) have been measured by Khan (5.9) who reported that plates methylated at room temperature became much more hydrophobic when subsequently heated at 160°C for several hours. Cleaned quartz plates appeared to give hydrophilic behaviour with film thickness increasing sharply up to 0.91, whereas methylated plates had a much smaller film thickness with no tendency to increase sharply at higher vapour pressures.

Table 7.11. Ellipsometric measurement of thin water films on methylated crystalline quartz plates

plate conditions	Δ (°)	Ψ (°)	corresponding water film thickness(nm)	thickness after correcting for blank value (nm)
($\theta \sim 80°$) methylated plate, washed in benzene, dried at 110°C for 15 h, sealed with saturated water vapour	6.5	4.5	4.8	2.2
as above but after 4 days with thin water film on methylated surface ($\theta \sim 70°$)	11.0	4.6	8.5	5.9
freshly methylated plate sealed with P/P_o = 0.95 solution	4.6	4.5	3.5	0.9
methylated plate washed in benzene dried at 110°C for 15 h.	3.6	4.4	2.6	-
methylated plate washed in benzene dried at 320°C for 15 h	3.6	4.3	2.6	-

From the results obtained it is apparent that quartz plates which have been heat de-hydroxylated, methylated or contaminated (by hydrophobic material) form definite, limiting water film thicknesses ($<$ 10 nm thick) at saturated vapour pressure. The experimental system used did not supersaturate the sample so as to form micro-droplets on the hydrophobic surface (the maximum relative vapour pressure never exceeding about 1.001); droplet formation would have been observed as an increase in film thickness and as a decrease in absolute reflected light intensity - neither of which was observed.

Investigation of the difference in the measured phase change between zones

For most of the measurements reported here the phase change obtained from different zones (say from zone 1 and zone 3) differed by up to 4°. The mean value, however, should be very near the true value (7.7). The effect of tightening of the vitreous silica windows (held down by screw caps) on this difference in phase change was investigated, with a quartz plate carrying a water film of about 12 nm in the cell. The phase changes (and ψ values) in zones 1 and 3 were measured before and after tightening the windows. Results are given in Table 7.12.

The difference between Δ_1 and Δ_3 was altered from 3° (which is acceptable (7.7)) to 21° by strong tightening of the windows. The ψ values hardly altered. The mean value $\Delta_{1/3}$ changed also but to a lesser extent than did either Δ_1 or Δ_3.

Strain in the windows (set to within 2° normal to the beam) therefore caused large deviations in the phase change of the transmitted light. In practice, the windows were lightly tightened and

7.12. Effect of strain in optical cell windows on the ellipsometric measurement of Δ and ψ measured for the case of a water film on crystalline quartz

set value of P or A	corresponding (measured) minimum value of A or P	corresponding value of Δ and ψ (see Table 7.3)
(a) with cell windows tightly screwed down:-		
Zone 1		
P = 136	A_m = 5.0	$\psi_1 = 5.0^\circ$
A = 5	P_m = 135.6	$\Delta_1 = 1.2^\circ$
Zone 3		
P = 56	A_m = 355.95	$\psi_3 = 4.05^\circ$
A = 356	P_m = 56.23	$\Delta_3 = 22.5^\circ$
(b) with cell windows loosely held:-		
Zone 1		
P = 142	A_m = 184.6	$\psi_1 = 4.6^\circ$
A = 185	P_m = 142.05	$\Delta_1 = 14.1^\circ$
Zone 3		
P = 54	A_m = 175.7	$\psi_3 = 4.3^\circ$
A = 176	$P_m = 53.5^\circ$	Δ_3 = 17.0

mean of zones 1 and 3 with strain in windows:

$\Delta = 11.9^\circ \pm 10^\circ$; $\psi = 4.5^\circ \pm 0.5^\circ$

mean of zones 1 and 3 with minimal strain:

in windows: $\Delta = 15.6^\circ \pm 1.5^\circ$; $\psi = 4.45^\circ \pm 0.15^\circ$

the system was then aligned with respect to the sample reflecting surface.

Discussion

(1) Validity of the results

From the temperature variation in the cell used in these measurements, any temporary supersaturation when using pure water cannot have exceeded $P/P_o = 1.001$; this is not capable of inducing nucleation of micro-droplets on a typical hydrophobic surface (e.g. contaminated quartz with a water contact angle of 20^o to 40^o). Similarly, it is very unlikely that the thick water films which are obtained only on exceptionally clean quartz plates could have been formed via supersaturation (i.e. passing through the region where $\Pi < 0$, see Chapter 1, Fig. 1.1b). That this did not occur is further substantiated by the observation that a clean quartz plate initially warmer than the vapour source water still formed thick water films after a few hours and that water films of up to 30 nm were observed on plates in equilibrium with salt solutions of relative vapour pressure substantially less than 1.0 (i.e. 0.98). It can be confidently concluded, therefore, that stable thick water films were formed on cleaned quartz plates and on varying the partial pressure a continuous transition was observed from very thin water films ($\sim$ 1 nm) to very thick water films (150 nm).

That these very thick films measured by the ellipsometer were not microdroplets of water can be shown by several observations:

(a) the presence of microdroplets on the reflecting surface would drastically reduce the absolute reflected intensity (i.e. parts of equal intensity about the minimum would be

separated by a larger angle - giving a wider minimum) - which was not observed.

(b) If droplets were formed there ought to be no limit to their size - hence the film thickness observed should increase beyond the observed 150 nm. The latter limiting value is in fact expected for the case of a thin water film supported on a vertical plate. (See following).

(c) from observations by naked eye, for a clean plate, high reflecting, uniform fringes are observed. Therefore, very thick continuous films were certainly present.

That a water film of about 150 nm was usually formed on a clean quartz plates sealed with water can be explained by the fact that the plate was held about 1-2 cm above the water surface. The region of measurement on the plate was about 0.75-1 cm from thebase of the plate. Thus the disjoining pressure in the film at the position where it was measured must be equal to the hydrostatic pressure in the water film which it is supporting (7.15), thus the disjoining pressure, where l is the height above the water surface, is given by:

$$\Pi = l \cdot \rho \cdot g \qquad 7.3$$

where ρ is the density of water and g acceleration due to gravity. For these very thick films it may be assumed that Π is determined entirely by Π_{el}. Using the limiting equation of Langmuir (3.1) for high potentials, the thickness of film corresponding to a given height above the water surface can be calculated. For heights of about 1 cm, the water film is estimated to be approximately 150 nm thick - this thickness agrees very well with that observed.

(2) Comparison with published data

The adsorption isotherm measured here for water on crystalline quartz is compared, in Fig. 7.13, with measurements reported by other workers using both glass and silica. The results obtained here clearly show that the isotherm is that of a perfectly hydrophilic solid (see Fig. 1.1(1). The measurements of Garbaski and Folman on glass surfaces also correspond to a hydrophilic surface but with a much larger water film thickness for a given relative vapour pressure. (This could be due to a gel layer on the glass). The measurements of Hall and of Derjaguin and Zorin on vitreous silica are roughly comparable to those obtained on quartz which had been made hydrophobic by heat de-hydroxylation or by hydrophobic surface contamination (see Fig. 7.14).

The observation by Zorin and Churaev (7.16) that films of different thickness exist in equilibrium (at 10 and 40 nm) via a contact angle with bulk water on vitreous silica (when a gas bubble was pressed against the plate) was not confirmed here. A finite contact angle was observed by these researchers, but was not obtained here for clean quartz; this difference may explain the fact that stepped films were not observed, during condensation, in this work.

Derjaguin et al (1.12) report that methylation of a quartz surface reduces the adsorbed water film thickness, at $P/P_o \approx 1.0$, to less than 0.3 - 0.4 nm (from 4.5 nm). This corresponds to a reported water contact angle change of 20° (for the untreated surface) to 105° (for the methylated surface). These results would correspond, from the results reported here, to a contaminated quartz plate (of contact angle 20°) further grossly contaminated to produce a surface with a very large water contact angle. The water film

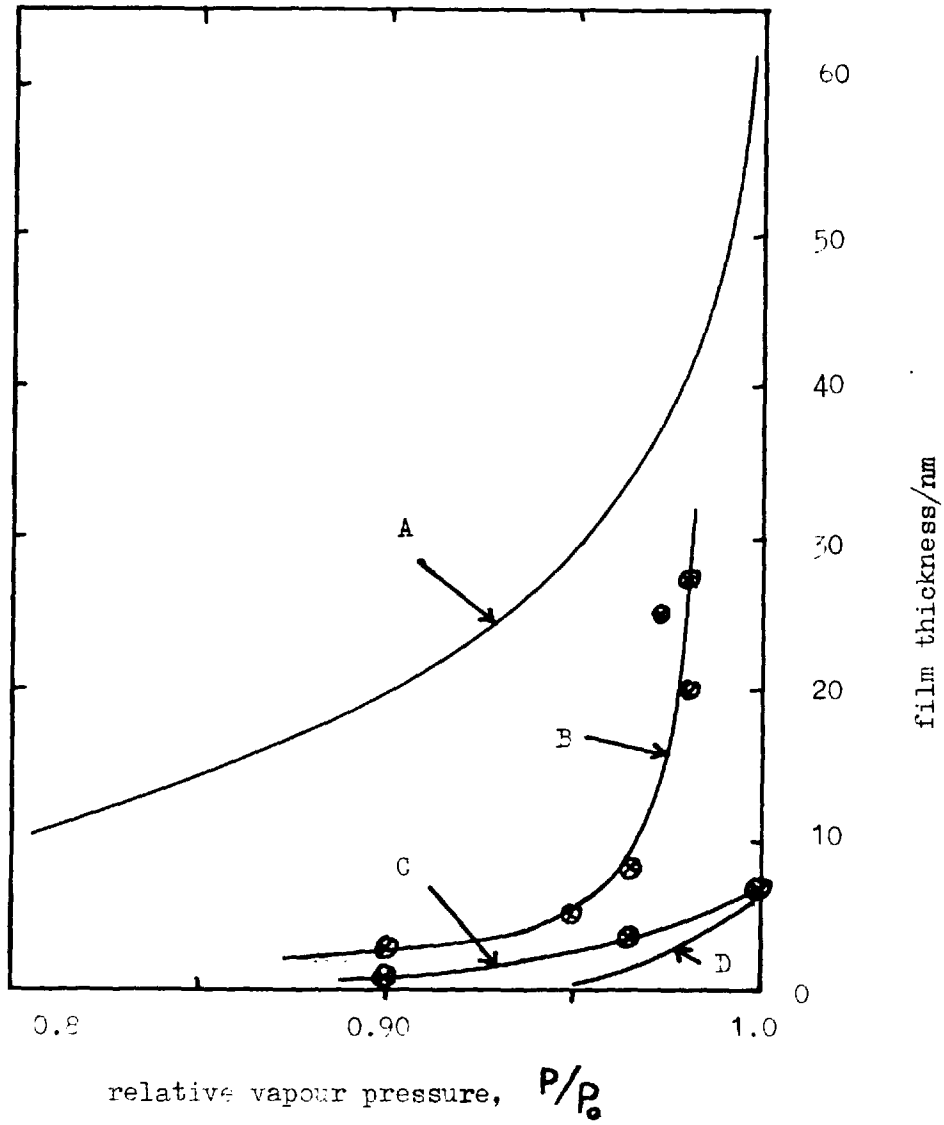

Figure 7.13. Relative vapour pressure as a function of water film thickness for glass, vitreous silica and quartz surfaces.

A - results of Garbatski and Folman on glass.

B - results obtained in this work on clean quartz.

C - results obtained in this work on heat dehydroxylated quartz.

D - results of Derjaguin and Zorin on vitreous silica.

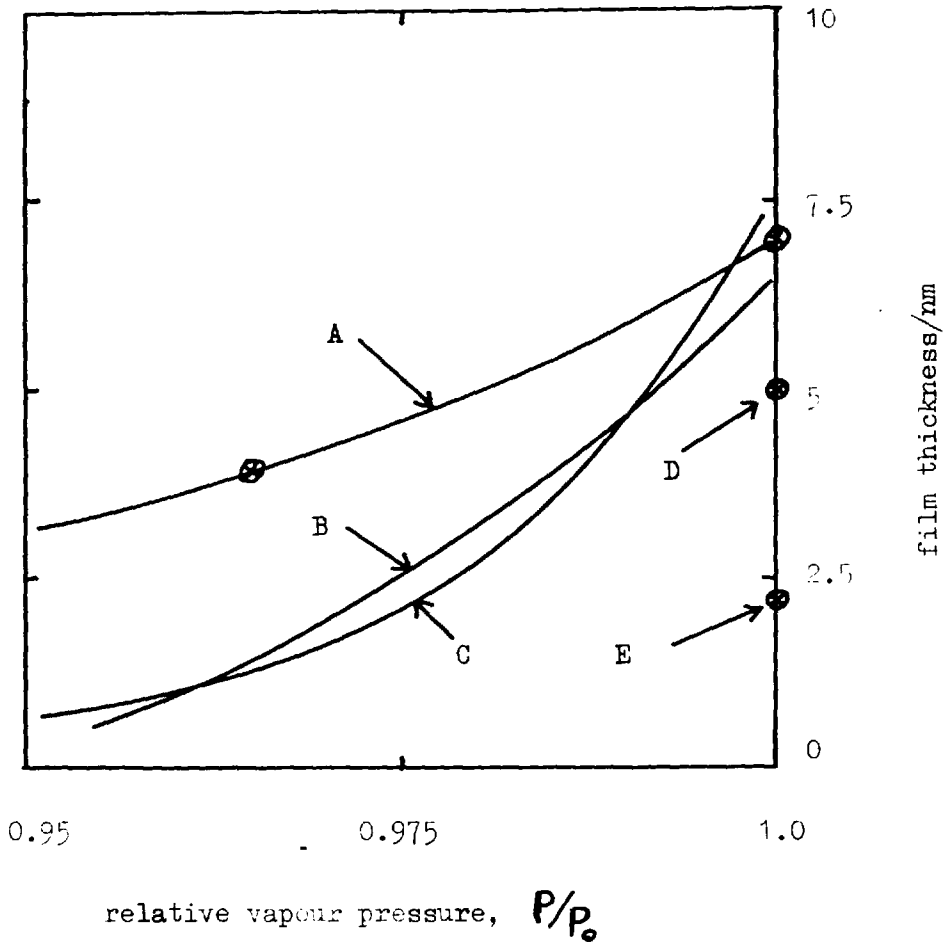

Figure 7.14. Relative vapour pressure as a function of water film thickness for hydrophobic quartz.

A - results obtained in this work for heat dehydroxylated quartz.

B - results of Derjaguin and Zorin on vitreous silica.

C - results of Hall on vitreous silica.

D - results measured in this work on a contaminated quartz plate.

E - results measured in this work on a methylated quartz plate.

thickness at $P/P_o \approx 1.0$ would therefore correspondingly be reduced with further contamination. No blank ellipsometric measurements on methylated surfaces appear to have been given by Derjaguin et al (1.12). Measurements on the variation in water film thickness with temperature were, however, reported for these quartz plates which had a 20° water contact angle. The film thickness decreased with increase in temperature, approaching zero thickness at about 65°C. These results suggest that a hydrogen-bonded lattice is important for interaction on such quartz surfaces (i.e. with 20° contact angle), which is broken up by increased thermal agitation.

(3) Comparison with the theory of surface forces

Using equation (1.1), relative vapour pressures were converted to the corresponding disjoining pressures and the latter are plotted as a function of film thickness in Fig. 7.15. Theoretically calculated disjoining pressures (see chapters 2 and 3), Π_{vdw} and Π_{el}, for thin water films on quartz are also plotted for comparison.

From Fig. 7.15 it is apparent that the form of the adsorption isotherm measured in this work for water on quartz is similar to that expected from theory, assuming that only electric double-layer forces and van der Waals forces are significant in the film. The film thicknesses measured at a given disjoining pressure (for thin films) are, however, distinctly greater than these expected from Π_{vdw} and Π_{el} theory. However, for the thicker water films (i.e. about 150 nm) electric double layer theory does appear to agree with experiment.

For the hydrophobic case (and for the measurements of Hall and Derjaguin and Zorin) the film thicknesses are not only somewhat greater than theoretically calculated values (for $P/P_o \lesssim 0.99$, from

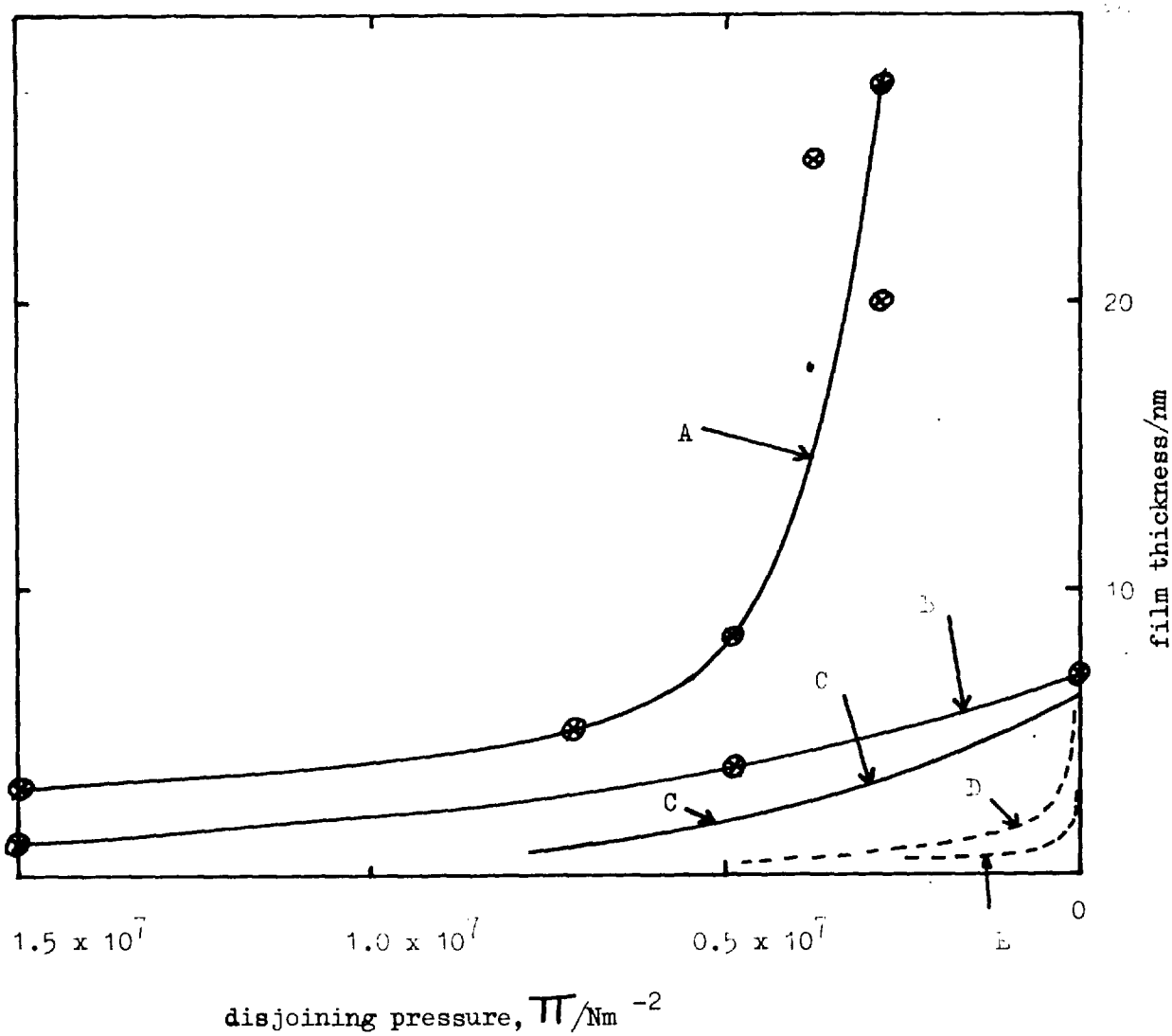

Figure 7.15. Disjoining pressure as a function of water film thickness for hydrophilic and hydrophobic quartz surfaces, compared with theoretically calculated values.

A - results obtained in this work on clean quartz.

B - results obtained in this work for heat dehydroxylated quartz.

C - results of Derjaguin and Zorin on vitreous silica.

D - disjoining pressure calculated from electrical double-layer theory (Lanmuir equation), Π_{el}.

E - disjoining pressure calculated from Lifshitz theory, Π_{vdw}.

Π_{el} and Π_{vdw} theory) but also have an entirely different form from that of the theory, as $P/P_o \rightarrow 1.0$. Thus as $P/P_o \rightarrow 1.0$ the film thickness should, according Π_{el} and Π_{vdw} theory, increase steeply; however, finite film thicknesses were reported and were measured here at $P/P_o = 1.0$ for the cases shown. Therefore, hydrophobicity is not accounted for by double layer or van der Waals forces.

The adsorption isotherm measured here for water on clean quartz corresponds roughly, in form, to that expected from Π_{vdw} and Π_{el} theory, but these Π contributions appear to be much greater than expected.

It is possible, for instance, that the electrical double-layer repulsive force is much larger than that calculated from models based on what may be unrealistic assumptions (see chapter 3). A much increased double-layer repulsion would explain the results obtained.

The hypothesis of Derjaguin and Churaev (1.3), that there may be a third component in the disjoining pressue due to short range interactions, Π_s, seems unquestionable for the hydrophobic surfaces. However, this component is expected to be important only over short distances (i.e. $\lesssim$ 11 nm (1.10)). Thus, this positive contribution to disjoining pressure may explain deviations from Π_{el} and Π_{vdw} theory up to about 11 nm but would not explain the increased disjoining pressure apparent up to about 60 nm (estimated from Fig. 7.15).

An increase in Π due to both Π_s (short range) and Π_{el} (short and long-range) may therefore have to be considered in order to account quantitatively for these results.

For the case of a hydrophobic surface a short range contribution

must be postulated to explain the deviation obtained from Π_{el} and Π_{vdw} theory. The Π_{el} and Π_{vdw} components for the case of a water film on heat-dehydroxylated quartz ought to be similar to those on clean, fully hydroxylated, quartz for the following reasons:

Firstly the zeta-potentials are only slightly reduced on heating (Chapter 5); secondly the van der Waals component should be almost unchanged because dehydroxylation merely removes most of the surface hydrogen atoms and about half a monolayer of oxygen atoms. The very large difference in adsorption isotherm must therefore be ascribed to a change in the structural component, Π_s. The effect of such an interaction in terms of disjoining pressure must be as a large positive contribution up to very near $P/P_o = 1.0$ and as a strongly negative contribution at $P/P_o = 1.0$, preventing the film thickening as P/P_o approaches 1.0.

The concept of additive disjoining pressure contributions is not really valid for these very thin structured layers. The Russian school consider very thin films on hydrophobic surfaces as different (α) forms of the liquid, and this theory seems very plausible to account for the non-wetting of low energy solids (such as dehydroxylated silica) by polar liquids such as water. The structure of the α-film is unknown. The film is attached to the solid (being left behind when a meniscus retreats over the surface), but it exhibits weak adhesion to ordinary liquid water. As Laskowski and Kitchener emphasized, the strong cohesion of liquid water is mainly due to its internal hydrogen bonding (rather than dispersion energy); and, since dispersion forces cannot account for hydrophobicity, conversely weak adhesion of water to the α-film may simply indicate reduced hydrogen bonding across the interfacial zone (α/β boundary).

It should be mentioned that heating of silica to 875°C (as used here) does not produce complete dehydroxylation of the surface; although two adjacent - SiOH groups fairly readily lose 1 H_2O, isolated silanols are left, and such groups probably act as sites for adsorption of clusters of water molecules. Furthermore, the surface of dehydroxylated crystalline quartz must not be thought of as a crystalline plane of uniform molecular type (as believed to exist in the siloxane sheets of talc). There must be pits and projections of more than atomic dimensions. Therefore these surfaces aremolecularly heterogeneous as adsorption substrates, and the macroscopic contact angle measures only a mean work of adhesion.

Since the magnitude of the electrical double-layer repulsion is not accurately known for the case of thin films condensed on to a solid surface it is unreasonable to attempt to estimate the Π_s contribution from the measurement of the total disjoining pressure, for the case of a water film on clean quartz. That a short-range force exists and is of great importance in wetting properties is apparent from the results obtained here for the case of heat dehydroxylated and fully hydroxylated quartz. That a "hydrophobic force" is also important for the case of methylated and contaminated surfaces is not quite so firmly proved from the present data, since these surfaces appear to carry fairly thick layers of hydrophobic materials which may alter both Π_{el} and Π_{vdw}. However, both contributions are almost certainly positive in sign, which leaves Π_s firmly negative to account for the hydrophobicity as P/P_o approaches 1.0.

(4) The role of contamination

From Fig. 7.13, 7.14 and 7.15 it is apparent that the reported measurements of Hall and of Derjaguin and Zorin were approximately reproduced in this work for the case of deliberately contaminated, methylated and heat-dehydroxylated quartz surfaces but were not obtained with exceptionally clean conditions, when great attention was paid to the cleaning of the quartz, the water and the cell. These results strongly suggest that the previously published isotherms were measured on contaminated surfaces. This view is further substantiated by the reported observation that the surfaces used by Derjaguin et (1.12) had a 20° contact angle with water and produced micro-droplets on supersaturation (1.6). Such behaviour was only observed here for contaminated surfaces. Clean quartz surfaces had zero or very low contact angle with clean water and produced uniform coloured fringes when exposed to supersaturation.

Low film thicknesses were observed in this work where vapour equilibrium was clearly not obtained - such an explanation could possibly be applied to some of the reported measurements.

Summary of conclusions

(1) Highly polished and lightly etched crystalline quartz plates cleaned with hot concentrated sodium hydroxide, hot concentrated nitric acid or hot ammoniacal hydrogen peroxide gave low "blank" ellipsometric values, indicating that surface gel layers, disturbed layers or surface roughness was no more than about 0.5 nm thick.

(2) Relatively strong etching (e.g. 1.5% NH_4HF_2 at room temperature for 24 hours) of crystalline quartz plates did not markedly increase the phase change (Δ) measured

by ellipsometry.

(3) Well cleaned, fully hydroxylated, crystalline quartz plates (or vitreous silica) when sealed in the presence of clean water, at thermal equilibrium, built up thick water films ($\sim$150 nm) on the surface which were stable for at least 3 days (apparently depending on the rate of ingress of contamination.) Under identical conditions heat-dehydroxylated, hydrophobically contaminated or methylated plates formed thin films, less than 10 nm thick.

(4) Water adsorption isotherms measured on clean, crystalline quartz plates were qualitatively of the form expected for a hydrophilic solid of zero (or very low) contact angle (Fig. 1.1(b)). Heat de-hydroxylated, contaminated or methylated plates behaved as hydrophobic solids (Fig. 1.1(b)), giving a definite intercept at $P/P_o = 1.0$.

(5) For the case of clean hydrophilic quartz the measured water film thicknesses at controlled vapour pressures, below $P/P_o = 1.0$, were found to be substantially greater than those expected from conventional electrical double-layer and van der Waals theory applied to the case of thin films.

(6) Previously reported measurements of the water adsorption isotherm on vitreous silica by Hall and by Derjaguin and co-workers were very similar to those measured here on quartz surfaces altered so as to become hydrophobic. It has been found that contamination is extremely difficult to avoid, and it therefore seems likely that the conditions used by the previous workers were not sufficiently rigorous.

(7) A major factor influencing the water wetting properties of quartz has been shown to be short-range forces between surface hydroxyl groups and adjacent liquid layers. Removal of surface hydroxyl groups leads to hydrophobicity.

Chapter 8

Main Conclusions

(1) In general, calculation of the macroscopic van der Waals interaction, on the basis of Lifshitz theory, should be more accurate and more fundamental if the Kramers-Kronig equation is used with the full spectral data (where available, up to far U.V.) rather than using a simplified oscillator-type spectral model. However, for the case of quartz and water close agreement was obtained with calculations using adequate oscillator models.

(2) The dispersion component of the disjoining pressure (Π_{vdw}) calculated with full spectral data and the Lifshitz theory, for the case of water films on quartz, was found to become negative for water films thicker than about 60 nm. This calculated negative disjoining pressure would, however, normally be masked by a much larger positive disjoining pressure due to electric double-layer repulsion.

(3) Polishing of crystalline quartz with hard materials (e.g. diamond or carborundum powder) produces latent disturbed lines in the apparently smooth surface. Quartz polished with a softer powder (e.g. cerium oxide) shows no such latent features or disturbed layers.

(4) Z-cut crystalline quartz surfaces are etched uniformly in dilute hydrofluoric acid (0.5%) and show neither crystalline faces nor any marked increase in surface roughness.

(5) Dehydroxylation of crystalline quartz by heating produces a hydrophobic surface but does not significantly affect its zeta-potential.

(6) Bubble rise velocity was found to be a very sensitive monitor of the cleanliness of water with respect to surfactant. It was not found possible to produce water (by either microflotation cleaning or double distillation/activated charcoal treatment) in which bubbles rose at a rate corresponding to that expected for perfectly pure water. However, microflotation cleaning was found to have a substantial surfactant removal action on contaminated water. Water obtained from double distillation/activated charcoal treatment was clean enough not to contaminate clean quartz plates after immersion for several days.

(7) Using the ellipsometric roughness theory of Fenstermaker and McCrackin, it has been theoretically shown in this work that large errors in the ellipsometric measurement of thin water films on quartz may occur where the surface roughness is of a similar order to the thickness of the film.

(8) Polished quartz (and vitreous silica) surfaces are remarkably difficult both to clean and to keep clean. Once clean, however, the surface is definitely hydrophilic with a zero or very low water contact angle. Such surfaces show a water adsorption isotherm corresponding to a perfectly hydrophilic solid (i.e. Figure 1.1(a)). The isotherm obtained was of the form predicted by Π_{el} and Π_{vdw} theory,

but thicker films were measured than expected from current theory.

(9) Quartz surfaces which have been heat-dehydroxylated, methylated or contaminated (by hydrophobic materials) show large contact angles with water (20° to 80°) and thin equilibrium water films (< 10 nm) in saturated water vapour. Adsorption isotherm results on such quartz surfaces resemble those reported on supposedly clean vitreous silica surfaces by Hall and by Derjaguin and Zorin.

(10) A short-range "structural" interaction appears to be responsible for the difference in wetting properties between fully hydroxylated (hydrophilic) and de-hydroxylated (hydrophobic) quartz.

REFERENCES

CHAPTER 1

1.1 DERJAGUIN, B.V. and SHCHERBAKOV, L.M. Colloid J. USSR, 23, 33 (1961).

1.2 BLAKE, T.D. J. Chem. Soc. Faraday Trans. I, 71, 192 (1975).

1.3 DERJAGUIN, B.V. and CHURAEV, N.V. J. Coll. Int. Sci. 49, 249 (1974)

1.4 LASKOWSKI, J. and KITCHENER, J.A. J. Coll. Int. Sci. 29, 670 (1969).

1.5 FREUNDLICH, H. "Colloid and capillary chemistry" Methuen Ltd. (1926).

1.6 DERJAGUIN, B.V. and ZORIN, Z.M. Proc. 2nd Int. Con. Surface Activity, 2, 145 (1957).

1.7 ADAMSON, A.W. and LING, I. Adv. Chem. Ser. 43, 57 (1964)

1.8 FRUMKIN, A.N. J. Phys. Chem. U.S.S.R. 12, 337 (1938)

1.9 DROST-HANSEN, W. J. Coll. Int. Sci. 58, 251 (1977)

1.10 DERJAGUIN, B.V. and CHURAEV, N.V. Soviet Physics - Doklady 17, 1080 (1973).

1.11 ERSHOVA, G.F., ZORIN, Z.M. and CHURAEV, N.V. Coll. J. U.S.S.R. 37, 190 (1975)

1.12 DERJAGUIN, B.V., ZORIN, Z.M. CHURAEV, N.V. and SHISHIN, V.A. Chap. 9 in "Wetting, Spreading and Adhesion", Edited by J.F. Padday (1978)

1.13 HALL, A.C. J. Phys. Chem. 74, 2742 (1970).

1.14 GARBATSKI, U. and FOLMAN, M. J. Chem. Phys. 22, 2086 (1954).

1.15 GARBATSKI, U. and FOLMAN, M. J. Phys. Chem. 60, 793 (1956).

CHAPTER 2

2.1 KEESOM, W.H. Commun. Phys. Lab. Suppl., 24 - 26 Univ. Leiden (1912).

2.2 DEBYE, P.J.W. Phys. Z. 21, 178 and 22,302 (1920).

2.3 LONDON, F. Z. Phys. Chem. B11, 222 (1930); Trans. Farad. Soc., 33, 8 (1936); J. Chem. Phys., 46, 305 (1942).

2.4 HAMAKER, H.C. Physica, 4, 1058 (1937)

2.5. CASIMIR, H.B.G. and POLDER, D. Phys. Rev. 73, 360 (1948).

2.6 LIFSHITZ, E.M. Sov. Phys. JETP 2, 73 (1956)

2.7 DZYALOSHINSKII, I.E., LIFSHITZ, E.M. and PITAEVSKII, L.P. Adv. Phys. 10, 165 (1959).

2.8 PARSEGIAN, V.A. and NINHAM, B.V. Nature 224, 1197 (1969)

2.9 ISRAELACHVILI, J.N. and TABOR, D. Prog. Surface Membrane Sci. 7, 1 (1973).

2.10 RICHMOND, P. in "Colloid Science 2" (D.H. Everett, Ed.) Chap. 4, The Chemical Society, London, 1975.

2.11 WITTMANN, F., SPLITTGERBER, H. and EBERT, K. Z. Physik., 245, 354 (1971).

2.12 SPLITTGERBER, H. and WITTMANN, F. Surface Sci. 41, 504 (1974).

2.13 SABISKY, E.S. and ANDERSON, C.H. Phys. Rev. (A) 7, 790 (1973)

2.14 CHAN, D. and RICHMOND, P. Proc. R. Soc. Lond. A. 353, 163, (1977)

2.15 ISRAELACHVILI, J. and ADAMS, G.E. J.C.S. Faraday Trans I., 74, 975 (1978).

2.16 MAHANTY, J. and NINHAM, B.W. "Dispersion forces" in Colloid Science. Edit. R.H. Ottewill and R.L. Powell, Acad. Press. London (1976)

2.17 RABINOWITZ, P. and WEISS, G., Maths. Tables and Other Aids to Computation 8 (68), 285 (1959).

2.18 GINGELL, D. and PARSEGIAN, V.A. J. Coll. Int. Sci. 44, 456 (1973)

2.19 GINGELL, D. and PARSEGIAN, V.A. J. Theor. Biol. 36, 41 (1972)

2.20 NIR, S., REIN, R. and WEISS, L. J. Theor. Biol. 34, 135 (1972)

2.21 INGRAM, B.T. J.C.S. Faraday Trans I, 70, 868 (1974)

2.22 LANDAU, L.D. and LIFSHITZ, E.M., "Electrodynamics of Continuous Media" Addison - Wesley, Reading, Mass, 1960.

2.23 LONDON, F. Trans. Farad. Soc. 33, 8 (1937)

2.24 VISSER, J., Advan. Colloid. Interface Sci. 3, 331 (1972)

2.25 NIR, S., J. Theor. Biol. 53, 83 (1975)

2.26 DONNERS, W.A.B., RIJNBOUT, J.B. and VRIJ, A. J. Coll. Int. Sci. 60, 540 (1977).

2.27 VASSILIEFF, C.S. and IVANOV, I.B. Colloid and Polymer Sci. 254, 431 (1976).

2.28 DZYALOSHINSKII, I.E., LIFSHITZ, E.M. and PITAEVSKII, L.P., Soviet Phys. JETP 37, 161 (1960).

2.29 BUCKLEY, F. and MARYOTT, A. Nat. Bur. Stand. U.S. Circ. 589, 18 (1958)

2.30 KISLOVSKII, L.D. Opt. Spectrosc. 7, 201 (1959)

2.31 POINTER, L. and DECHAMBENOY, C., Ann. Geophys. 22, 633 (1966).

2.32 HELLER, J.M. Jr., HAMM, R.N., BIRKHOFF, R.D. and PAINTER, L.R. J. Chem. Phys. 80, 3483 (1974).

2.33 DEREILHAC, L., and DAMANY, N. Spectrochim. Acta. A. 26, 801 (1970).

2.34 RUSSELL, E.E. and BELL, E.E. J. Opt. Soc. Am. 57, 341 (1967)

2.35 SPITZER, W.G. and KLEINMAN, D.A. Phys. Rev. 121, 1324 (1961)

2.36 PHILLIP, H.R. Solid State Communication 4, 73 (1966)

2.37 BUECHNER, U. J. Phys. C. Solid State Phys. 8, 2781 (1975)

2.38 ARAKAWA, E.T., HAMM, R.N. and WILLIAMS, M.W. Phys. Rev. B, 15, 3243 (1977)

2.39 NIR, S., ADAMS, S., and REIN, R., J. Coll. Int. Sci. 49, 196 (1974).

CHAPTER 3

3.1 LANGMUIR, I. Science 88, 430 (1938)

3.2 JONES, G. and RAY, W.A. J. Amer. Chem. Soc. 59, 187 (1937)

3.3 BABCHIN, A.J., GUR, Y. and LIN, I.J. Adv. Coll. Int. Sci. 9, 105 (1978).

3.4 DERJAGUIN, B.V. and KUSAKOV, M. Acta. Physicochim. USSR, 10(1), 25 (1939); 10(2), 153 (1939)

3.5 READ, A.D. and KITCHENER, J.A. J. Coll. Int. Sci. 30, 391 (1969)

3.6 BLAKE, T.D. and KITCHENER, J.A. J.C.S. Faraday Trans. I. 68, 1435 (1972).

3.7 CALLAGHAN, I.C. and BALDRY, K.W. Chapter 7 in "Wetting, Spreading and Adhesion". Edited by J.F. Padday Academic Press, London (1978)

3.8 SCHULZE, H.J. and CICHOS, C. Z. Phys. Chem. 251, 252 (1972)

3.9 USHI, S. and SASAKI, H. J. Coll. Int. Sci. 65, 36 (1978)

3.10 BELL, G.M. and PETERSON, G.C. J. Coll. Int. Sci. 41, 542 (1972)

3.11 JONES, G. and FRIZZELL, L.D. J. Chem. Phys. 8, 986 (1940)

3.12 DEVEREUX, O.F. and de BRUYN, P.L. "Interaction of plane-parallel double layers" M.I.T. Press (1963).

3.13 READ, A.D. and KITCHENER, J.A. Soc. Chem. Ind. Monograph. 25, 300 (1967).

3.14 DERJAGUIN, B.V. Discuss. Faraday Soc., 18, 85 (1954)

3.15 USUI, S. Prog. Surface Membrane Sci. 5, 223 (1972)

3.16 BELL, G.M. and PETERSON, G.C. J. Coll. Int. Sci. 60, 376 (1977).

CHAPTER 4

4.1 AZZAM, R.M.A. and BASHARA, N.M. Ellipsometry and polarised light, North Holland Pub. Co. (1977).

4.2 MULLER, R.H. Adv. Electrochem. Electrochem. Eng. 9, 167 (1973)

4.3 VASICEK, A. "Optics of thin films". (1960)

4.4 VEDAM, K. and MALIN, M Mat. Res. Bull. 9, 1503 (1974)

4.5 FENSTERMAKER, C.A. and McCRACKIN, F.L. Surface Sci. 16, 85 (1969).

4.6 ARCHER, R.J., in Ellipsometry and the measurement of surfaces and thin films; Nat . Bur. Std. (Washington) Misc. Publ. 256, 255 (1964)

4.7 LOSCHKE, K. and G. KUHN. Kristall und Technick 11, 645 (1976)

4.8 GARNETT, M. Phill. Trans. Roy. Soc. (London) 203, 385 (1904); 205, 237 (1906)

4.9 CHAN, E.C. and MARTON, J.P. J. Appl. Phys. 45, 5004 (1974)

4.10 MARTON, J.P. and CHAN, E.C. J. Appl. Phys. 45, 5008 (1974)

4.11 McCRACKIN, F.L. and COLSON, J.P. in: Ellipsometry and the measurement of surfaces and thin films. Nat . Bur. Std. (Washington) Misc. Publ. 256, 61 (1964).

CHAPTER 5

5.1 VEDAM, K. and MALIN, M. Mat. Res. Bull. 9, 1503 (1974)

5.2 VEDAM, K. Surf. Sci. 56, 221 (1976)

5.3 HODGKINSON, I.J. J. Phys. E. 3, 300 (1970)

5.4 GRITSAENKO, G.S. and SAMOTOYIN, N.D. Proc. Int. Clay. Conf. 1, 391 (1966)

5.5 BASSETT, G.A. Philos. Mag. 3, 1042 (1958)

5.6 SERNA, J. and BRU, L. Surface Sci. 12, 369 (1968)

5.7 FREDERICK, P.S. and HRUSKA, S.J. J. Appl. Phys. 45, 3213 (1974)

5.8 GAUDIN, A.M. and FUERSTENAU, D.W. Trans. A.I.M.E. 202, 66 (1955)

5.9 KHAN, G.M. Can. J. Chem. 50, 125 (1972)

5.10 BLAKE, T.D. and KITCHENER, J.A. J.C.S. Faraday Trans. I. 68, 1435 (1972)

5.11 VIG, J.R., COOK, C.F., SCHWIDTAL, K., LEBUS, J.W. and HAFNER, E. Proc. Ann. Freq. Control Symp. 28, 96 (1974)

5.12 FEDER, D.O. and KOONTZ, D.E. A.S.T.M. Special Tech. Pub: No. 246, 40 (1959).

5.13 WHITE, M.L. Proc. Ann. Freq. Control Symp. 27, 79 (1973)

5.14 VIG, J.R., LEBUS, J.W. and FILLER, R.L. Proc. Ann. Freq. Control Symp. 29, 220 (1975)

5.15 VIG, J., WASSHAUSEN, H., COOK, C., KATZ, M. and HAFNER, E. Proc. Ann. Freq. Control Symp. 27, 98 (1973)

5.16 KRIEGER, G.L. et al. Sandia Corp. Technical Memorandum SC-TM-66-428 pp. 49, 66, Sandia Corp., Albuquerque, N.M. (1966).

5.17 BOLON, D.A. and KUNZ, C.O. Poly. Engng. and Sci., 12, 109 (1972)

5.18 McLACHLAN, A.D. and GIBBS, W.E.K. Appl. Optics. 16, 544 (1977).

5.19 WARREN, L.J. and KITCHENER, J.A. Trans. Instn. Min. Metall. 81, 137 (1972)

5.20 ELMER, T.H., CHAPMAN, I.D. and NORDBERG, M.E. J. Phys. Chem. 67, 2219 (1963)

5.21 DAELLENBACH, C.H.B. and TIEMANN, T.D. Trans. A.I.M.E. 229, 59 (1964)

5.22 MACKENNA, R.M.B., WHEATLEY, V.R. and WORMALL, A. J. Investig. Dermat. 15, 33 (1950).

5.23 HETHERINGTON, G. and BELL, L.W. Chapt. 15 in Ultrapurity-methods and techniques. Edit. M. Zief and R. Speights (1972).

5.24 SMIT, W., HOLLEN, C.L.M., STEIN, H.N., DEGOEIJ, J.J.M. and THEELEN, H.M.J. J. Coll. Int. Sci. 63, 120 (1978)

5.25 JONES, G. and WOOD, L.A. J. Chem. Phys. 13, 106 (1945)

5.26 BERGMAN, I. and LANGRISH, B. J. Electroanal. Chem. 34, 203 34, 203 (1972)

5.27 LI, H.C. and DE BRUYN, P.L. Surface. Sci. 5, 203 (1966)

5.28 FUJII, Y. Unpublished work referred to in: KULKARNI, R.D. and SOMASUNDARAN, P. Int. J. Min. Process. 4, 89 (1977).

5.29 KNOZINGER, H. in Vol. III, Chapt. 27, of "The Hydrogen Bond" Edited by P. Schuster, G. Zundel and C. Sandorfy.

5.30 LASKOWSKI, J. and KITCHENER, J.A. J. Coll. Int. Sci. 29, 670 (1969)

5.31 WHITE, M.L. in "Clean Surfaces" Edited by G. Goldfinger pp. 361 - 373 (1970).

5.32 DE BOER, J.H., HERMANS, M.E.A. and VLEESKEN, J.M. Koninkl. Ned. Akad. Wetenschap. Proc. Ser. B. 60, 45 (1957)

5.33 HAIR, M.L. J. non-crystal. solids. 19, 299 (1975)

5.34 BERMUDEZ, V.M. J. Phys. Chem. 75, 3249 (1971)

CHAPTER 6

6.1 MYSELS, K.J. and FLORENCE, A.T. in "Clean Surfaces" Edited by G. Goldfinger. pp. 227 (1970).

6.2 KAYE, W. J. Coll. Int. Sci. 46, 543 (1974); J. Coll. Int. Sci. 44, 384 (1973).

6.3 SMITH, V.C. in "Ultrapurity" Edited by M. Zief and R. Speights. Chapter 10 (1972).

6.4 SCHENKEL, J.H. and KITCHENER, J.A. Nature. 182, 131 (1958)

6.5 MATTSON, J.S. and MARK, H.B. Jr. "Activated Charcoal" (1971)

6.6 CROLL, B.T. Progress in water technology v6, 149 (1974)

6.7 SCOTT, J.C. J. Fluid Mech. 69, 339 (1975)

6.8 CINI, R., FICALBI, A. and LOGLIO, G. Mikrochemica Acta. (Wien) 203, (1974)

6.9 KITCHENER, J.A. and COOPER, C.F. Quart. Rev. 13, 71 (1959)

6.10 HABERMAN, W.L. and MORTON, R.K. Trans. Am. Soc. Civil. Engrs. 121, 227 (1956)

6.11 HARPER, J.F. Adv. Appl. Mech. 12, 59 (1972)

6.12 BACHHUBER, C. and SANFORD, C. J. Appl. Physics 45(6), 2567(1974)

6.13 GORODETSKAYA, A. J. Phys. Chem. Acad. Sci. (USSR) 23, 71 (1949)

6.14 DETWILER, A. and BLANCHARD, D.C. Chem. Eng. Sci. 33, 9 (1978)

6.15 COLLINS, G.L. and JAMESON, G.J. Chem. Eng. Sci. 32, 239 (1977)

6.16 MELVILLE, J.B. and MATIJEVIC, E. in Foams, Brunel University Conference 8 - 10 Sept., 1975, P199.

6.17 LESSARD, R.R. and ZIEMINSKI,S.A. Ind. Eng. Chem. Fundan. 10(2), 260 (1971)

CHAPTER 7

7.1 WADE, W.H. and SLUTSKY, L.J. J. Chem. Phys. 40, 3394 (1964)

7.2 WARNER, A. in "Ultra micro weight determination in controlled environments" Edited by S.P. Wolsky pp. 137-162 (1969).

7.3. WADE, W.H. and SLUTSKY, L.J. in "Vacuum microbalance techniques" vol. 2. Edited by R.F. WALKER pp. 115-128(1962).

7.4 BLAKE, T.D. J.C.S. Faraday Trans. I, 71, 192 (1975)

7.5 ISRAELACHVILI, J.N. J. Coll. Int. Sci. 44, 259 (1973).

7.6 ROTHEN, A. in "Ellipsometry and the measurement of surfaces and thin films". N.B.S. Misc. Pub. 256, p. 7 (1964).

7.7. McCRACKIN, F.L. PASSAGLIA, E., STROMBERG, R.R. and STEINBERG, H.L. Journal of Research. N.B.S. 67A, 363 (1963).

7.8 JENKINS, F.A. and WHITE, H.E. Fundamentals of optics. 3rd Edition, McGraw-Hill Book Co., Inc. (1957).

7.9 VEDAM, K. Surface Sci. 56, 221 (1976).

7.10 PEARCE, J.N. and NELSON, A.F. J. Am. Chem. Soc. 54, 3544 (1932).

7.11 PEPELA, C.N. and DUNLOP, P.J. J. Chem. Thermodynamics 4, 255 (1972).

7.12 ZORIN, Z.M. in "Research in surface forces" v2. Edited by B.V. Derjaguin, Consultants Bureau, N.Y. p. 134 (1966)

7.13 ADAMSON, A.W. "Physical chemistry of surfaces" 3rd Edition, J. Wiley & Sons. 1976.

7.14 COTTON, F.A. and WILKINSON, G. "Advanced Inorganic Chemistry" Pg. 116, 3rd Edition, Interscience (1972).

7.15 PADDAY, J.F. Disc. Faraday Soc., "Thin liquid films and boundary layers", 64 (1971).

7.16 ZORIN, Z.M. and CHURAEV, N.V. Coll. J. USSR, 30, 279 (1968).

Appendix 2.1

Equation 2.2 can be written as:

$$G(1,T) = \frac{kT}{8\pi l^2} \sum_{n=0}^{\infty'} \int_{P_s}^{\infty} dp\, F(p)\, e^{-P} \qquad A.1$$

(i.e. extracted e^{-P} from inner integral function)

now from Gauss-Laguerre integration procedure:

$$\int_0^{\infty} f(p)\, e^{-P} dp = \sum_{n=1}^{N} W_N\, f(P_N) \qquad A.2$$

where P_N is the value of the function at a sampling point (of which there are sixteen) and W_N is the weight given to this value.

Flow Chart

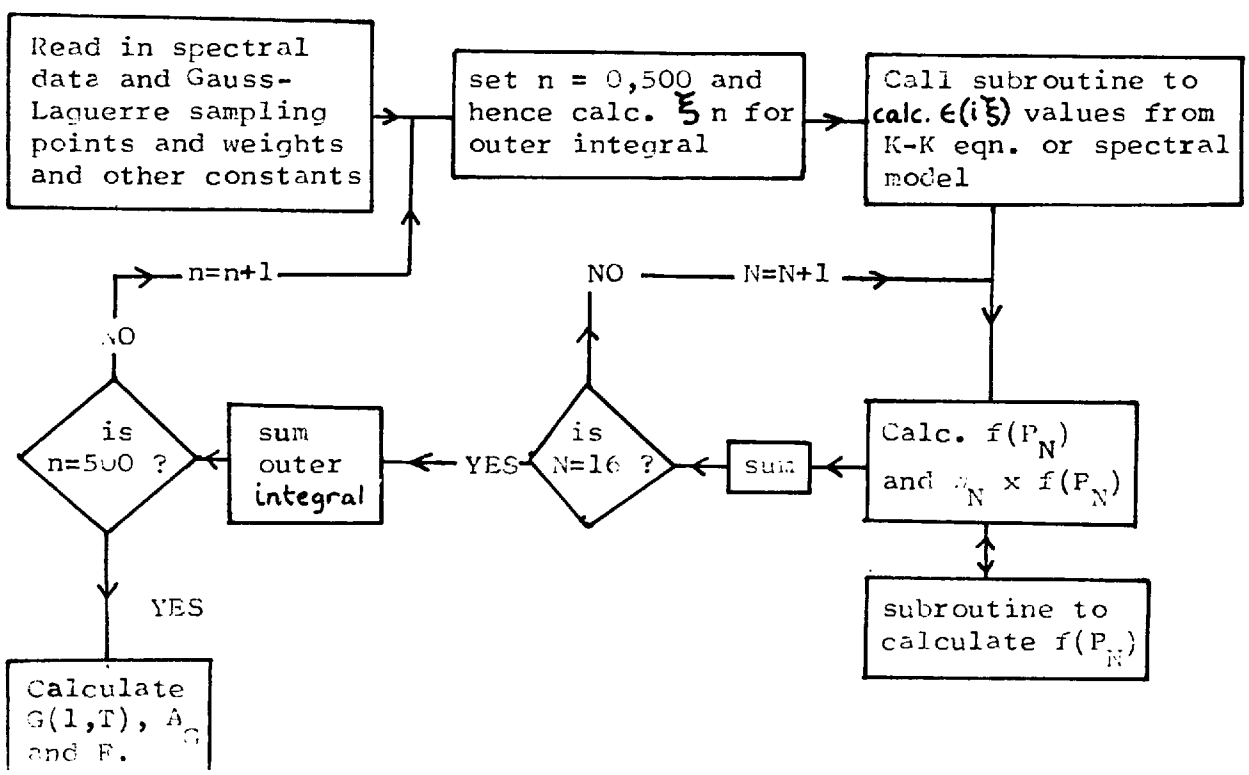

Appendix 2.2

NOTES

The van der Waals Interaction for Liquid Water: A Comparison of the Oscillator Model Approximation and Use of the Kramers–Kronig Equation with Full Spectral Data

INTRODUCTION

In order to calculate the dispersion force between two semi-infinite half-spaces on the basis of the Lifshitz theory, the complex dielectric constant, $\epsilon(i\xi)$, of the media as a function of imaginary frequency must be known throughout the electromagnetic spectrum. Usually this means from far infrared to far ultraviolet, depending on the distance between the bodies and the dielectric constant of the intervening media.

There are two methods of calculating this data: (a) by use of a simplified oscillator model equation derived from an expression ascribed to Debye in 1929 (1), whereby the dielectric constant is directly related to frequency via an equation involving oscillator strengths (related to F_i) and oscillator frequencies (ω_i) corresponding to the absorption spectrum of the material:

$$\frac{\epsilon(i\xi) - 1}{\epsilon(i\xi) + 2} = \sum_{i=1}^{n} \frac{F_i}{\omega_i^2 + \xi^2} \qquad [1]$$

($n = 2$ in this study, corresponding to IR and UV absorption for water) and (b) by use of the Kramers–Kronig equation (2) applied to full spectral data for the material:

$$\epsilon(i\xi) - 1 = \frac{2}{\pi} \int_0^\infty \frac{x\epsilon''(x)dx}{x^2 + \xi^2}, \qquad [2]$$

where $\epsilon''(x)$ is the imaginary component of the complex dielectric constant at frequency x.

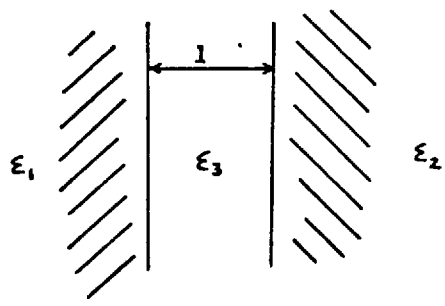

FIG. 1. Two semi-infinite half-spaces separated by distance l.

For the case of water Nir, Rein, and Weiss (3) suggested values for the oscillator strengths and corresponding frequencies by comparison of directly calculated refractive indices, using such an oscillator equation, with observed values for liquid water over the frequency range 2.36×10^{14} rad/sec (IR, 80,000 Å) to 1.03×10^{16} rad/sec (UV, 1832 Å).

Instead of assuming the validity of an oscillator model equation, it is perhaps more fundamental to use the Kramers–Kronig equation to calculate $\epsilon(i\xi)$ from the available spectral data for liquid water, and hence calculate the dispersion force which may then be compared with that obtained using the oscillator model.

METHOD

A computer program was written to calculate the van der Waals interaction free energy per unit area, $G(l)$, for the situation shown in Fig. 1; the required expression is given by Richmond (4), namely:

$$G(l) = \frac{kT}{8\pi l^2} \sum_{\xi_n}{}' \left(\frac{\xi_n}{\xi_a}\right)^2 \int_1^\infty dp\, p \times \ln\left[\left\{1 - \Delta(p; s_1)\Delta(p; s_2)\cdot\exp\left(-\frac{\xi_n p}{\xi_a}\right)\right\} \cdot\left\{1 - \bar{\Delta}(p; s_1)\bar{\Delta}(p; s_2)\exp\left(-\frac{\xi_n p}{\xi_a}\right)\right\}\right]$$

TABLE I

Spectral Data Sources for Water

Region	Frequency range (rad/sec)	Source	Error in $\epsilon''(x)$
IR	6.1×10^{7}–7.6×10^{12}	(6)	
IR	9.1×10^{12}–3.8×10^{13}	(7)	
IR	4.6×10^{13}–1.8×10^{15}	(8)	
UV	1.2×10^{16}–3.8×10^{16}	(9)	±15%
UV	3.8×10^{16}–1.5×10^{17}	(10)[a]	±25%

[a] This source reported absorption coefficients for water vapor. These latter data were normalized for liquid water by comparison with source (9) values at 3.8×10^{16} rad/sec.

Journal of Colloid and Interface Science, Vol. 62, No. 2, November 1977
ISSN 0021-9797

TABLE II

Comparison of $\epsilon(i\xi)$ Calculated Using Full Spectral Data and Oscillator Equation [1]

	Frequency (ξ) (rad/sec) $\times 10^{16}$				
	0.4816	3.853	6.742	9.632	12.04
Full spectral data (K–K equation)	1.832	1.255	1.120	1.068	1.047
Oscillator model ($\omega_{UV} = 3 \times 10^{16}$ rad/sec)	1.882	1.282	1.117	1.062	1.041

where

$$\Delta(p; s_j) = \frac{\epsilon_j p - \epsilon_3 s_j}{\epsilon_j p + \epsilon_3 s_j}, \quad \bar{\Delta}(p; s_j) = \frac{p - s_j}{p + s_j},$$
$$s_j^2 = p^2 - 1 + \epsilon_j/\epsilon_3, \quad j = 1, 2, \qquad [3]$$
$$\xi_s = c/2l(\epsilon_3)^{\frac{1}{2}}.$$

c = velocity of light in a vacuum, T = temperature, 20°C here. For the case considered here, $\epsilon_1 = \epsilon_2 = \epsilon_{H_2O}$; $\epsilon_3 = 1.0$.

The method used here follows that recommended by Dr. L. White (private communication) whereby the inner integral is solved using Gauss–Laguerre quadrature (5). The outer summation was carried out up to $n = 2000$ for small separations ($l < 50$ Å) and up to $n = 500$ for $l > 50$ Å.

A subroutine was used to numerically integrate the spectral data according to the equation

$$y = \frac{x\epsilon''(x)}{x^2 + \xi^2}; \quad \int_0^\infty y dx \qquad [4]$$

for each value of $\xi = \xi_n$, up to $n = 2000$, if required. The value of $\epsilon''(x)$ was obtained from available spectral data for liquid water (Table I) over the ranges shown, using the equation

$$\epsilon''(x) = 2n(x) \cdot k(x), \qquad [5]$$

where $n(x)$ and $k(x)$ are the real and imaginary parts (usually quoted) of the complex refractive index. The error in $\epsilon''(x)$ is also given for the important UV data.

RESULTS

$\epsilon(i\xi)$ values were calculated using the oscillator model equation and the full spectral data (via the Kramers–Kronig equation). Some of the results are summarized in Table II and Fig. 2, together with those of Nir, Adams, and Rein (11). Nir *et al.* apparently did not use the Kramers–Kronig method, for $\epsilon(i\xi)$, in calculating

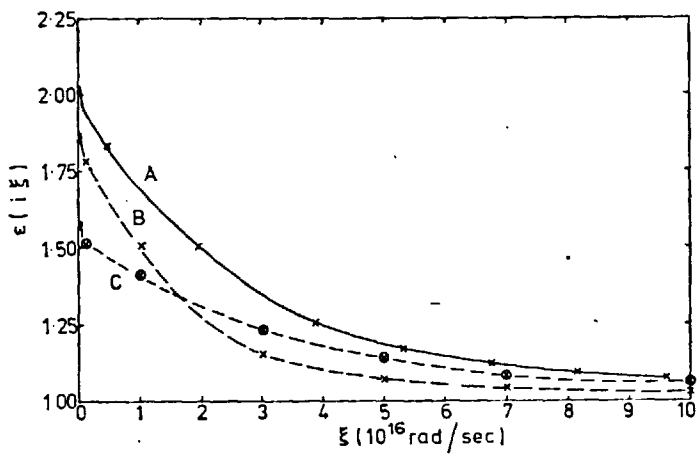

FIG. 2. Calculated dielectric "constant" as a function of imaginary frequency: (A) this study, full spectral data and Kramers–Kronig equation; (B) Nir *et al.* (11), oscillator model equation ($\omega_{UV} = 1.906 \times 10^{16}$ rad/sec); (C) Nir *et al.* (11), full spectral data and Kramers–Kronig equation. At $\xi = 0.001$ rad/sec Nir *et al.* (11) reported $\epsilon(i\xi) = 93.6 \pm 21.4$ (from full spectral data). This study, $\epsilon(i\xi) = 85.2$.

TABLE III

Comparison of $\epsilon(i\xi)$ Calculated Using Full Spectral Data and Limiting Equation [5]

	Frequency (ξ) (rad/sec) × 10^{18}			
	0.2504	0.3468	0.4045	0.4816
Full spectral data (K–K equation)	1.013	1.007	1.005	1.003
Limiting equation	1.016	1.008	1.006	1.004

the dispersion force, but compared the $\epsilon(i\xi)$ values obtained with those calculated using an oscillator model equation.

For large frequencies the limiting equation

$$\epsilon(i\xi) = 1 + (4\pi Ne^2/m\xi^2) \qquad [6]$$

may be derived (2), where $(4\pi Ne^2/m)^{\frac{1}{2}}$ is the plasma frequency (ω_p) and N is the number of electrons per unit volume (m and e are the electronic mass and charge). This equation is valid in the region $\omega_p \ll \xi \ll 2\pi c/a$, where a is a length of atomic dimensions. For liquid water, $\omega_p^2 \simeq 10^{33}$ (rad/sec)^2 and $2\pi c/a \simeq 6 \times 10^{18}$ rad/sec. Thus, for water, Eq. [6] is valid over the approximate range 0.2×10^{18} to 1.0×10^{18} rad/sec. The results obtained from Eq. [6] over this range are compared, in Table III, with those calculated using the Kramers–Kronig equation.

Tables IV and V show the results obtained for the dispersion force as a function of separation distance using the oscillator model for $\epsilon(i\xi)$. The oscillator strengths and frequencies used are also given. The results obtained using the full spectral data (Table I) and the Kramers–Kronig equation are given in Table VI. The 50-Å calculation was repeated using the UV data with maximum positive and negative errors in $\epsilon''(x)$, as indicated in Table I. The results are shown in brackets in Table VI.

DISCUSSION

In order to solve Eq. [3] the function $\epsilon(i\xi)$ must be known as far as 0.5×10^{18} rad/sec for the water–water calculation. The spectral data used here (to 0.15×10^{18} rad/sec) in the Kramers–Kronig equation may be seen, from Table III, to be adequate as compared with the limiting equation [6], up to the required frequency.

From the dispersion force results obtained, it is apparent that the full spectral data (Kramers–Kronig method) give values very similar to those obtained by an oscillator model equation of assumed UV frequency 3.0×10^{16} rad/sec. It is of interest to note that this frequency is, in fact, the effective frequency used by London [12] in 1937.

Using an approximate form of Eq. [3], for small separations, a value for the Hamaker "constant" may be calculated that is independent of separation distance. Visser (13) recommends the value 4.4×10^{-20} J for this calculated Hamaker constant, which corresponds to the value calculated here for a separation of about 50 Å.

Nir (14) reported values for Hamaker constants for the system considered here using a microscopic approach which included a retardation effect. These values are given in square brackets in Table VI. For separations of 100 to 500 Å, the two different approaches appear to give similar results.

ACKNOWLEDGMENTS

The author wishes to thank Dr. J. A. Kitchener for many valuable and interesting discussions and to thank Dr. B. T. Ingram for several helpful suggestions.

TABLE IV

Dispersion Force and Hamaker "Constant" Calculated Using Oscillator Model Equation[a]

	Separation distance (Å)					
	2	50	100	200	500	1000
Dispersion force (nm^{-2})	7.4×10^{7}	1.4×10^{4}	1.5×10^{3}	1.5×10^{2}	6.0	5.3×10^{-1}
Hamaker "constant" ($\times 10^{-20}$ J)	3.7	3.3	2.8	2.2	1.4	1.0

[a] For the oscillator model used here:
$\omega_{UV} = 1.906 \times 10^{16}$ rad/sec; $F_{UV}/\omega_{UV}^2 = 0.202$,
$\omega_{IR} = 5.66 \times 10^{14}$ rad/sec; $F_{IR}/\omega_{IR}^2 = 0.377$.

TABLE V

Dispersion Force and Hamaker "Constant" Calculated Using Oscillator Model Equation[a]

	Separation distance (Å)					
	2	50	100	200	500	1000
Dispersion force (nm^{-2})	3.7×10^{8}	1.8×10^{4}	1.8×10^{3}	1.65×10^{2}	6.3	5.3×10^{-1}
Hamaker "constant" ($\times 10^{-20}$ J)	5.5	4.3	3.4	2.5	1.5	1.0

[a] For the oscillator model used here:
$\omega_{UV} = 3.0 \times 10^{16}$ rad/sec; $F_{UV}/\omega_{UV}^2 = 0.203$;
$\omega_{IR} = 5.66 \times 10^{14}$ rad/sec; $F_{IR}/\omega_{IR}^2 = 0.377$.

TABLE VI

Dispersion Force and Hamaker "Constant" Calculated Using Full Spectral Data

	Separation distance (Å)					
	2[a]	50	100	200	500	1000
Dispersion force (nm^{-2})	3.8×10^{8}	(2.3×10^{4}) 1.8×10^{4} (1.4×10^{4})	1.8×10^{3}	1.6×10^{2}	5.9	4.8×10^{-1}
Hamaker "constant" ($\times 10^{-20}$ J)	5.7	[3.6] (5.3) 4.3 (3.4)	[3.3] 3.4	[2.7] 2.4	[1.7] 1.4	0.9

[a] This calculation was also carried out using $n = 4000$; dispersion force = 3.8×10^{8} nm^{-2}, Hamaker "constant" = 5.7×10^{-20} J.

REFERENCES

1. Debye, P., "Polar Molecules." Dover, New York, 1929.
2. Landau, L. D., and Lifshitz, E. M., "Electrodynamics of Continuous Media." Addison–Wesley, Reading, Mass., 1960.
3. Nir, S., Rein, R., and Weiss, L., *J. Theor. Biol.* 34, 135 (1972).
4. Richmond, P., *in* "Colloid Science 2" (D. H. Everett, Ed.), Chap. 4. The Chemical Society, London, 1975.
5. Rabinowitz, P., and Weiss, G., *Maths. Tables and Other Aids to Computation* 8(68), 285 (1959).
6. Buckley, F., and Maryott, A., *Nat. Bur. Stand. U. S. Circ.* 589, 18 (1958).
7. Kislovskii, L. D., *Opt. Spectrosc.* 7, 201 (1959).
8. Pointer, L., and Dechambenoy, C., *Ann. Geophys.* 22, 633 (1966).
9. Heller, J. M., Jr., Hamm, R. N., Birkhoff, R. D., and Painter, L. R., *J. Chem. Phys.* 80, 3483 (1974).
10. DeReilhac, L., and Damany, N., *Spectrochim. Acta A* 26, 801 (1970).
11. Nir, S., Adams, S., and Rein, R., *J. Colloid Interface Sci.* 49, 196 (1974).
12. London, F., *Trans. Faraday Soc.* 33, 8 (1937).
13. Visser, J., *Advan. Colloid Interface Sci.* 3, 331 (1972).
14. Nir, S., *J. Theor. Biol.* 53, 83 (1975).

R. M. Pashley

Department of Mineral Resources Engineering
Imperial College
London S.W. 7, England

Received June 21, 1976; accepted January 24, 1977.

Appendix 2.3. Comparison of interaction energy (G) calculated using full spectral data for water/vacuum/water (a) and vacuum/water/vacuum (b)

separation (nm)		1	3	6	9
interaction energy $G(mJm^{-2})$	(a)	$-1.44x10^{0}$	$-1.43x10^{-1}$	$-3.04x10^{-2}$	$-1.17x10^{-2}$
	(b)	$-1.44x10^{0}$	$-1.41x10^{-1}$	$-2.93x10^{-2}$	$-1.11x10^{-2}$

Appendix 3.1. A suggested method of solution for the calculation of the electrical double-layer force in a thin water film on quartz.

The thin film system considered here is defined in Figure A.3.1:

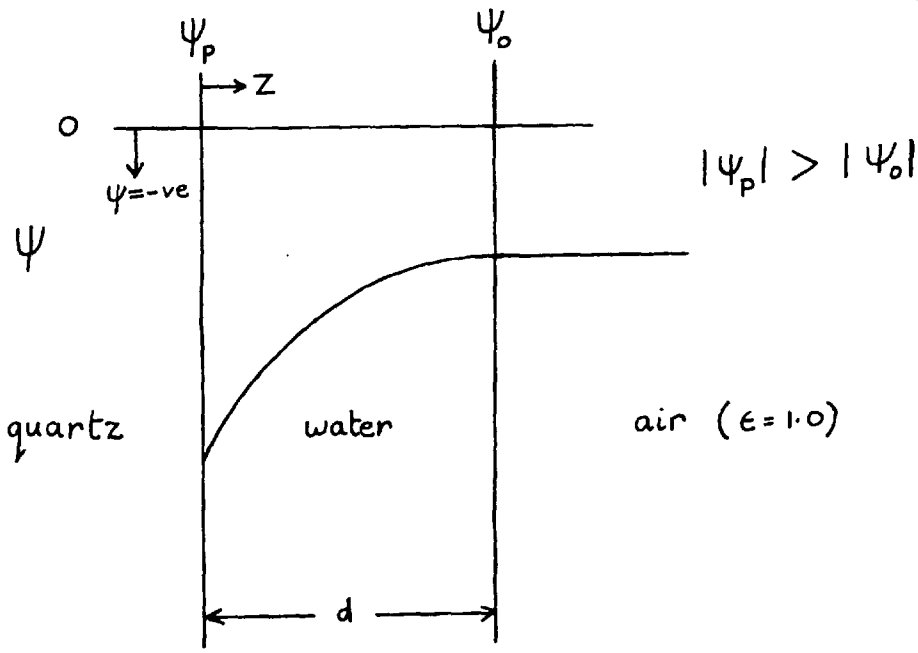

The basic physical assumption is that the surface charge density on the quartz is governed by the concentration of hydrogen ions in the adjoining water film. The boundary conditions defined for the two interfaces are:-

(a) at the silica/water interface (Z = 0):

$$\left(\frac{d\psi}{dz}\right)_{z=o} = \frac{4\pi q \alpha N}{\epsilon} \qquad \text{A.3.1.}$$

and $$\psi(o) = \psi_p \qquad \text{A.3.2.}$$

where ϵ is the dielectric constant of water in the film,

q is the electronic charge, α is the fraction of surface hydroxyl groups dissociated and N is the total number of surface groups. It is assumed here that the surface is ionised ($-SiOH \rightleftharpoons -SiO^- + H^+$) according to the equation:

$$\frac{n_\oplus \alpha}{1-\alpha} = K \qquad \text{A.3.3.}$$

Where $n_\oplus$ is the hydrogen ion concentration at the silica/water interface (i.e. at z = 0) and K is a dissociation constant. As a reasonable simplification the equilibria: $-SiOH + H^+ \rightleftharpoons -SiOH_2^+$ is ignored here.

(b) <u>at the air/water interface (z = d)</u>:

$$\left(\frac{d\psi}{dz}\right)_{z=d} = 0 \qquad \text{A.3.4.}$$

and

$$\psi(d) = \psi_o \qquad \text{A.3.5.}$$

Thus, for simplicity, it is assumed that ψ_o is a function of film thickness, d, but that there is no charge at the air/water interface. Ideally, however, a similar equilibrium to that assumed for the silica/water interface should be applied to the air/water interface also; however, the charging mechanism of the air/water interface is problematical.

Using the Boltzmann equation the cation charge density (n_c) is:

$$n_c = n_\oplus \exp -\left[q(\psi - \psi_p)/kT\right] \qquad \text{A.3.6.}$$

and applying the Poisson equation:

$$\nabla^2\psi = \frac{-4\pi\rho}{\epsilon} \qquad \text{A.3.7.}$$

where ρ is the charge density. For the case of plane-parallel surfaces:

$$\frac{d^2\psi}{dz^2} = -\frac{4\pi n_{\oplus} q}{\epsilon} \exp\left[-q(\psi - \psi_p)/kT\right] \qquad \text{A.3.8.}$$

For simplicity, in this equation only the cation charge density is considered since in a thin water film adjacent to silica, it may be assumed that $[H^+] \gg [OH^-]$

In equations A.3.1. to A.3.5., the unknown constants (for an assumed film thickness) are ψ_o , $n_{\oplus}$ and α , as well as two constants from the integration of equation A.3.8. It should be possible to obtain all five constants from equations A.3.1 to A.3.5.

Equation A.3.8. may be integrated using the fact that:

$$2\int \frac{d^2y}{dx^2}\, dy = \left(\frac{dy}{dx}\right)^2 - C \qquad \text{A.3.9.}$$

where C is a constant which may be determined using the boundary conditions given. Hence $\psi = \psi(z)$ for a given film thickness may be obtained.

If it is assumed that an osmotic force may exist in the thin water film (via vapour transfer, since the film is not directly in contact with bulk water) then the repulsive force per unit area is given by (see reference 3.10):

$$F = kT\left(n_c - 2n_B\right) - \frac{\epsilon E^2}{8\pi} \qquad \text{A.3.10.}$$

where $E = -\partial\psi/\partial z$ and $\epsilon E^2/8\pi$ is the tensional stress in a dielectric due to the electric field E. The first term on the right hand side of equation A.3.10 is the difference between the osmotic pressure at a point in the diffuse region (at potential ψ)

and at a point in bulk solution (i.e. in a very thick film, where n_β is the concentration of electrolyte in water).

It should be possible, using the equations given here and with the aid of a computer, to calculate the potential distribution and hence the force in the thin film.

Acknowledgement

I would like to thank Professor G. M. Bell and Dr. P. Richmond for invaluable advice on this electrical double-layer problem.

Appendix 4.1

Surface Science 71 (1978) 139–147

THEORETICAL ESTIMATE OF ERRORS IN ELLIPSOMETRIC MEASUREMENT OF THIN FILMS OF WATER ON SLIGHTLY ROUGH QUARTZ SURFACES

R.M. PASHLEY

Department of Mineral Resources Engineering, Imperial College of Science and Technology, London SW7 2BP, England

Received 18 May 1977; manuscript received in final form 19 August 1977

The simple Fenstermaker–McCrackin method has been used to estimate possible errors that may be incurred on interpretation of the ellipsometric measurement of the thickness of thin water films on model rough surfaces of quartz. Two different methods are used to interpret the results expected from such a system. Both give very nearly the same result which indicates large errors for systems where the quartz substrate roughness is of the same magnitude as the thickness of the water film.

1. Introduction

While it is true that the apparent refractive index of the substrate, deduced by ellipsometry, has been shown to be little affected by surface roughness up to 300 Å, for glass of refractive index 1.5 [1], the effect of substrate roughness on thin film measurement may be very considerable.

Archer [2] used a simple periodic cube model surface to estimate the effect of a rough silicon surface on the ellipsometric measurement of thin carbon tetrachloride films. Using a linear relation between the phase change and film thickness and by calculating volume-averaged refractive indices, Archer estimated that the measured film thickness could be more than 50% less than the true value for a 50 Å peak–peak cubic surface roughness.

Errors in thin film measurement due to substrate roughness must depend on the refractive indices of the substrate, film and vapour (or solution) and may also be a function of the type of surface roughness. It is intended in this work to theoretically calculate errors which may be expected from ellipsometric measurement of thin water films on various model rough surfaces of quartz.

It is hoped that this work will be of use to experimentalists as an indication of the possible errors in interpretation of measurements on systems where the substrate roughness is large relative to the film thickness.

2. Theoretical model and calculations

Fenstermaker and McCrackin [1] used the Garnett theory [3–5] to calculate refractive indices for horizontal sections of a rough substrate surface. The method uses the Clausius–Mossotti relation to calculate polarisabilities of the components which are then volume averaged. A series of layers of different refractive indices (n_e) are obtained. The refractive index and film thickness that is ellipsometrically equivalent to these combined layers may be calculated using the equations of McCrackin and Colson [6]:

$$N_{cal} = [\int_0^t n_e(n_e - n_1)\,dt]\,[\int_0^t (n_e - n_1)\,dt]^{-1}, \tag{1}$$

$$T_{cal} = [\int_0^t (n_e - n_1)\,dt]\,(N_{cal} - n_1)^{-1}, \tag{2}$$

where N_{cal} is the average refractive index, T_{cal} the effective thickness, n_1 the refractive index of the surrounding media and t the thickness of the sections.

Thus Fenstermaker and McCrackin were able to calculate the thickness and refractive index of a film which was ellipsometrically equivalent (with respect to observed phase change (Δ) and azimuth (ψ)) to various rough model surfaces on several substrates. The Δ and ψ values calculated could then be used to calculate the refractive index of the substrate assuming its surface were perfectly smooth. This procedure was followed for the quartz (refractive index = 1.543) substrate considered here.

All the ellipsometric calculations were carried out by computer programs written by the author using the Drude equations [6].

If a water film (refractive index = 1.332) is placed on a rough surface and we assume the form of the surface and film (i.e. contoured or flat surface film, fig. 2), we may again calculate the thickness and refractive index of an ideal smooth film which is ellipsometrically equivalent to that model. From this equivalent film system the values Δ and ψ which would be measured may be calculated. This method assumes that the Fenstermaker–McCrackin treatment may be applied to a three component system.

By this procedure we thus obtain the Δ and ψ values which would be measured both on bare rough quartz substrates and on substrates with water films present.

In this work we have used two different methods of analysing the Δ and ψ values which would be measured:

(a) For thin water films (<200 Å) on quartz, it has been shown (fig. 4b) that for measured Δ and ψ accuracy of $\pm 0.01^\circ$ (usual error limit, at present) ellipsometric measurements, at a single angle of incidence, do not accurately define the refractive index of a film as well as its thickness. Thus we must assume a refractive index and

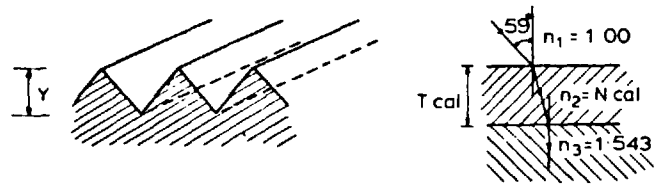

Fig. 1. (a) Triangualr ridge substrate; (b) ellipsometrically equivalent film.

hence calculate the corresponding film thickness [7]. Fig. 4a gives more complete values for calculated Δ and ψ angles for different film thicknesses (in Å) for films of refractive indices 1.250, 1.332 and 1.400.

From tables 1 and 3 it is apparent that rough surfaces on quartz are ellipsometrically equivalent to films of refractive index near to that of water. Hence, for convenience in this method, we assume that the rough substrate surface and the rough surface with water film are both equivalent to different thicknesses of films with the same refractive index, 1.332. The actual measured water film thickness on a rough substrate is then simply, the difference between these two thicknesses.

(b) The second method: The values of Δ and ψ measured for a rough substrate (which are theoretically calculated here) are different from those expected for a smooth surface. If the substrate refractive index is calculated from these different values then the refractive index is found to be apparently complex. In this second method the substrate surface was assumed to be smooth and the substrate to possess this complex refractive index. The thickness of the transparent film of refractive index 1.332 present on this absorbing substrate corresponding to the measured (theoretically calculated here) Δ and ψ values was then calculated. The results from the two methods were compared.

An iterative computer solution (written by the author) was used to calculate the thicknesses of the films in both methods. Two solutions were obtained in each case; one each from equating both real and imaginary parts of the equations. The valid solution was proven in each case by re-calculation to obtain the starting values. In both cases the imaginary solution gave the original starting values and was hence the correct one.

The models used in this paper are shown in figs. 1, 2 and 3. In order to calculate

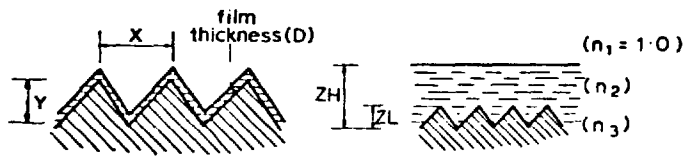

Fig. 2. (a) Rough triangular ridge with contoured film; (b) thick film on low roughness triangular ridge surface.

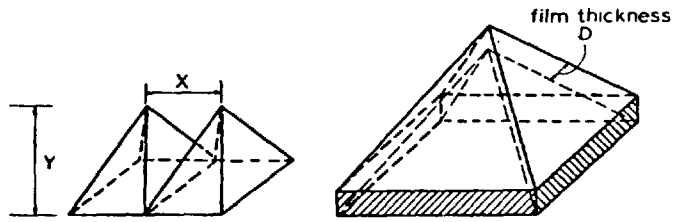

Fig. 3. (a) Square based pyramid model; (b) square based pyramid model with contoured film.

the film equivalent (i.e. thickness and refractive index, T_{cal} and N_{cal}) to a rough surface using the Fenstermaker–McCrackin method the averaged horizontal layer indices, n_e, are required as a function of vertical height, t. In the case of a triangular ridge surface n_e is a direct function of t which is easily integrated, hence eqs. (1) and (2) were solved directly. However, for the square-based pyramid model this was not the case and n_e was therefore calculated for 1 Å intervals and the summation, for N_{cal} and T_{cal}, was carried out numerically.

The average horizontal layer indices (n_e) are calculated for a 3-component system using the following equation which is directly analogous to that used by Fenstermaker–McCrackin:

$$\frac{n_e^2-1}{n_e^2+2}=q_1\frac{N_1^2-1}{N_2^2+2}+q_2\frac{N_2^2-1}{N_2^2+2}+q_3\frac{N_3^2-1.}{N_3^2+2},$$

where n_e is calculated from the volume fractions (q_n) and refractive indices (N_n) of the three components in a horizontal layer of thickness dt in the model surface/film system.

3. Results and discussion

Typical experimental conditions for angle of incidence (59.0, 2° above Brewster angle [8]) and wavelength (6328.0 Å, He–Ne laser wavelength) were used in the calculations.

Table 1 gives the results of using the Fenstermaker–McCrackin method to calculate Δ and ψ from the dimensions of the triangular-ridge model rough surface. D_i is the thickness of a film of refractive index 1.332 (on a 1.543 smooth substrate) which would give the same Δ and ψ values. It may be seen, as expected from fig. 4b, that for Δ and ψ of ±0.01° a film of a particular index and thickness is ellipsometrically equivalent to a thinner film of a lower index.

It may be of interest to note that the values N_{cal} and T_{cal} in table 1 are independent of the X dimension (see fig. 2), assuming that the latter is small compared with the wavelength of the incident light.

Table 1
Calculation of apparent thickness of film of 1.332 equivalent to triangular ridge rough surface of quartz

Y (A)	T_{cal} (A)	tan ψ exp(iΔ)	Δ (deg)	ψ (deg)	D_i (A)
5	3.655	0.05298 + i0.0006105	0.66	3.03	3.45
10	7.3102	0.05299 + i0.001221	1.32	3.03	6.93
15	10.965	0.05299 + i0.001832	1.98	3.035	10.40
20	14.620	0.05300 + i0.002442	2.64	3.04	13.87
25	18.276	0.05301 + i0.003052	3.295	3.04	17.33
50	36.55	0.05312 + i0.006104	6.556	3.06	34.5
100	73.10	0.05355 + i0.01238	13.02	3.15	69.4
200	146.2	0.05520 + i0.02439	23.84	3.45	138.5
300	219.3	0.05802 + i0.03653	32.20	3.92	207.4
500	365.5	0.06727 + i0.06056	41.99	5.17	343.9

N_{cal} = 1.3512, λ = 6328.0 A, ϕ_1 = 59.0°, n_3 = 1.543.

Table 2, 3 and 4 similarly give calculated values of tan Δ. exp(iψ) (from which Δ and ψ are easily calculated) and the corresponding 1.332 index film thickness to which they are equivalent. By subtracting this latter value from that given in table 1, the values for water film thicknesses which would be ellipsometrically measured on these rough surfaces (using this method) are obtained, and are given here, with approximate percentage errors, in table 6.

The complex substrate refractive indices which would give the same Δ and ψ values as those from rough substrate surfaces are given in table 5. The thicknesses of water films on these, apparently absorbing, smooth substrates corresponding to the values of Δ and ψ which would be measured, are given in parentheses in table 6 for comparison.

From table 6 it is apparent that either analysis of the Δ and ψ values, which would be measured on model rough surfaces, with and without films, give almost identical errors. These errors are large if the surface roughness is comparable with

Table 2
Results of calculation for 1.332 film thickness for rough triangular ridge substrate with contoured film

D (A)	Y (A)	X (A)	T_{cal} (A)	N_{cal}	tan ψ exp(iΔ)	D_i (A)
25	50	500	54.82	1.3945	0.05330 + 0.007724i	43.6
25	100	500	90.01	1.3895	0.05385 + 0.01298i	73.7
25	200	500	164.55	1.3802	0.05591 + 0.02465i	140.0
25	300	500	241.00	1.3765	0.05929 + 0.03651i	207.25
25	500	500	395.91	1.3738	0.07033 + 0.05976i	339.40
25	50	2000	54.41	1.3945	0.05330 + 0.007665i	43.6

Table 3
Results of calculation for 1.330 film thickness for square-based pyramid model with and without the contoured water film (n_3 = 1.51 in this case, otherwise same conditions)

D (Å)	Y (Å)	X (Å)	T_{cal} (Å)	N_{cal}	tan ψ exp(iΔ)	D_i (Å)
0	100	300	53.84	1.298	0.06895 + i0.009216	58.5
25	100	300	73.61	1358	0.06924 + i0.01041	66.3

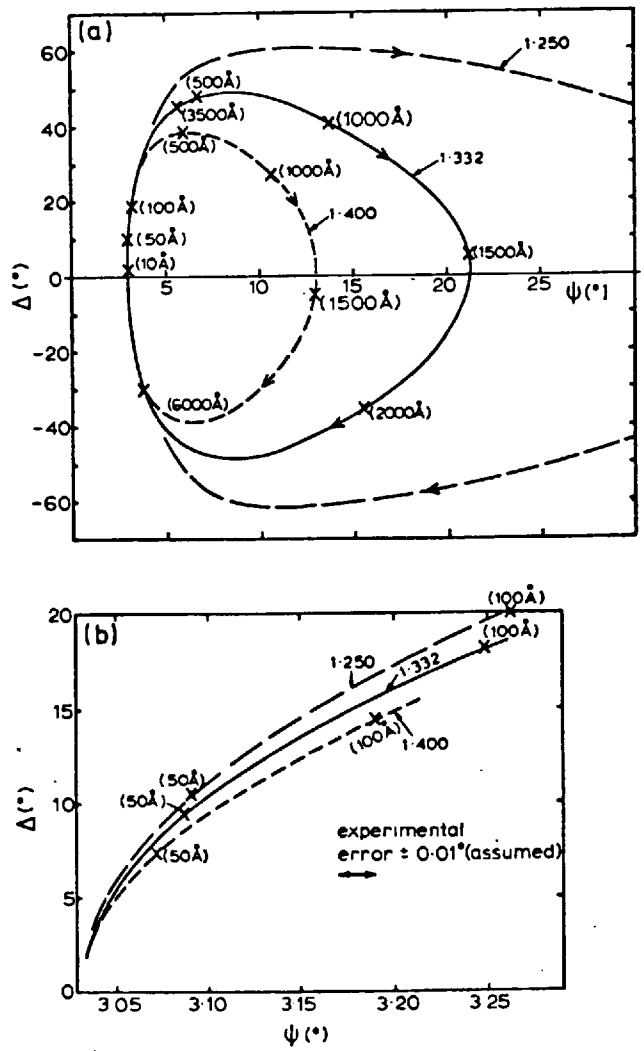

Fig. 4. Calcualted values of Δ and ψ for various thicknesses of films of refractive index 1.250, 1.332 and 1.400 on smooth quartz.

Table 4
Results of calculation for 1.332 film thickness for small roughness squared-based pyramid

ZL (A)	ZH (A)	T_{cal} (A)	N_{cal}	tan ψ exp(iΔ)	D_i (A)
5	100	99.4	1.339	0.05397 + i0.01718	97.6
10	100	98.9	1.346	0.05398 + i0.01676	95.6
25	100	97.9	1.346	0.05400 + i0.01554	88.2
30	100	97.5	1.372	0.05400 + i0.01514	86.0
50	100	97.0	1.395	0.05400 + i0.01361	77.3
70	100	97.14	1.416	0.05397 + i0.01215	69.0
90	100	97.68	1.435	0.05393 + i0.01074	60.9

the water film thickness. By comparison, in table 6, between squared-based pyramid and triangular ridge surfaces it may be also observed that the exact form of the surface roughness is also relevant although not as important as the peak–peak height. These results, of course, only apply to thin water films on quartz or glass.

Thus it appears that for accurate measurement of thin water films on quartz, very smooth surfaces are required. Hodgkinson [9] reports a rms roughness obtained from analysis of fringes of equal chromatic order (feco) for polished fused silica, of about 2.5 Å after polishing with cericouge followed by water addition only, for long periods. However, the horizontal resolution of such an analysis is about 2 μm [10]. Thus it is doubtful that such analyses are of relevance to smoothness with respect to ellipsometric substrates. Shadowed replicas studied by electron microscopy may be of more value. Some work done by the author indicates that cerirouge polished surfaces of crystalline quartz possess undulations of about 100 Å peak–peak and about 500 Å periodicity. This latter result agrees well with an electron microscopy study on polished silica plates by Derjaguin et al. [11].

Table 5
Results of calculation of complex substrate refractive indices (N_s^*) ellipsometrically equivalent to surface rough triangular-ridge quartz

Y (A)	N_s^*
5	1.5430–i0.001306
10	1.5430–i0.002613
15	1.5430–i0.003920
20	1.5429–i0.005225
25	1.5429–i0.006530
50	1.5426–i0.01306
100	1.5414–i0.02645
200	1.5367–i0.05186
300	1.5287–i0.07707
500	1.5035–i0.1245

Table 6
Comparison of apparent film thickness deduced by ellipsometry with actual film thickness (compiled from tables 1–5)

Type of surface and film	Peak–peak height (Å)	Real-film thickness (Å)	Measured value (Å)	± % error
Low roughness	5	97.5	94.1	−3
triangular ridge	10	95	88.3 (88.2)	−7
substrate	25	87.5	70.9	−19
	50	75	42.8 (42.6)	−43
High roughness	50	25	9.1 (9.2)	−64
triangular ridge	100	25	4.3 (3.5)	−84
substrate with	500	25	Negative	–
contoured film				
Square-based pyramid substrate with contoured film	100	25	7.8	−69

Clearly, from the analysis given the surface roughness for these samples cannot be ignored when ellipsometrically measuring the thickness of thin water films. If the exact from of the surface roughness were known, then assuming the Fenstermaker–McCrackin method were valid, the gross errors could be significantly corrected for.

Smith [12] has compared the validity of the Fenstermaker–McCrackin method with that of Ohlidal and Lukes [13] with respect to interpretation of characterised rough surfaces of aluminium. Smith concluded that the F–M treatment was most promising for pit-type roughnesses, whereas the O–L method was better for bump-like surfaces.

Acknowledgement

The author would like to thank Dr. J.D. Hibbs for serveral helpful suggestions.

References

[1] C.A. Fenstermaker and F.L. McCrackin, Surface Sci. 16 (1969) 85.
[2] R.J. Archer, in: Ellipsometry and the Measurement of Surfaces and Thin films, Natl. Bur. Std. (Washington) Misc. Publ. 256 (1964) p. 255.
[3] M. Garnett, Phil. Trans. Roy. Soc. (London) 203 (1904) 385; 205 (1906) 237.

[4] E.C. Chan and J.P. Marton, J. Appl. Phys. 45 (1974) 5004.
[5] J.P. Marton and E.C. Chan, J. Appl. Phys. 45 (1974) 5008.
[6] F.L. MaCrackin and J.P. Colson, in: Ellipsometry and the Measurement of Surfaces and Thin Films, Natl. Bur. Std. (Washington) Misc. Publ. 256 (1964) p. 61.
[7] A.C. Hall, J. Phys. Chem. 74 (1970) 2742.
[8] K. Vedam and M. Malin, Mater. Res. Bull. 9 (1974) 1503.
[9] I.J. Hodgkinson, J. Phys. E3 (1970) 341.
[10] J.M. Bennett, Appl. Opt. 15 (1976) 2705.
[11] B.V. Derjaguin, Z.M. Zorin, N.V. Churaev and V.D. Sobolev, to be published.
[12] T. Smith, Surface Sci. 56 (1976) 252.
[13] I. Ohlidal and F. Lukes, Opt. Acta 19 (1972) 817.